

Advanced optical materials for light control

Citation for published version (APA):

Timmermans, G. H. (2021). *Advanced optical materials for light control: On the road towards smart greenhouses*. [Phd Thesis 1 (Research TU/e / Graduation TU/e), Chemical Engineering and Chemistry]. Technische Universiteit Eindhoven.

Document status and date:

Published: 06/04/2021

Document Version:

Publisher's PDF, also known as Version of Record (includes final page, issue and volume numbers)

Please check the document version of this publication:

- A submitted manuscript is the version of the article upon submission and before peer-review. There can be important differences between the submitted version and the official published version of record. People interested in the research are advised to contact the author for the final version of the publication, or visit the DOI to the publisher's website.
- The final author version and the galley proof are versions of the publication after peer review.
- The final published version features the final layout of the paper including the volume, issue and page numbers.

[Link to publication](#)

General rights

Copyright and moral rights for the publications made accessible in the public portal are retained by the authors and/or other copyright owners and it is a condition of accessing publications that users recognise and abide by the legal requirements associated with these rights.

- Users may download and print one copy of any publication from the public portal for the purpose of private study or research.
- You may not further distribute the material or use it for any profit-making activity or commercial gain
- You may freely distribute the URL identifying the publication in the public portal.

If the publication is distributed under the terms of Article 25fa of the Dutch Copyright Act, indicated by the "Taverne" license above, please follow below link for the End User Agreement:

www.tue.nl/taverne

Take down policy

If you believe that this document breaches copyright please contact us at:

openaccess@tue.nl

providing details and we will investigate your claim.

Advanced optical materials for light control

On the road towards smart greenhouses

Gilles Timmermans



Advanced optical materials for light control

On the road towards smart greenhouses

PROEFSCHRIFT

ter verkrijging van de graad van doctor aan de Technische Universiteit Eindhoven, op
gezag van de rector magnificus prof.dr.ir. F.P.T. Baaijens,

voor een commissie aangewezen door het College voor Promoties, in het openbaar te
verdedigen op dinsdag 6 april 2021 om 16:00 uur

door

Gilles Hubert Timmermans

geboren te Heerlen

Dit proefschrift is goedgekeurd door de promotoren en de samenstelling van de promotiecommissie is als volgt:

voorzitter:	Prof.dr. F. Gallucci
1 ^e promotor:	Prof.dr. A.P.H.J. Schenning
copromotor:	Dr. M.G. Debije
leden:	Prof.dr. A.H.M.E. Reinders Prof.dr. W.G.J.H.M van Sark (Universiteit Utrecht) Dr. R.C. Evans (University of Cambridge) Dr. S.C.J. Meskers
adviseur:	Dr. S. Hemming (Universiteit Wageningen)

Het onderzoek of ontwerp dat in dit proefschrift wordt beschreven is uitgevoerd in overeenstemming met de TU/e Gedragscode Wetenschapsbeoefening.

*“Yesterday is history,
tomorrow is a mystery,
but today is a gift.
That is why it is called the present.”*

- Bil Keane

A catalogue record is available from the Eindhoven University of Technology Library
ISBN: 978-90-386-5239-9

Copyright © 2021 Gilles Timmermans

Cover: Photo by Nahil Naseer on Unsplash and Peter Timmermans
Design by Gilles Timmermans

Printed by Proefschriftmaken

The research described in this thesis was financially supported by PPS Smart Materials

Table of Contents

Summary		VII
Chapter 1	Introduction	1
Chapter 2	Dual thermal-/electrical- responsive luminescent 'smart' window	25
Chapter 3	Color tunable triple state 'smart' window	37
Chapter 4	Temperature and light responsive 'smart' window based on a diarylethene sunlight responsive dye	49
Chapter 5	Flexible Nanoporous Liquid Crystal Networks as Matrixes for FRET	61
Chapter 6	Technological assessment	75
Samenvatting		85
Acknowledgments		87
Curriculum Vitae		91
List of Publications		92

Summary

Better quality and greater quantity of crops are needed to help feed the growing and wealthier global population. Greenhouses are excellent systems to increase the productivity of a fixed land area. Many factors have been investigated to improve yields in greenhouses but the quantity and distribution of light that reaches the crops is still a limiting factor in many modern greenhouses. Currently, there are only limited options to control the incoming sunlight and almost no systems are available that can rapidly change their optical properties. In this thesis we show several systems that can rapidly change their optical properties in response to external stimuli. These ‘smart’ windows can change their absorbance and/or light scattering in response to triggers such as heat, light and electrical fields.

First an absorption based ‘smart’ window was fabricated where a liquid crystal (LC) host was doped with a dichroic fluorescent dye in Chapter 2. The alignment of the LCs can be changed by application of an electrical field or by changes in the temperature. The dichroic dye follows the alignment of the LCs and thus the absorption of the system changes. As the temperatures increase more light is being absorbed, helping to stabilize the temperatures inside a greenhouse. If so desired, the ‘smart’ window can be manually switched to a more transparent state by an electrical field. As the dichroic dye is fluorescent, part of the absorbed light is reemitted and will be concentrated at the edges of the window as in a luminescent solar concentrator (LSC). The concentrated light could be converted to electricity using photovoltaic cells or redirected to plants to increase their growth.

In Chapter 3, a ‘smart’ window is fabricated where not only the alignment of the fluorescent dye is changed but the dye itself is temperature responsive. At higher temperatures the dye is fluorescent but upon cooling aggregates to a colorless non-fluorescent form. Addition of a second fluorescent dye results in yellow color at lower temperatures and a bright red color at high temperatures facilitated by Förster resonance energy transfer (FRET). At application of an electrical field both the LC host and fluorescent dye reorientate, making the ‘smart’ window transparent. Creation of a supertwist LC alignment results in a scattering state at intermediate voltages. Scattering of light is generally beneficial to crop growth in greenhouses and can function as a privacy state in the built environment. As the system makes use of a fluorescent dye, an LSC design is also possible.

To be able to quickly protect crops from harsh lighting conditions, a photo responsive ‘smart’ window was fabricated in Chapter 4. Unlike the systems in Chapter 2 and 3, this

system can directly respond to changes in light, before the temperature in the greenhouse has increased. This system is based on a fluorescent photochromic diarylethene dye that becomes more colored when exposed to light of 340 nm and less colored when exposed to 440 nm light. A manual override towards a transparent state remains possible upon application of an electrical field. Again, this system could also be deployed as an LSC to generate electricity. The 'smart' window was also converted into a 'smart' photo responsive coating to allow for easier applications in greenhouses or buildings.

Contrary to Chapters 2-4, in Chapter 5 a system in which efficient FRET could take place is fabricated that is not a 'smart' window. LCs are used to align a fluorescent dye and to create an ordered matrix. After a base treatment the LC matrix becomes nanoporous and a second dye is absorbed bringing the two dyes in close contact. The ordering and short distance between the two fluorescent dyes greatly facilitates FRET. Such systems are not only interesting for sensing applications but this efficient energy transfer could also be beneficial for photovoltaic systems, LSC and greenhouses.

In conclusion, this thesis provides multiple examples of potential 'smart' windows based on fluorescent dyes and LCs. These windows can alter their absorbance both on demand or in response to changing environmental factors to help keep the inside temperature of buildings and greenhouses more constant. The absorbed light could be used to generate electricity in a LSC configuration or redirected to the crops in greenhouses. Outside of greenhouses, these systems are also interesting in the built environment, electricity generation and sensors.

Chapter 1

Introduction

The increasing demand for efficiently growing crops in greenhouses requires continual improvement of the control of the growth environment experienced by the plants. The single most important factor in maximizing the crop's growth is the quantity, quality and geometrical distribution of radiation intercepted at every moment. Few available greenhouse coverings are capable of responding to changes in sunlight conditions by themselves, which limits the grower's control, and to better manage growth conditions the grower must employ additional technologies, including screens, artificial lighting, heating, and cooling. This Chapter considers existing efforts in providing adaptable greenhouse covering systems and advanced optical materials for controlling the color, intensity and/or distribution of sunlight transmitted into greenhouse-like structures by describing existing static materials and their responsive equivalents. The Chapter also offers speculation on potential applications of other light-control elements, mostly designed for use in the urban environment that could be adapted for greenhouse use in the future.

This chapter is partially reproduced from: G. H. Timmermans, S. Hemming, E. Baeza, E. A. J. van Thoor, A. P. H. J. Schenning, and M. G. Debije, "Advanced Optical Materials for Sunlight Control in Greenhouses," *Adv. Opt. Mater.* 8, 2000738 (2020)

1.1 Introduction

Advanced optical materials have many potential applications; one which is often overlooked is the horticultural sector. About 38% of dry land area worldwide is dedicated to agriculture, which is close to the maximum suitable for this purpose.^{1,2} Greenhouses and similar constructions are designed to help meet growing food demands by increasing the production on existing land³ and allowing use of areas otherwise unsuitable for agriculture.⁴ The total global area for growth of fruits and vegetables in greenhouses (permanent structures) covered with glass and plastic is about 500,000 hectares, 40,000 hectares of which are glass.⁵ The average production volume of vegetables per greenhouse increased about 36% between 2000 and 2017. The largest single crop, tomatoes, showed a 75% increase, while zucchini production more than doubled (138%), and strawberries were even greater at 177% (see **Figure 1.1**).⁶

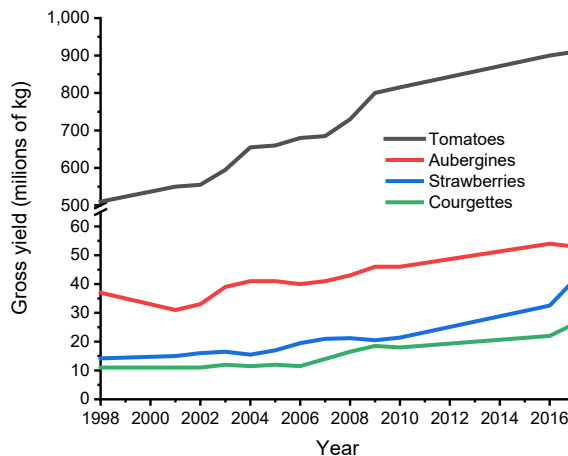


Figure 1.1: Worldwide greenhouse production 2000-2017 as determined by the Agricultural Census 2017, conducted by Statistics Netherlands (CBS).⁶

The primary roles of greenhouses are to protect crops from harmful weather phenomena (such as hail, snow, and rainstorms), birds, pest insects, help maintain stable temperatures to improve quantity and quality of the crops,³ and control of solar irradiance, key to plant growth.⁷ Solar irradiance consists of several wavelength regimes, with ultraviolet (UV, <400 nm), photosynthetically active radiation (PAR, 400-700 nm), and near infrared (NIR, 700-2500 nm) having the greatest relevance for greenhouses (see **Figure 1.2a**,^{3,8} and **Figure 1.2b**⁹ for a depiction of light intensity distribution around the globe). To make the growth requirements even more complex, the radiation needs of plants can vary between species, the time of day, or the day of the year, and less than optimum conditions can curtail crop production.^{7,10}

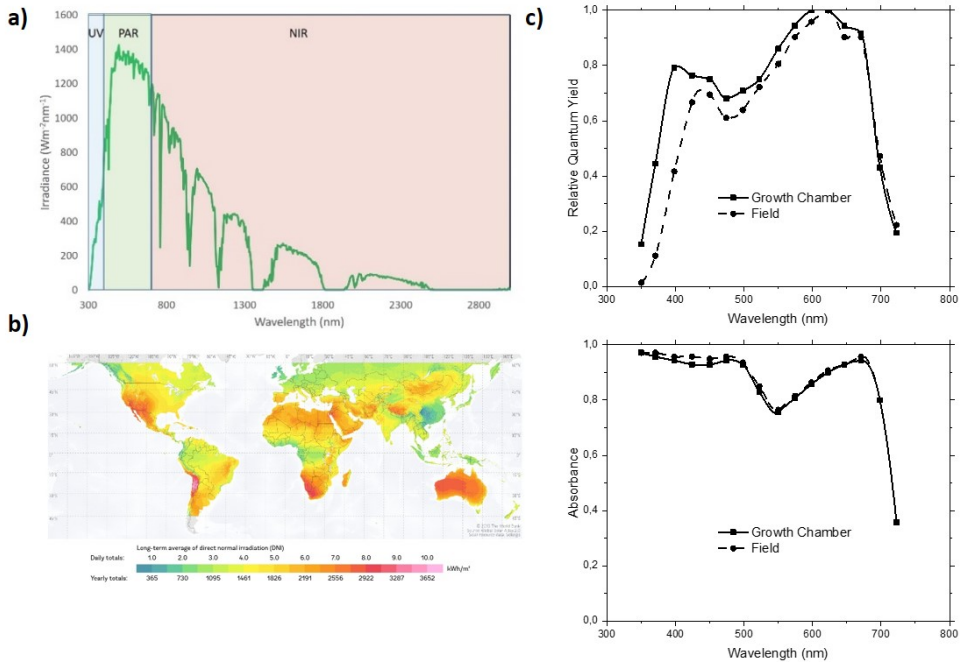


Figure 1.2: a) Calculated AM1.5 spectrum showing the spectral coverage and relative contributions from UV, PAR, and NIR radiation. b) Global direct normal irradiation. Reproduced with permission.⁹ Copyright 2019, Solargis c) Data showing the quantum yields (uptake of CO₂ per absorbed photon) and spectral absorbances of leaves averaged for 22 species of plants grown in controlled locales and in the field. Adapted with permission.¹¹ Copyright 1972, Elsevier.

UV light plays a key role in the morphology of specific plants and their secondary metabolites,⁷ and can influence the behavior of pests,^{3,12–15} but is also helpful to insects and pollinators.^{16,17} UV also influences the generation of diseases within greenhouses.¹⁸

The most important irradiance for photosynthesis is PAR. In high latitude (*e.g.* Dutch) greenhouses, the availability of PAR light often limits plant growth, the rule of thumb being a ~1% variation in the available amount of light for a crop results in a ~0.8% change in crop yield.¹⁹ In these Dutch greenhouses, considerable effort is made to increase the amount of PAR light that enters greenhouses, including regular roof cleaning²⁰ and applying antireflection (AR) surface treatments,^{3,18} while research is done on new surface structures, such as zigzag shaped plastics,²¹ new plastic compounds and lighter materials,²² and using fluorescent materials to convert shorter wavelengths of light into PAR.^{23,24}

PAR direction and geometrical distribution can be separated into direct and diffuse components. Direct radiation reaches the earth unimpeded from the sun. However, at overly high intensities, direct radiation is likely to damage some type of crops.^{25,26} Diffuse radiation occurs when solar light is scattered before encountering the crop, for example by

clouds and particles in the atmosphere, or by special scattering greenhouse cover materials. While diffuser materials can reduce the absolute intensity of incident light, they often enhance light penetration deeper into the crop canopy, resulting in better horizontal and vertical light distributions, improving growth and development.^{27,28}

NIR, on the other hand, is only *ca.* 60% absorbed by crops, mostly being converted into latent and sensible heat inside the greenhouse. This heating can have positive or negative effects. In cold periods when it is desirable to increase the interior temperature of the greenhouse, NIR heating is an advantage; however, in hot periods when the temperature inside the greenhouse must be artificially reduced, it is a significant disadvantage.²⁹ As an added complication, the requirements of NIR often vary with the seasons and even during the course of a day.³⁰

Both glass and most plastics that are used as greenhouse coverings transmit UV, PAR, and NIR to certain extents. Control of light, in directionality, intensity and color, is vitally important for attaining ideal growth conditions. Many of these growth characteristics depend on plant type, variety, stage of growth, position on the globe, type of greenhouse structure and equipment, and a host of other variables (see **Figure 1.2c**¹¹).

The control of solar radiation is generally not regulated by the greenhouse structure itself, but only by add-on technologies such as screens, supplementary lighting, heating, cooling, and so forth.^{31,32} Because the growth requirements of the plant is constantly changing, it could revolutionize greenhouse growing if the materials making up the greenhouses themselves could directly alter light transmission, direction or quality in response to these changes. Doing so could increase crop production and profitability, enhancing their nutritional value and appearance.^{33,34} In this Chapter, we will consider advanced optical materials and architectures designed for the control of all important bandwidths of solar radiation. While there are only limited instances of adaptive optical materials currently being integrated in greenhouse structures, we will extrapolate possibilities for new devices based on existing research that could be transferred to greenhouses. This Chapter will focus on manipulation of natural sunlight, and will not discuss the common use of artificial lighting such as LEDs to influence plant growth.^{7,35}

1.2 Sunlight intensity and distribution control

The quantity and quality of light are both important elements in plant growth. Too much light may be as damaging as too little light. The distribution of light also plays a key role: diffuse light has shown to improve plant yields by decreasing the chance of plant stress, altering crop morphology and light interception,^{28,36,37} resulting in a particular interest in materials that give rise to diffusion for construction of greenhouses.^{28,38} In this section, we will discuss systems designed to control both of these aspects of sunlight.

1.2.1 Intensity and distribution control via scattering

Modified light transmission through a greenhouse roof can be achieved by coverings^{39–41} or permanent coatings.¹⁸ In warm regions, shading is often required to decrease temperatures. The most common shading methods use temporary coatings that scatter the incoming light, such as simple whitewashes using calcium oxide or calcium carbonate applied to the external roof surfaces before anticipated hot periods, and removed for cooler periods,⁴² although there are examples of scattering material being applied directly to plant leaves themselves.⁴³ While simple, there are potential disadvantages, including premature washing away by rain,⁴⁴ spatial heterogeneity,⁴⁵ or excessive shading, reducing plant growth by the removal of the PAR.^{46,47} Movable shading screens allow for more control of light transmission on a daily basis. However, an interior screen often interferes with ventilation,⁴⁸ and exterior screens have other drawbacks such as foiling by dust, damage by wind, in spite of the good ventilation performance.^{49,50} Only a highly porous, movable internal screen seems to perform better than a whitewash for the purpose of shading during high intensity light conditions..⁵¹

Devices that can switch from a transparent to a light scattering state to actively control sunlight intensity might have benefits. Considerable research has already been done on 'smart' windows that can switch from a transparent to a light scattering state for use in the built environment. Many different systems are under investigation, including polymer dispersed liquid crystals (PDLCs),^{52–54} polymer stabilized liquid crystals (PSLCs),⁵⁵ electrodynamic instabilities^{56,57} and other techniques.^{58–60} Some switchable PDLC/PSLC windows are already commercially available.^{61,62}

PDLCs are made by dispersing liquid crystal (LC) droplets throughout a polymer matrix. Light is scattered due to the refractive index mismatch between the randomly ordered LC and the host polymer matrix. Application of an electrical field aligns the birefringent LC droplets. By aligning the LC, the effective LC refractive index matches the refractive index of the polymer matrix, and a transparent state is attained. The system has maximum

transparency for incoming PAR normal to the PDLC, allowing it to be used as an angular discriminating device.⁵³ For greenhouse applications, this might be adapted to become more or less transparent over the course of a day, as the angle of the sun changes. Most PDLC systems are scattering in the 'off' state, but reverse mode PDLCs that are transparent in the 'off' state also exist.⁵⁴ A variation of PDLCs are PSLCs where the polymer content is greatly reduced which lowers the voltage required for switching between states. These systems are maturing rapidly, with large ($40 \times 50 \text{ cm}^2$) prototypes (see **Figure 1.3**) stable for over 100,000 switches being demonstrated.⁵⁵ A key research challenge is to extend the photostability of these devices, as UV light is often quite damaging to the liquid crystal components. While 5-year guarantees are now offered on some windows,^{63,64} these times must be extended to allow widespread adoption in the greenhouse industry.

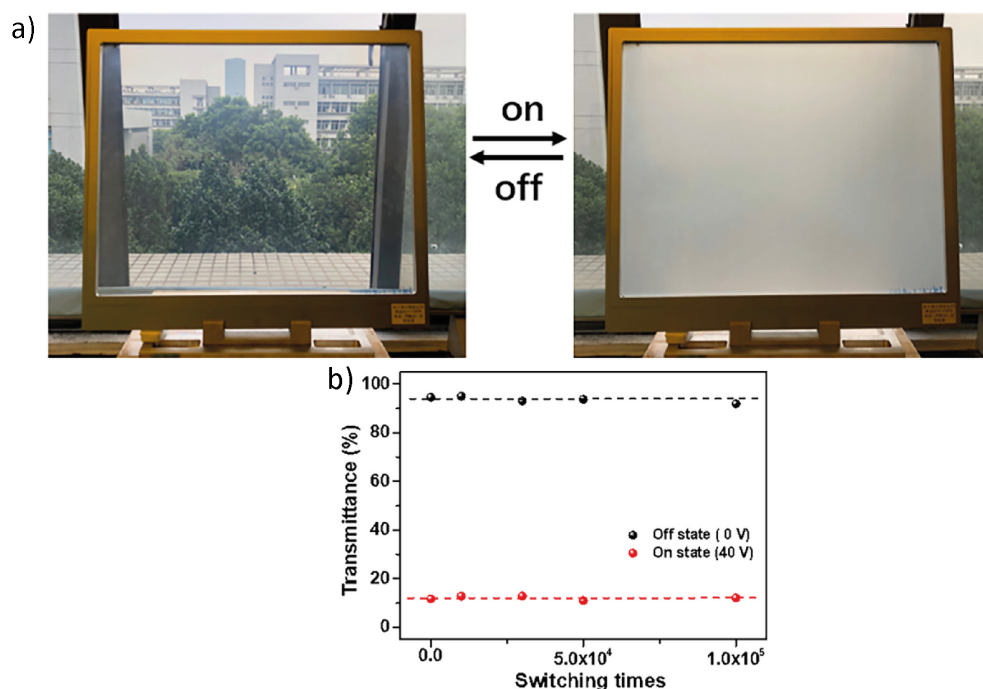


Figure 1.3: a) Prototype of a $40 \times 50 \text{ cm}^2$ PSLC window in the 'off' (0 V) and 'on' (40 V) states. b) Transmittance of sample windows as a function of applied voltage and switching time. Reproduced with permission.⁵⁵ Copyright 2020, Wiley Periodicals.

A technique that could help improve the UV-stability of switchable scatterers is the use of electrohydrodynamic instabilities. Electrohydrodynamic instabilities in LCs have been investigated since the 1960s,⁶⁵ and may be used to create 'smart' windows by doping a nematic liquid crystal with an ionic dye, which upon application of an electrical field generate vortices in the LC host that scatter the light: see **Figure 1.4**.^{56,57} A main advantage of such a system is that it does not contain any polymer, thus removing the polymerization

step and potentially increasing device lifetimes. Such devices have been shown to be capable of switching thousands of times from >95% transmission and almost no scattering to ~10% transparent with >90% scattering.⁵⁶

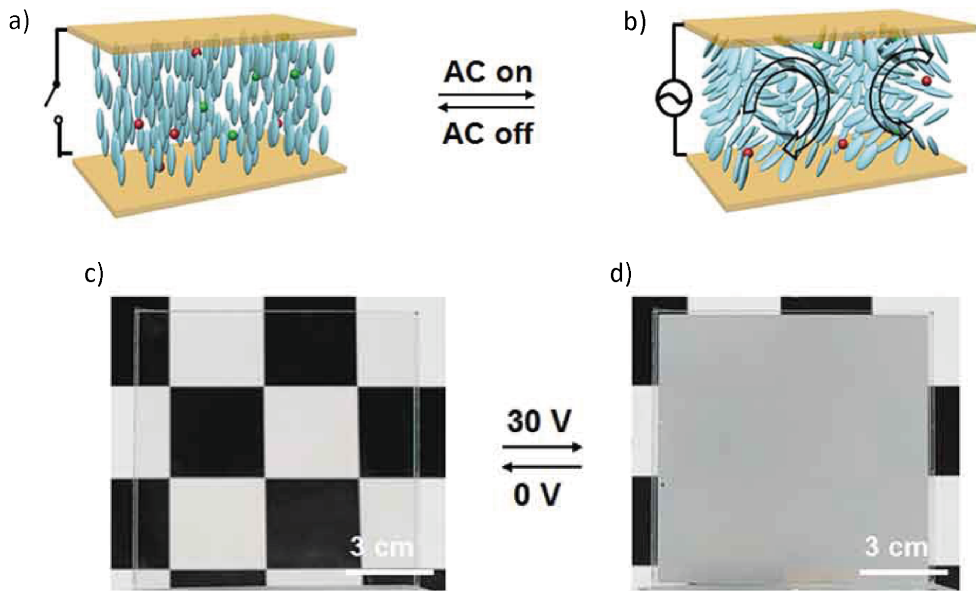


Figure 1.4: Schematic displaying electrohydrodynamic instability at: a) 0 V and b) > 0 V AC field. Photographs of the 9 x 9 cm² cell at: c) 0 V and d) 30 V. Reproduced with permission.⁵⁶ Copyright 2019, Taylor & Francis Group.

Creating roughened surfaces is a common way of inducing light scattering, but this is usually not reversible. However, a ‘smart’ window using randomly dispersed nanowires on the top of an elastomer demonstrated reversible surface deformations, forming a scattering state when a voltage was applied (see **Figure 1.5**).⁵⁸ This system could easily be scaled to large areas as it is suitable for roll-to-roll fabrication and uses commercially available materials. Challenges that remain are the high voltages required (>1500 V) and the low transmission in the transparent state (~60%).

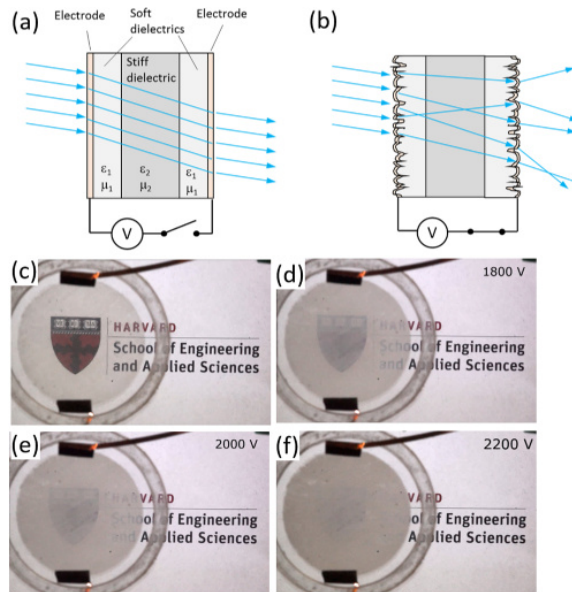


Figure 1.5: a) Schematic of the nanowire-topped device, which in the 'off' state has a smooth surface. b) Schematic of the device in the 'on' state where the randomly dispersed electrodes deform the surface causing the incoming light to scatter. c-f) The increase in scattering as the voltage is increased from 0 V to 2200 V. Reproduced with permission.⁵⁸ Copyright 2016, Optical Society of America.

Since most of these scattering systems were originally designed for privacy states for domestic use, the literature only reports decreases in directly transmitted light intensity, and not the hemispherical transmitted light or amount and distribution of forward scattered light. For greenhouse applications, a high 'hortiscatter' is desirable for optimal plant growth. In future, both light diffusion and total hemispherical light transmission should be reported to be able to evaluate the application of these systems for greenhouses.

1.2.2 Intensity (only) control

Systems that can switch from completely transparent to completely opaque states may control both light availability and regulate temperatures inside the greenhouse.⁶⁶ Generally, a higher transmission in the (hemispherical) PAR light is desired for crop photosynthesis, but there are exceptions: shade-loving plants, such as ornamental pot plants, must be protected against higher light intensities. Other crops, such as chrysanthemum, are sensitive to the day length. In these crops, blackout screens are used to shorten natural long days, and block all light to control flowering.^{67,68} For switchable blackout screens, transition metal oxides,⁶⁹ conjugated polymers,⁷⁰ Prussian blue,⁷¹ and dichroic dye⁷² based systems have received the most attention. Mechanical solutions are also encountered, such as switchable blinds with absorbers on one face and reflectors on the other.⁷³

Recently, the movement of magnetic nanoparticles to create a squid-inspired ‘smart’ window has been proposed.⁷⁴ In this device, an array of pyramidal voids is created in a transparent polymer. These voids are filled with a refractive index matching fluid containing magnetic nanoparticles. By applying a magnetic field, the nanoparticles move to the top of the pyramidal voids and become concentrated, significantly increasing the total transparency of the system (see **Figure 1.6**). An advantage of this device is its simplicity, which could translate into good durability. The main disadvantages are the requirements of a switchable magnetic field, and the concentrated dark regions present even in the transparent state. The research showed decrease of the dark area by replacing the pyramidal structures with hopper-like structures.

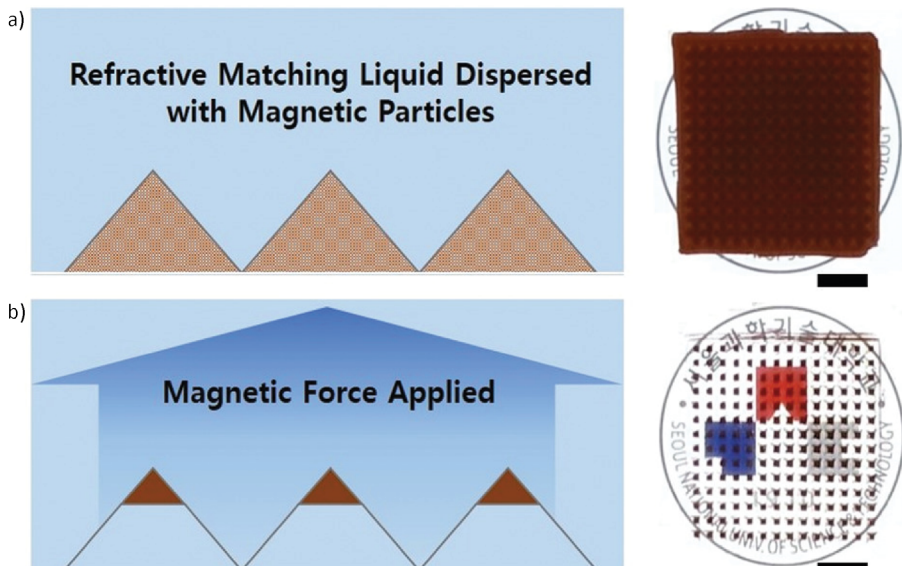


Figure 1.6: a) Magnetic particles dispersed inside pyramidal voids filled with a refractive index matching liquid causing a colored state. b) An applied magnetic field concentrates the particles at the top of the pyramidal voids creating a mostly transparent state. Reproduced with permission.⁷⁴ Copyright 2019, WILEY-VCH Verlag GmbH & Co. KGaA.

Another study used the phase change of VO_2 , which converts from an effective insulator into a metal upon heating. When coated on a glass fiber cloth, the VO_2 can be used as a negative feedback material:⁷⁵ at low temperatures, the coated glass releases heat, but when the temperature is high, the VO_2 absorbs heat, resulting in a decreased interior temperature. In experiments, with a temperature increase from 30 °C to 40 °C (a desired range for greenhouse applications), the reflection of VO_2 on glass fiber cloth decreased by 22% for the wavelength range of 400 nm to 800 nm, meaning more light was absorbed. However, reflection of PAR even in the most transmissive case is very high, and probably not applicable to an actual greenhouse.

Another option that does not require a continuous power supply is to make use of holographic optical elements suggested for use in buildings for light control.⁵⁹ Applied to a greenhouse, the transmission of light would change throughout the day as the windows would be angularly dependent, so one could conceivably tune the light distribution changes to occur for specific solar positions, presumably when the incident intensity would be highest. By accounting for the position of the sun throughout the year, the window could be designed to block more light in summer than in winter. These systems are relatively simple, so cost should be low but cannot be modified after installation to adapt to different lighting needs for different plants.

1.3 Near infrared control

Temperature plays an important role in most crop development processes. Optimal growth temperatures usually range between 15 °C and 30 °C.⁷⁶ Growth, yield and quality of most greenhouse crops will be affected whenever the temperature is below 12 °C or above 30 °C.⁷⁷ During summer months and in warmer climates, the application of (permanent) NIR selective filters is considered an advantage:^{78,79} the energy demand for cooling can be reduced while PAR light is unimpeded, as PAR is the driving force for crop photosynthesis, growth and development.^{19,80} There has been a great deal of research demonstrating blocking NIR in greenhouses is desired during warm periods but not during cold periods,^{81,82} with many different materials investigated, including plastic films or coated glass for greenhouse covers,^{83–85} movable screens,^{86–88} and NIR-filtering temporary coatings.^{89,90} However, the reduction of energy for cooling is often less than could be expected, as the crops themselves already have a high reflectivity for NIR radiation (about 50%), so that NIR radiation transmitted by partially reflective NIR greenhouse coverings or screens will end up being partially trapped within the greenhouse between two reflective surfaces (the roof covering and crop), suggesting 100% NIR reflectors are greatly preferred.⁸⁶

Adaptive coverings responding to seasonal energy demands could be important, especially in unheated greenhouses.⁹¹ Solar light incident on greenhouses changes hourly in incidence angle, intensity, and spectral quality. To better control the ingress of NIR radiation, it would be an advantage to have materials that can respond to these changing conditions, becoming more transparent when more light is needed, but less transparent when it is desirable to reject heat entering the growing space.³⁴

Mobile Fresnel lenses are employed in controlling both PAR and NIR,^{82,92} and switchable shutters⁹³ are used to control temperature in greenhouses. Such systems are especially effective in warm climates when combined with ventilation;⁹⁴ however, these technologies can be complex and are not yet introduced commercially on a larger scale.

Recently, research into using advanced optical materials for control of infrared light while retaining high transmission in the visible light has begun.⁹⁵ A promising class of materials for light control are nematic LCs doped with a chiral guest, forming a chiral-nematic mesophase, commonly referred to as a cholesteric liquid crystal (CLC). CLCs reflect specific wavelengths of light, while remaining almost completely transparent to other wavelengths. The wavelength reflected may be easily tuned by changing the amount of chiral dopant added to the host LC. CLCs selectively reflect only one circular polarization of incident light matching the 'handedness' of the helical structure of the CLC: that is, a right-handed CLC film can reflect a specific bandwidth of right-circularly polarized light. Thus, the CLC can reflect 50% of incident sunlight, given solar radiation is equally distributed between right- and left-circular polarizations.⁹⁶ It is possible to make 100% CLC reflectors by layering individual right- and left-handed CLCs, using two like-handed CLCs separated by a halfwave plate, or other techniques.^{97,98} However, intriguing research suggests plants are sensitive to the polarization of sunlight: for example, lentils and peas appeared to grow more swiftly under left-handed circularly polarized light,⁹⁹ perhaps a single layer of CLC could be effective at controlling incident sunlight without affecting the growth of the plants. Many CLC-based 'smart' window architectures feature an additional 'hazy' state where the LCs have lost their alignment and scatter most of the incoming light.¹⁰⁰⁻¹⁰³ Usually this is presented as an intermediate 'privacy' state between the reflective and transparent states, but it could potentially be of further benefit to greenhouses in addition to the IR reflecting state. While CLC systems have shown good switching properties and the wavelength that need to be reflected can be easily controlled, they have not yet been proven to be stable enough for long term continual outdoor exposure.

Normally, the bandwidth of a cholesteric reflector is too narrow to be of much use as a greenhouse heat control element (~100 nm in the NIR). Broadening the CLC reflection band (to >500 nm) may be attained using diffusion of mono- and di-acrylates to form a pitch gradient in the depth of a CLC,¹⁰³ or associating two layers of polymer-stabilized CLCs, labeled PSCLCs.¹⁰⁴ In the former case, by mixing photoreactive and non-reactive LC species, it was possible of making an electrically switchable broadband reflector that could have a significant impact on the infrared energy passing through the window (see **Figure 1.7a**).¹⁰³ In the latter case, two individual reflective layers are produced independently and brought into contact, allowing them to diffuse together to create the broadened reflector. This latter system also demonstrated an intermediate, scattering state, which could also be used in light management for greenhouses (**Figure 1.7b**).¹⁰⁴ The potential needed to switch these two reflecting windows was somewhat high, over 150 V each, and would need to be lowered for practical application.

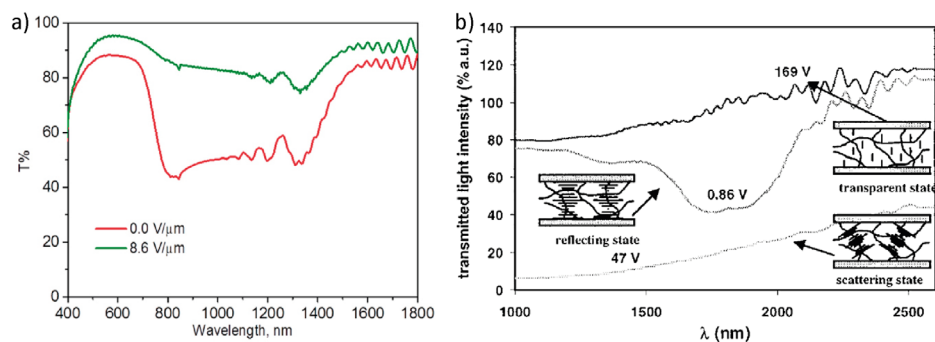


Figure 1.7: a) Transmission spectrum of reflective and transmissive states of a cholesteric gel at 0 V/μm and 8.6 V/μm, respectively. Reproduced with permission.¹⁰³ Copyright 2015, Nature Research. b) Intensity of transmitted light intensity vs wavelength for the sandwich cell at three different voltages with drawings of the postulated structures of the polymer stabilized CLC material. Reproduced with permission.¹⁰⁴ Copyright 2001, American Institute of Physics.

Electrically broadened reflection bands of over 1000 nm were demonstrated in CLC systems employing ethylene glycol twin diacrylate crosslinkers using a nematic LC host with negative dielectric anisotropy (see **Figure 1.8a**).¹⁰⁵ Even more extended reflection bands are possible by exploiting the phase transition between smectic and nematic phases, leading to reflection spectra thousands of nm wide, see **Figure 1.8b**, increasing the potential heat reduction:¹⁰⁶ however, unlike the previous reflectors, this reflector is not switchable making it only applicable in regions that always have an excess of heat.

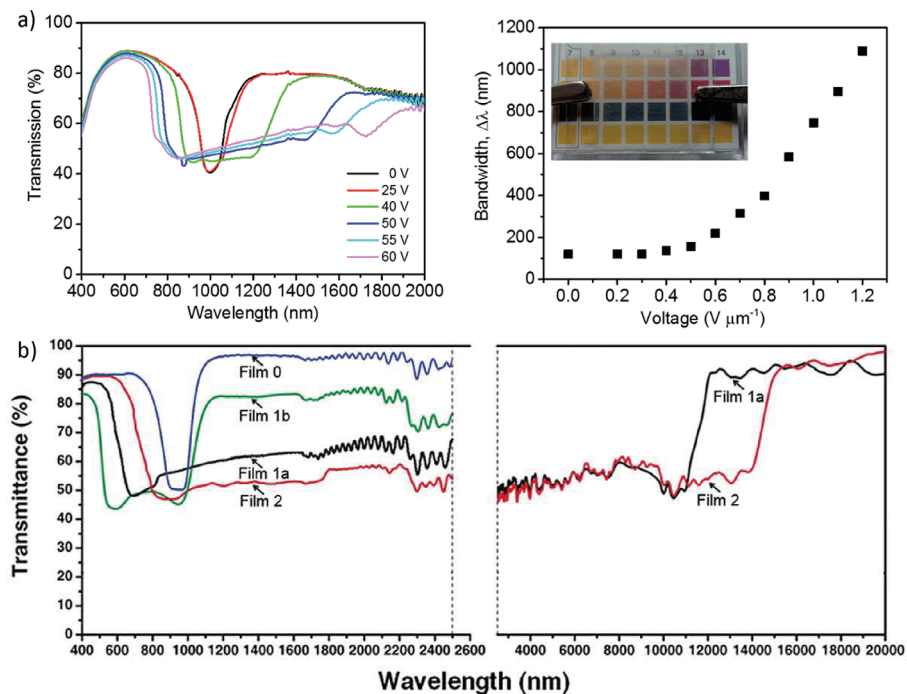


Figure 1.8: a) (left) Transmission spectra of Ch-LC mixture in applying 0–60 V; (right) reflection bandwidth as a function of the applied voltage per micron cell thickness with photograph of reflector demonstrating visible light transparency at 0 V. Reproduced with permission.¹⁰⁵ Copyright 2016, The Royal Society of Chemistry. b) Transmission spectra of films with various internal structures demonstrating the possibility of forming extremely broad reflectors. Reproduced with permission.¹⁰⁶ Copyright 2016, Taylor & Francis.

In addition to electrically responsive systems, thermally responsive cholesterics have been developed which automatically reflect more of the incident sunlight at higher temperatures. A major advantage is the devices would not need to be connected to the power grid. A downside is that the temperature response is set during production and cannot be changed later and thus needs to be set for the exact crop and climate. Some cholesterics are designed to reflect more light as the temperature increases,^{107–110} or have red^{111,112} or blue shifts^{113–116} of the reflection band.^{117,118} Shifting the reflection band can be used to control the temperature by designing the shift to coincide with maximal NIR reflection at the desired temperature. The disadvantage of using a red shifting cholesteric is the layer will reflect PAR light at lower temperatures, potentially hindering growing conditions. Blue shifting cholesterics can be tuned to initially reflect at >1400 nm where the sunlight intensity is low, and shift at higher temperatures to the NIR where the sun intensity is higher (see Figure 1.2a). Thermally responsive systems can also be made into surface coatings,^{114–116} something that is difficult to do with electrically responsive systems. Other cholesterics have been developed that trigger on both temperature and humidity, which could be particularly interesting in a greenhouse environment.¹¹⁹

The use of temperature-sensitive hydrogels combined with graphene oxide produces windows that switch automatically, from between full transparency to fully absorbing, in this case at around 28 °C (an appropriate switching temperature).¹²⁰ The disadvantage is that, while IR is effectively absorbed, so too is the useful PAR light, often not a desired situation.

1.4 Color changes

Within PAR, changes in the color of the light reaching the crops can cause photomorphogenetic responses: these effects are extensively studied.^{7,121} Plants behave based on photoreceptors which function as light sensors to analyze the light quality, quantity, duration and direction.^{24,122} Changes in light spectrum influence shoot elongation, formation of side shoots, leaf area and leaf thickness, germination processes, tropisms, flowering induction and development, color of flowers and leaves.⁷ Photosensitive films have shown to be able to effect a variety of crops such as delaying the flowering of strawberry plants,¹²³ and controlling the height (by influencing the red: far red ratio) of poinsettia,¹²⁴ antirrhinum,^{125,126} chrysanthemum,^{126,127} and cherry and peach trees.¹²⁸ Many static materials are used to control the color of the light reaching the crops, including colored screens and nets,^{8,129–132} reflectors,^{133,134} photosensitive films,^{23,121,124,135,136} fluorescent pigments,^{137–139} doped glass,^{140,141} and luminescent solar concentrators (LSC).^{24,142} These devices often reduce the total amount of PAR, although fluorescent dyes that absorb UV radiation and shifting this to PAR may theoretically increase the effective irradiance.^{23,24}

Dynamic control of sunlight color quality is uncommon, although screens and nets can be simply (re)moved, and temporary coatings can be seasonally applied. There don't yet exist systems that change instantaneously.

Fluid pumps that circulate liquids through the roofs of greenhouses for cooling purposes have been researched. Additives in the cooling fluid can promote scattering, or the absorption of specific wavelengths of light. By using far red (700-780 nm) absorbing filters (such as CuSO_4), the height of 'Spears' chrysanthemums could be influenced, with the advantage that the additives to the fluid can be further altered to achieve different purposes.¹⁴³ Replacing the absorber with fluorescent dyes could act to alter the spectral content experienced by the plants. A downside of these systems is that they require the installation of a plumbing network and pumps to control the flow, but the specific absorbance could be easily modified. A similar technique for controlling the color of incoming light is by mixing a liquid containing dye together with an unmixable liquid or a gas in a window architecture. An increase in temperature is followed by a corresponding

change in density and pressure, causing the liquid containing dye to cover a larger surface of the window, without the need for pumps, thus absorbing more of the incident light (see **Figure 1.9**).¹⁴⁴

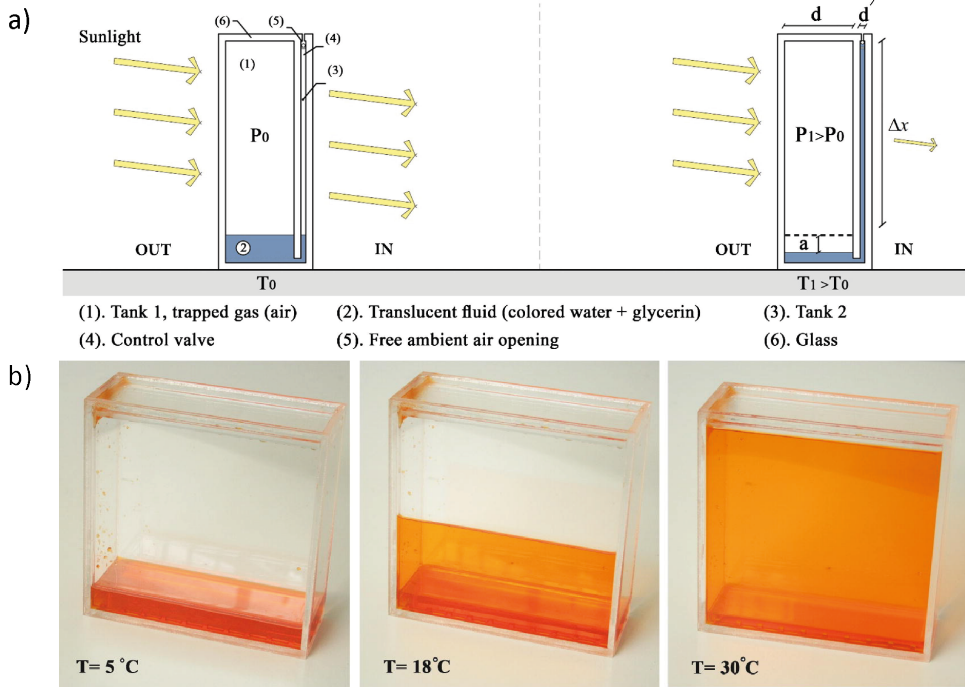


Figure 1.9: a) Schematic for liquid-based window in the (left) transparent and (right) light blocking states. b) Photographs of the prototype window taken at 5 °C, 18 °C and 30 °C. Reproduced with permission.¹⁴⁴ Copyright 2016, Elsevier Ltd.

1.5 Electricity Generation

Greenhouses can also be used to generate electricity by converting excess light to electricity^{10,29,82,145–148} or using the generated power for water /temperature control.¹⁴⁹ Care must be taken when using PV greenhouses that the crop production is not hindered.¹⁵⁰ For this reason PV systems that do not use photons in the PAR regime, or can be switched on and off, are of particular interest.

In some situations the top of a greenhouse can be partially covered with PV to generate electricity while ensuring enough light still reaches the crops.^{2,151–153} Fresnel lenses can be used to redirect part of the direct sunlight to PV modules, while allowing the diffuse

component of the light to pass.^{147,154} Semitransparent, wavelength-selective PV cells have been designed that allow some light to be transmitted to the crops below.^{155–157} As a decrease of PAR is detrimental to production, NIR absorbing devices that are mostly transparent for PAR are being researched.^{158,159} For application in greenhouses the PAR transmission of these systems needs to be significantly increased or they can only find application in regions with very high sunlight intensity.

Devices with switchable transmission could generate electricity in the future.^{160,161} A recent example combines the switchable scattering of a normal PDLC, which could help with light distribution, with a PV to make the device self-powering, thus lowering the installation and operating costs (see **Figure 1.10**).¹⁶¹

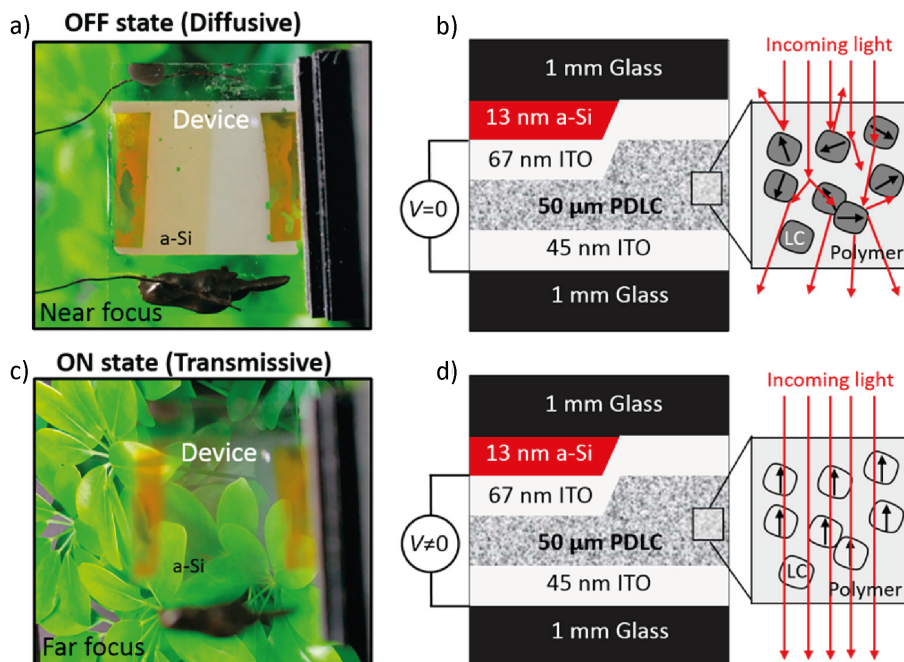


Figure 1.10: a) Photograph and b) schematic of the combination PDLC/PV device in the diffusive state with no applied bias. c) Photograph and d) schematic of the device in the transmissive state at 150 V. Reproduced with permission.¹⁶¹ Copyright 2016, American Chemical Society.

Another semitransparent concept for generation of electricity in greenhouses is the LSC, which consists of a transparent lightguide (usually plastic or glass) that either contains or is coated with a fluorescent dye. This dye can absorb incident radiation, re-emitting it as down-shifted light, guiding this emission by total internal reflection to the edges of the lightguide. By placing PV cells at these edges, this concentrated light can be converted to electricity.^{162,163} LSCs have been industrially deployed in the roofs of greenhouses and

shown to be able to generate electricity as well as enhance crop growth via color conversion.¹⁶⁴ As they lower the amount of PAR available for the crops, these systems best deployed in regions with high sun intensities.

1.6 Liquid crystals

Many of the devices described in Sections 1.2-1.5 have relied on the use of liquid crystals which have become ubiquitous in our modern lives as a major component of our smart phones and television screens. LC materials as described in these works are generally calamitic LCs, which consist of a rod-like core and flexible side chains and have some degree of molecular ordering while being in a (viscous) liquid state. They are an interesting material to use for responsive systems as they can easily be ordered and aligned and their order and alignment can be changed upon exposure to external stimuli. For thermotropic liquid crystals, the simplest stimulus is thermal. At low temperatures, the material is in the crystalline solid state with 3-dimensional ordering; heating can generate one or several different LC states¹⁶⁵ such as the smectic and the nematic states. In the smectic state, the molecules are aligned in layers with the long axis of the molecules all facing in a common direction. Positional order is lost when heated to the nematic state where only directional order remains. When heated beyond the nematic state, an isotropic liquid is obtained (see **Figure 1.11**).

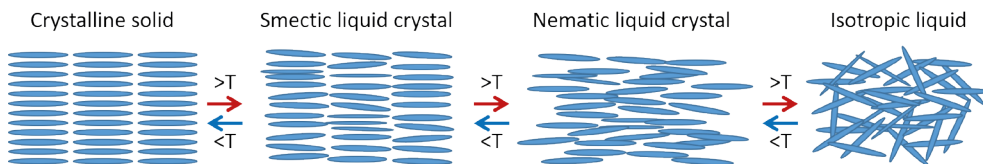


Figure 1.11: Different states of LC materials. From left to right with increasing temperature: the solid state, the smectic state, the nematic state and the liquid state.

The order of LC is often described using the order parameter S which quantifies the deviation of the molecular axis from the average molecular direction. If $S = 1$ the system is perfectly ordered and if $S = 0$ the system is completely isotropic. LC generally have an S -value that varies between 0.3 - 0.8.¹⁶⁵

The most common approach to aligning LCs is by using polyimide alignment layers, which can then form a rest state to which the LC can return upon removal of the stimulus. LC alignment is called planar when the individual molecules are aligned parallel to the surface and homeotropic when aligned perpendicular to the surface.

Another commonly-used alignment stimulus is an electrical field, making use of the dielectric anisotropy that most LCs have to align them to an applied electrical field. By using such a system in combination with a dichroic fluorescent dye, switchable LSC have been fabricated as shown in **Figure 1.12a**. In these systems the LC is used to change the alignment of the dye resulting in changes of PAR transmission which would greatly increase the ease of use in temperate climates.¹⁶⁶ Recently, switchable LSCs with a third, scattering state were fabricated using ‘supertwisted’ LCs which could provide even more functionality for greenhouse applications, as they combine color change, electricity generation and can provide diffuse light: see **Figure 1.12b**.

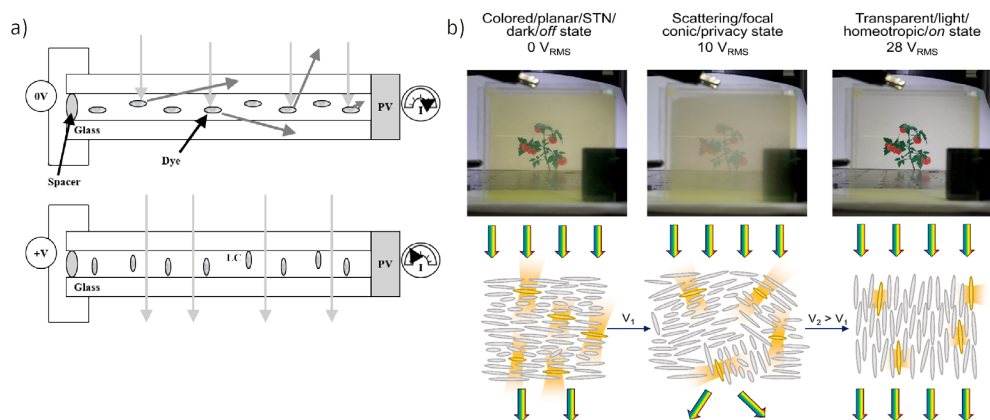


Figure 1.12. a) Working principle of the LSC switchable window. (Top) At rest, the dye molecules can absorb incoming light and re-emit this light at longer wavelengths, a fraction of which is trapped by total internal reflection and reaches the edge with PV attached; (bottom) after electrically switching, the guest dye molecules are reoriented to align parallel to direction of the incoming light; less light is absorbed and allowed to pass through the lightguide into the space beyond. Reproduced with permission.¹⁶⁶ Copyright 2010, WILEY-VCH Verlag. b) (Top) Photographs of the dye-doped supertwist LC cell at (left) 0 V_{RMS} , (middle) 10 V_{RMS} , and (right) 28 V_{RMS} . (Bottom) Schematic showing the alignment of the LCs, dyes, and the light emission direction. Reproduced with permission.¹⁶⁷ Copyright 2018, WILEY-VCH Verlag.

1.7 Aim and outline of this thesis

In this thesis, devices are described that can change their optical properties in response to external stimuli. By doing so they can control the amount, intensity and wavelength range of light passing through them. Furthermore, as the systems are fluorescent, they can function as LSCs where the absorbed light is re-emitted and concentrated at the edges of the device where it could be collected for other purposes such as electricity generation. These devices could be used for multiple applications including ‘smart’ windows for the greenhouse industry.

In Chapter 2 we fabricate a responsive LSC by combining a dichroic fluorescent dye with a LC matrix. In this configuration the LC is responsive to electrical and thermal stimuli, providing control over the orientation of the dichroic dye: when the LCs are rotated, they rotate the fluorescent dye with them. As the fluorescent dye is dichroic, the absorption changes when dye is rotated to different alignments. The resulting device can be used to control the amount of light entering buildings and the excess light could be used to generate electricity. The color change could be beneficial for plants as described in section 1.4.

In Chapter 3, the fluorescent dye itself is temperature responsive in addition to the alignment of the dye being controlled by the LC. At low temperatures, the dye aggregates to a non-fluorescent state and dissolves at high temperatures to a fluorescent state. Furthermore, the change in color is made more pronounced by addition of a non-temperature sensitive yellow fluorescent dye that at higher temperatures facilitates Förster Resonance Energy Transfer (FRET). The electrical response of the LCs is expanded by creating a supertwist structure to also include a scattering state. The scattering state could be beneficial for use in greenhouses (see section 1.2.1) but could also function as a privacy state in 'smart' windows.

Some crops need protection from harsh light conditions (see section 1.2.2). When lighting conditions change, an immediate response is required rather than a delayed response as is the case for temperature responsive systems. To create system that can directly respond to changes in light, a photo responsive fluorescent dye was developed in Chapter 4. The photo responsive dye becomes more colored when exposed to light of 340 nm and less colored at when exposed to 440 nm light. The dye could also be electrically switched for a manual override when in a LC host. To increase the ease of application, this dye was also incorporated in a polymer coating that could be printed in visually attractive patterns while retaining its light response.

More focused on dyes in polymer films and less application oriented, in Chapter 5 we use liquid crystals to fabricate a nanoporous matrix that facilitates FRET between two fluorescent dyes. To bring the two dyes in close contact, the first dye is aligned in the LC matrix, which is then made nanoporous by base treatment, to absorb a second dye, greatly enhancing the FRET efficiency. The system allows for efficient energy transfer and in the future this system can be used to improve output in LSCs, but is also of potential interest in other applications such as greenhouses.

Finally, in Chapter 6 we provide a brief outlook on some of the main issues that limit the introduction of these systems towards actual applications (*i.e.* stability and scalability). In addition, we introduce two promising new concepts: 'smart' blinds and switchable light guiding that could help to improve light control for the greenhouse industry.

1.8 References

- 1 N. Ramankutty and J. A. Foley, *Global Biogeochem. Cycles*, 1999, **13**, 997–1027.
- 2 C. S. Allardyce, C. Fankhauser, S. M. Zakeeruddin, M. Grätzel and P. J. Dyson, *Sol. Energy*, 2017, **155**, 517–522.
- 3 D. Waaijenberg, *Acta Hortic.*, 2006, **710**, 31–42.
- 4 S. Thomaier, K. Specht, D. Henckel, A. Dierich, R. Siebert, U. B. Freisinger and M. Sawicka, *Renew. Agric. Food Syst.*, 2015, **30**, 43–54.
- 5 *World vegetable map, RaboResearch Food & Agribusiness*, 2018.
- 6 <https://www.cbs.nl/en-gb/news/2018/16/upscaling-of-greenhouse-vegetable-production> (accessed March 2020).
- 7 S. Hemming, *Acta Hortic.*, 2011, **907**, 25–35.
- 8 C. Lamnatou and D. Chemisana, *Renew. Sustain. Energy Rev.*, 2013, **27**, 175–190.
- 9 © 2019 The World Bank, Source: Global Solar Atlas 2.0, Solar resource data: Solargis. (accessed March 2020).
- 10 R. H. E. Hassanien, M. Li and W. Dong Lin, *Renew. Sustain. Energy Rev.*, 2016, **54**, 989–1001.
- 11 K. J. McCree, *Agric. Meteorol.*, 1972, **10**, 443–453.
- 12 U. N. Mutwiwa, C. Borgemeister, B. Von elsner and H. Tantau, *J. Econ. Entomol.*, 2005, **98**, 1221–1228.
- 13 D. Doukas and C. C. Payne, *J. Econ. Entomol.*, 2007, **100**, 389–397.
- 14 F. Monci, S. García-Andrés, F. Sánchez, E. Moriones, E. Espí and A. Salmerón, *Acta Hortic.*, 2004, **633**, 537–542.
- 15 C. Rapisarda, G. Tropea, G. Cascone, R. Mazzarella, A. Colombo and T. Serges, *Acta Hortic.*, 2006, **719**, 597–604.
- 16 A. G. Dyer and L. Chittka, *J. Exp. Biol.*, 2004, **207**, 1683–1688.
- 17 M. H. Koski and T.-L. Ashman, *Funct. Ecol.*, 2014, **28**, 868–877.
- 18 S. Hemming, F. L. K. Kempkes and V. Mohammadkhani, *Acta Hortic.*, 2011, **893**, 217–226.
- 19 L. F. M. Marcelis, A. G. M. Broekhuijsen, E. Meinen, E. M. F. M. Nijs and M. G. M. Raaphorst, *Acta Hortic.*, 2006, **711**, 97–104.
- 20 G. Manor, A. Geva, D. Jacobs, I. Secker, S. Tabak and L. Singer, *Acta Hortic.*, 2005, 641–648.
- 21 D. Waaijenberg and P. J. Sonneveld, *Acta Hortic.*, 2004, **633**, 137–143.
- 22 F. Kempkes, G. J. Swinkels and S. Hemming, *Acta Hortic.*, 2018, 133–140.
- 23 S. Hemming, E. A. van Os, J. Hemming, J. A. Dieleman, E. A. Van Os, J. Hemming and J. A. Dieleman, *Eur. J. Hortic. Sci.*, 2006, **71**, 145–154.
- 24 M. E. Loik, S. A. Carter, G. Alers, C. E. Wade, D. Shugar, C. Corrado, D. Jokerst and C. Kitayama, *Earth's Futur.*, 2017, **5**, 1044–1053.
- 25 M. P. N. Gent, *HortScience*, 2004, **39**, 759A – 759.
- 26 W. Chirachint and D. W. Turner, *Sci. Hortic. (Amsterdam)*, 1988, **36**, 1–15.
- 27 S. Hemming, T. A. Dueck, J. Janse and F. van Noort, *Acta Hortic.*, 2008, **801**, 1293–1300.
- 28 S. Hemming, V. Mohammadkhani and T. Dueck, *Acta Hortic.*, 2008, **797**, 469–475.
- 29 E. Cuce, D. Harjunowibowo and P. M. Cuce, *Renew. Sustain. Energy Rev.*, 2016, **64**, 34–59.
- 30 P. J. M. Van Beveren, J. Bontsema, G. Van Straten and E. J. Van Henten, *Appl. Energy*, 2015, **137**, 97–109.
- 31 L. D. Albright, *Acta Hortic.*, 2002, **578**, 47–54.
- 32 L. D. Albright, A.-J. Both and A. J. Chiu, *Trans. ASAE*, 2000, **43**, 421–431.
- 33 E. J. Baeza, A. J. B. van Breugel, S. Hemming and C. Stanghellini, *Acta Hortic.*, 2020, **1268**, 213–224.
- 34 E. Baeza, S. Hemming and C. Stanghellini, *Biosyst. Eng.*, 2020, **193**, 157–173.
- 35 Y. J. Yun, J. K. Kim, J. Y. Ju, S. K. Choi, W. I. Park, J. Y. Suh, H. Jung, Y. Kim and S. Choi, *Phys. Chem. Chem. Phys.*, 2017, **19**, 11111–11119.
- 36 T. Li, E. Heuvelink, F. van Noort, J. Kromdijk and L. F. M. Marcelis, *Sci. Hortic. (Amsterdam)*, 2014, **179**, 306–313.
- 37 T. Li, E. Heuvelink, T. A. Dueck, J. Janse, G. Gort and L. F. M. Marcelis, *Ann. Bot.*, 2014, **114**, 145–156.
- 38 S. Hemming, V. Mohammadkhani and J. Van Ruijven, *Acta Hortic.*, 2014, **1037**, 883–896.
- 39 E. Baeza and J. C. López, *Acta Hortic.*, 2012, **956**, 425–440.
- 40 H. J. Tantau, J. Hinken, B. Von Elsner, T. Hofmann, J. F. J. Max, A. Ulbrich, U. Schurr and G. Reisinger, *Acta Hortic.*, 2012, **956**, 441–448.
- 41 J. F. J. Max, G. Reisinger, T. Hofmann, J. Hinken, H. J. Tantau, A. Ulbrich, S. Lambrecht, B. Von Elsner and U. Schurr, *Energy Build.*, 2012, **50**, 298–307.

- 42 H. A. Ahemd, A. A. Al-Faraj and A. M. Abdel-Ghany, *Sci. Hortic. (Amsterdam)*, 2016, **201**, 36–45.
- 43 E. M. Costa, T. Miranda, T. Xavier, J. Eduardo, M. Pezzopane, S. O. Guimarães, A. Pereira, S. Neto, M. Duarte and S. Fonseca, *J. Exp. Agric. Int.*, 2018, **22**, 1–7.
- 44 A. Ganguly and S. Ghosh, *Iran. J. Energy Environ.*, 2011, **2**, 32–46.
- 45 E. J. Fernandez-Rodriguez, J. Fernandez Vadillos, F. Camacho Ferre, J. J. Vazquez and A. Kenig, in *Acta Horticulturae*, 2000, vol. 534, pp. 125–130.
- 46 M. L. García, E. Medrano, M. C. Sánchez-Guerrero and P. Lorenzo, *Biosyst. Eng.*, 2011, **108**, 133–143.
- 47 T. Boulard and A. Baille, *Agric. For. Meteorol.*, 1993, **65**, 145–157.
- 48 A. J. Callejón-Ferre, F. Manzano-Agugliaro, M. Díaz-Pérez, A. Carreño-Ortega and J. Pérez-Alonso, *Spanish J. Agric. Res.*, 2009, **7**, 41.
- 49 P. Lorenzo, M. C. Sánchez-Guerrero, E. Medrano, M. L. García, I. Caparrós and M. Giménez, in *Acta Horticulturae*, International Society for Horticultural Science (ISHS), Leuven, Belgium, 2003, vol. 609, pp. 181–186.
- 50 P. Lorenzo, M. C. Sánchez-Guerrero, E. Medrano, M. L. García, I. Caparrós, G. Coelho and M. Giménez, in *Acta Horticulturae*, International Society for Horticultural Science (ISHS), Leuven, Belgium, 2004, vol. 659, pp. 189–194.
- 51 M. L. García-Balaguer, M. C. Sánchez-Guerrero, E. Medrano, E. J. Baeza, M. J. Sánchez-González, M. E. Porras, M. Giménez and P. Lorenzo, in *Acta Horticulturae*, International Society for Horticultural Science (ISHS), Leuven, Belgium, 2017, vol. 1170, pp. 959–965.
- 52 H. Hakemi, *Mol. Cryst. Liq. Cryst.*, 2019, **684**, 7–14.
- 53 B. Wu, J. L. West and J. W. Doane, *J. Appl. Phys.*, 1987, **62**, 3925–3931.
- 54 F. Ahmad, M. Jamil and Y. J. Jeon, *Electron. Mater. Lett.*, 2014, **10**, 679–692.
- 55 X. Hu, X. Zhang, W. Yang, X. Jiang, X. Jiang, L. T. Haan, D. Yuan, W. Zhao, N. Zheng, M. Jin, L. Shui, A. P. H. J. Schenning and G. Zhou, *J. Appl. Polym. Sci.*, 2020, **48917**, 48917.
- 56 Y. Zhan, H. Lu, M. Jin and G. Zhou, *Liq. Cryst.*, 2019, **00**, 1–7.
- 57 S. V. Serak, U. Hrozhyk, J. Hwang, N. V. Tabiryran, D. Steeves and B. R. Kimball, *Appl. Opt.*, 2016, **55**, 8506.
- 58 S. Shian and D. R. Clarke, *Opt. Lett.*, 2016, **41**, 1289.
- 59 C. G. Stojanoff, J. Schulat and M. Eich, in *Solar Optical Materials XVI*, 1999, vol. 3789, pp. 38–49.
- 60 Y. Zhou, X. Dong, Y. Mi, F. Fan, Q. Xu, H. Zhao, S. Wang and Y. Long, *J. Mater. Chem. A*, 2020, **8**, 10007–10025.
- 61 <https://www.eyrise.com> (accessed March 2020).
- 62 <https://www.privalite.com/> (accessed March 2020).
- 63 <https://www.eyrise.com/eyrise-frequently-asked-questions/> (accessed March 2020).
- 64 https://www.privalite.com/sites/privalite.com/files/download/priva_lite_classic_xl_eng.pdf (accessed March 2020).
- 65 R. Williams, *J. Chem. Phys.*, 1963, **39**, 384–388.
- 66 T. Jarosz, K. Gebka, A. Stolarczyk and W. Domagala, *Polymers (Basel)*, 2019, **11**, 273.
- 67 K.-J. I. Bergstrand, *Folia Hortic.*, 2017, **29**, 63–74.
- 68 H. K. Schüssler and K.-J. Bergstrand, *Acta Hortic.*, 2012, **956**, 409–415.
- 69 J. Pan, R. Zheng, Y. Wang, X. Ye, Z. Wan, C. Jia, X. Weng, J. Xie and L. Deng, *Sol. Energy Mater. Sol. Cells*, 2020, **207**, 110337.
- 70 M. İçli, M. Pamuk, F. Algi, A. M. Önal and A. Cihaner, *Org. Electron.*, 2010, **11**, 1255–1260.
- 71 R. Yan, L. Liu, H. Zhao, Y. G. Zhu, C. Jia, M. Han and Q. Wang, *J. Mater. Chem. C*, 2016, **4**, 8997–9002.
- 72 J. W. Huh, J. H. Seo, S. W. Oh, S. H. Kim and T. H. Yoon, *J. Mol. Liq.*, 2019, **281**, 81–85.
- 73 F. Horowitz, M. B. Pereira and G. B. de Azambuja, *Appl. Opt.*, 2011, **50**, C250-2.
- 74 J. Yang, H. Lee, S. G. Heo, S. Kang, H. Lee, C. H. Lee and H. Yoon, *Adv. Mater. Technol.*, 2019, **4**, 1900140.
- 75 N. Cai, W. Zhang, W. Wang, Y. Zhu, I. Zada, J. Gu, Q. Liu, H. Su, C. Guo, Z. Zhang, J. Zhang, L. Wu and D. Zhang, *Sci. Rep.*, 2016, **6**, 37264.
- 76 S. Hemming, J. C. Bakker, J. B. Campen and F. L. K. Kempkes, in *Achieving sustainable greenhouse cultivation*, eds. L. F. M. Marcelis and E. Heuvelink, Burleigh Dodds Science Publishing Limited, London, 2019, pp. 445–492.
- 77 N. Castilla and J. Hernandez, in *Acta Horticulturae*, 2007, vol. 761, pp. 285–297.
- 78 J. López-Marín, A. González, Y. García-Alonso, E. Espí, A. Salmerón, A. Fontecha and A. I. Real, in *Acta Horticulturae*, International Society for Horticultural Science (ISHS), Leuven, Belgium, 2008, vol. 801 PART 1, pp. 181–186.
- 79 Y. García-Alonso, E. Espí, A. Salmerón, A. Fontecha, A. González and J. López, *Acta Hortic.*, 2006, **719**,

- 131–137.
- 80 K. J. McCree, *Agric. Meteorol.*, 1971, **9**, 191–216.
- 81 S. Hemming, F. Kempkes, N. Van Der Braak, T. Dueck and N. Marissen, in *Acta Horticulturae*, 2006, vol. 711, pp. 411–416.
- 82 C. Lamnatou and D. Chemisana, *Renew. Sustain. Energy Rev.*, 2013, **18**, 271–287.
- 83 A. M. Abdel-Ghany, T. Kozai and C. Chun, *Japanese J. Trop. Agric.*, 2001, **45**, 242–250.
- 84 I. Impron, S. Hemming and G. P. A. Bot, *Biosyst. Eng.*, 2008, **99**, 553–564.
- 85 K. S. Kumar, K. N. Tiwari and M. K. Jha, *Energy Build.*, 2009, **41**, 1269–1275.
- 86 C. Stanghellini, J. Dai and F. Kempkes, *Biosyst. Eng.*, 2011, **110**, 261–271.
- 87 E. S. Runkle, R. D. Heins, P. Jaster and C. Thill, in *Acta Horticulturae*, International Society for Horticultural Science (ISHS), Leuven, Belgium, 2002, vol. 578, pp. 181–185.
- 88 E. S. Runkle, R. D. Heins, P. Jaster and C. Thill, in *Acta Horticulturae*, International Society for Horticultural Science (ISHS), Leuven, Belgium, 2002, vol. 580, pp. 137–143.
- 89 M. G. Blanchard and E. S. Runkle, *Trans. ASABE*, 2010, **53**, 939–944.
- 90 B. Von Elsner, in *Acta Horticulturae*, 2006, vol. 711, pp. 417–422.
- 91 F. Kempkes, C. Stanghellini, S. Hemming and J. Dai, *Acta Hortic.*, 2008, **797**, 477–482.
- 92 P. J. Sonneveld, G. L. A. M. Swinkels, B. A. J. Van Tuijl, H. Janssen and G. P. A. Bot, in *Acta Horticulturae*, International Society for Horticultural Science (ISHS), Leuven, Belgium, 2012, vol. 927, pp. 43–50.
- 93 J. Korecko, V. Jirka, B. Sourek and J. Cerveny, *Sol. Energy*, 2010, **84**, 1794–1808.
- 94 C. Kittas, T. Bartzanas and A. Jaffrin, *Biosyst. Eng.*, 2003, **85**, 87–94.
- 95 H. Khandelwal, A. P. H. J. Schenning and M. G. Debije, *Adv. Energy Mater.*, 2017, **7**, 1602209.
- 96 M. Mitov, *Adv. Mater.*, 2012, **24**, 6260–76.
- 97 M. Mitov and N. Dessaud, *Nat. Mater.*, 2006, **5**, 361–4.
- 98 J. Guo, H. Cao, J. Wei, D. Zhang, F. Liu, G. Pan, D. Zhao, W. He and H. Yang, *Appl. Phys. Lett.*, 2008, **93**, 201901.
- 99 P. P. Shibayev and R. G. Pergolizzi, *Int. J. Bot.*, 2011, **7**, 113–117.
- 100 K.-H. Kim, H.-J. Jin, K.-H. Park, J.-H. Lee, J. C. Kim and T.-H. Yoon, *Opt. Express*, 2010, **18**, 16745.
- 101 I.-H. Lee, Y.-C. Chao, C.-C. Hsu, L.-C. Chang, T.-L. Chiu, J.-Y. Lee, F.-J. Kao, C.-K. Lee and J.-H. Lee, in *Emerging Liquid Crystal Technologies V*, ed. L.-C. Chien, 2010, vol. 7618, p. 761816.
- 102 R. Bao, C.-M. Liu and D.-K. Yang, *Appl. Phys. Express*, 2009, **2**, 112401.
- 103 H. Khandelwal, R. C. G. M. Loonen, J. L. M. Hensen, M. G. Debije and A. P. H. J. Schenning, *Sci. Rep.*, 2015, **5**, 11773.
- 104 C. Binet, M. Mitov and M. Mauzac, *J. Appl. Phys.*, 2001, **90**, 1730–1734.
- 105 H. Khandelwal, M. G. Debije, T. J. White and A. P. H. J. Schenning, *J. Mater. Chem. A*, 2016, **4**, 6064–6069.
- 106 L. Zhang, M. Wang, L. Wang, D. K. Yang, H. Yu and H. Yang, *Liq. Cryst.*, 2016, **43**, 750–757.
- 107 H. Yang, K. Mishima, K. Matsuyama, K.-I. Hayashi, H. Kikuchi and T. Kajiyama, *Appl. Phys. Lett.*, 2003, **82**, 2407–2409.
- 108 X. Yuan, L. Zhang and H. Yang, *Liq. Cryst.*, 2010, **37**, 445–451.
- 109 M. E. McConney, V. P. Tondiglia, J. M. Hurtubise, L. V. Natarajan, T. J. White and T. J. Bunning, *Adv. Mater.*, 2011, **23**, 1453–1457.
- 110 A. J. J. Kragt, I. P. M. Gessel, A. P. H. J. Schenning and D. J. Broer, *Adv. Opt. Mater.*, 2019, 1901103.
- 111 M. T. Brannum, A. M. Steele, M. C. Venetos, L. T. J. Korley, G. E. Wnek and T. J. White, *Adv. Opt. Mater.*, 2019, **7**, 1801683.
- 112 Y. Wang, Z. Zheng, H. K. Bisoyi, K. G. Gutierrez-Cuevas, L. Wang, R. S. Zola and Q. Li, *Mater. Horizons*, 2016, **3**, 442–446.
- 113 L. V. Natarajan, J. M. Wofford, V. P. Tondiglia, R. L. Sutherland, H. Koerner, R. A. Vaia and T. J. Bunning, *J. Appl. Phys.*, DOI:10.1063/1.2913326.
- 114 E. P. A. van Heeswijk, T. Meerman, J. de Heer, N. Grossiord and A. P. H. J. Schenning, *ACS Appl. Polym. Mater.*, 2019, **1**, 3407–3412.
- 115 W. Zhang, S. Kragt, A. P. H. J. Schenning, L. T. de Haan and G. Zhou, *ACS Omega*, 2017, **2**, 3475–3482.
- 116 P. Zhang, A. J. J. Kragt, A. P. H. J. Schenning, L. T. de Haan and G. Zhou, *J. Mater. Chem. C*, 2018, **6**, 7184–7187.
- 117 M. E. McConney, T. J. White, V. P. Tondiglia, L. V. Natarajan, D. Yang and T. J. Bunning, *Soft Matter*, 2012, **8**, 318–323.
- 118 S. a. Cazzell, M. E. McConney, V. P. Tondiglia, L. V. Natarajan, T. J. Bunning and T. J. White, *J. Mater. Chem. C*, 2014, **2**, 132–138.
- 119 E. P. A. van Heeswijk, J. J. H. Kloos, N. Grossiord and A. P. H. J. Schenning, *J. Mater. Chem. A*, 2019, **7**,

- 6113–6119.
- 120 H.-T. Chou, Y. Chen, C. Lee, H.-Y. Chang and N. Tai, *Sol. Energy Mater. Sol. Cells*, 2017, **166**, 45–51.
- 121 F. R. De Salvador, G. Scarascia Mugnozza, G. Vox, E. Schettini, M. Mastrorilli and M. Bou Jaoudé, *Acta Hortic.*, 2008, **801**, 115–121.
- 122 H. Smith, *Annu. Rev. Plant Physiol.*, 1982, **33**, 481–518.
- 123 F. Takeda, D. M. Glenn, A. Callahan, J. Slovin and G. W. Stutte, *Int. J. Fruit Sci.*, 2010, **10**, 134–142.
- 124 S. C. Clifford, E. S. Runkle, F. A. Langton, A. Mead, S. A. Foster, S. Pearson and R. D. Heins, *HortScience*, 2004, **39**, 383–387.
- 125 A. M. Khattak and S. Pearson, *J. Zhejiang Univ. Sci.*, 2005, **6 B**, 119–124.
- 126 C. J. van Haeringen, J. S. West, F. J. Davis, A. Gilbert, P. Hadley, S. Pearson, A. E. Wheldon and R. G. C. Henbest, *Photochem. Photobiol.*, 1998, **67**, 407.
- 127 E. Oyaert, E. Volckaert and P. Debergh, *Sci. Hortic. (Amsterdam)*, 1999, **79**, 195–205.
- 128 E. Schettini and G. Vox, *J. Agric. Eng.*, 2010, **41**, 19.
- 129 Y. Shahak, in *Acta Horticulturae*, International Society for Horticultural Science (ISHS), Leuven, Belgium, 2008, vol. 770, pp. 161–168.
- 130 Y. Shahak, K. Ratner, N. Zur, Y. Offir, E. Matan, H. Yehezkel, Y. Messika, I. Posalski and D. Ben-Yakir, in *Acta Horticulturae*, International Society for Horticultural Science (ISHS), Leuven, Belgium, 2009, vol. 807, pp. 79–84.
- 131 R. H. Stamps, *HortScience*, 2009, **44**, 239–241.
- 132 C. Edser, *Plast. Addit. Compd.*, 2002, **4**, 20–24.
- 133 B. E. Shlesinger, R. E. Shesin and M. K. Shlesinger, US3372513A, 1968, 3.
- 134 M. J. Kasperbauer and P. G. Hunt, *Photochem. Photobiol.*, 1992, **56**, 579–584.
- 135 J. M. Fletcher, A. Tatsiopoulou, P. Hadley, F. J. Davis and R. G. C. Henbest, in *Acta Horticulturae*, International Society for Horticultural Science (ISHS), Leuven, Belgium, 2004, vol. 633, pp. 99–106.
- 136 N. C. Rajapakse and S. Li, in *Acta Horticulturae*, International Society for Horticultural Science (ISHS), Leuven, Belgium, 2004, vol. 631, pp. 193–199.
- 137 S. Pearson, A. E. Wheldon and P. Hadley, *J. Agric. Eng. Res.*, 1995, **62**, 61–69.
- 138 C. Kittas and A. Baille, *J. Agric. Eng. Res.*, 1998, **71**, 193–202.
- 139 K. Murakami, H. Cui, M. Kiyota, I. Aiga and T. Yamane, in *Acta Horticulturae*, International Society for Horticultural Science (ISHS), Leuven, Belgium, 1997, vol. 435, pp. 123–130.
- 140 Y. Han, F. Song, Q. Li, F. Wang, C. Ming and J. Tian, *Opt. Mater. (Amst.)*, 2014, **37**, 756–759.
- 141 G. Gao and L. Wondraczek, *J. Mater. Chem. C*, 2014, **2**, 691–695.
- 142 N. S. Makarov, K. Ramasamy, A. Jackson, A. Velarde, C. Castaneda, N. Archuleta, D. Hebert, M. R. Bergren and H. McDaniel, *ACS Nano*, 2019, **13**, 9112–9121.
- 143 M. McMahon and J. Kelly, *Sci. Hortic. (Amsterdam)*, 1999, **79**, 207–215.
- 144 A. Fazel, A. Izadi and M. Azizi, *Sol. Energy*, 2016, **133**, 274–282.
- 145 V. Jirka, V. Kučeravý, M. Malý, F. Pech and J. Pokorný, *Renew. Energy*, 1999, **16**, 660–664.
- 146 K. Kurata, *Sol. Energy*, 1991, **46**, 53–57.
- 147 P. J. Sonneveld, G. L. A. M. Swinkels, B. A. J. van Tuijl, H. Janssen and H. F. de Zwart, *Acta Hortic.*, 2012, **952**, 531–537.
- 148 C. Zisis, E. M. Pechlivani, S. Tsimikli, E. Mekeridis, A. Laskarakis and S. Logothetidis, *Mater. Today Proc.*, 2019, **19**, 65–72.
- 149 P. Hung and K. Peng, *Int. Rev. Spat. Plan. Sustain. Dev.*, 2017, **5**, 55–70.
- 150 C. Poncet, M. M. Muller, R. Brun and H. Fatnassi, *Acta Hortic.*, 2012, **927**, 75–79.
- 151 J. Pérez-Alonso, M. Pérez-García, M. Pasamontes-Romera and A. J. Callejón-Ferre, *Renew. Sustain. Energy Rev.*, 2012, **16**, 4675–4685.
- 152 R. H. E. Hassani, M. Li and F. Yin, *Renew. Energy*, 2018, **121**, 377–388.
- 153 Z. Li, A. Yano, M. Cossu, H. Yoshioka, I. Kita and Y. Ibaraki, *Energies*, 2018, **11**, 1681.
- 154 P. Sonneveld, H. Zahn, G.-J. Swinkels, A. W. Bett, R. D. McConnell, G. Sala and F. Dimroth, in *AIP Conference Proceedings*, 2010, vol. 1277, pp. 264–267.
- 155 J. J. Kim, M. Kang, O. K. Kwak, Y. J. Yoon, K. S. Min and M. J. Chu, *Int. J. Photoenergy*, 2014, **2014**, 1–7.
- 156 C. J. M. Emmott, J. A. Röhr, M. Campoy-Quiles, T. Kirchartz, A. Urbina, N. J. Ekins-Daukes and J. Nelson, *Energy Environ. Sci.*, 2015, **8**, 1317–1328.
- 157 A. Marucci, D. Monarca, M. Cecchini, A. Colantoni, A. Manzo and A. Cappuccini, *Math. Probl. Eng.*, 2012, **2012**, 1–14.
- 158 R. R. Lunt and V. Bulovic, *Appl. Phys. Lett.*, 2011, **98**, 113305.
- 159 S. H. Moon, S. J. Park, Y. J. Hwang, D.-K. Lee, Y. Cho, D.-W. Kim and B. K. Min, *Sci. Rep.*, 2015, **4**, 4408.
- 160 E. Amasawa, N. Sasagawa, M. Kimura and M. Taya, *Adv. Energy Mater.*, 2014, **4**, 1400379.

- 161 J. Murray, D. Ma and J. N. Munday, *ACS Photonics*, 2017, **4**, 1–7.
- 162 W. H. Weber and J. Lambe, *Appl. Opt.*, 1976, **15**, 2299.
- 163 M. G. Debije and P. P. C. Verbunt, *Adv. Energy Mater.*, 2012, **2**, 12–35.
- 164 C. Corrado, S. W. Leow, M. Osborn, I. Carbone, K. Hellier, M. Short, G. Alers and S. A. Carter, *J. Renew. Sustain. Energy*, 2016, **8**, 043502.
- 165 G. Vertogen and W. H. de Jeu, *Thermotropic Liquid Crystals, Fundamentals*, Springer Berlin Heidelberg, Berlin, Heidelberg, 1988, vol. 45.
- 166 M. G. Debije, *Adv. Funct. Mater.*, 2010, **20**, 1498–1502.
- 167 J. A. H. P. Sol, G. H. Timmermans, A. J. van Breugel, A. P. H. J. Schenning and M. G. Debije, *Adv. Energy Mater.*, 2018, **8**, 1702922.

Chapter 2

Dual thermal-/electrical- responsive luminescent ‘smart’ window

Here, we describe a ‘smart’ window that could reduce both interior temperatures and the use of electricity normally consumed for air conditioning and lighting, by absorbing excess solar radiation with dichroic fluorescent dye molecules aligned in a switchable liquid crystal host and guiding the re-emitted light energy to the edges of the device, where it can be used to generate electricity via attached photovoltaic cells. The liquid crystals are responsive both to temperature changes and applied electrical fields. At higher temperatures, transmission decreases due to increased disorder in the liquid crystals, while the application of an electrical field increases transmission by effectively realigning the dyes for minimal absorption. Using alternative configurations, a window with a transparent rest state was also produced, in which transmission can be decreased by applying an electrical field; the thermal response remains unchanged with applied field.

This chapter is partially reproduced from: G. H. Timmermans, R. F. Douma, J. Lin, and M. G. Debije, "Dual Thermal-/Electrical-Responsive Luminescent ‘Smart’ Window," *Appl. Sci.* 10, 1421 (2020)

2.1 Introduction

This Chapter will show a responsive system based on the alignments of liquid crystals (LCs) and the dichroic dye dissolved therein. Such systems were already discussed in the introduction chapter of this thesis. For ‘smart’ windows, the nature of the external stimuli is of importance: temperature responsive systems can automatically change their properties without user input but often manual overrides (*e.g.* via an electrical trigger) are preferred. Recent work by Oh *et al.*¹ has shown that the transmission of a ‘smart’ window can be thermally controlled using a dichroic dye in an LC. Three different LC phases (*i.e.*, smectic, nematic and isotropic) were used to create high-, mid- and low- light-transmitting states. Inspired by this system and previous works on switchable LSCs^{2,3}, in this Chapter we show a dual electrically and thermally responsive LSC based on a fluorescent dye doped LC mixture. This system decreases its transmission with increasing temperature with a manual override that can be used to either increase or decrease the transmission by application of an electric potential, depending on the design. The edge-emitted light can then be used for the generation of electricity by attaching photovoltaic cells or redirected for crop growth or daylighting.

2.2 Experimental

Liquid crystal 8CB (4'-octyl-4-biphenylcarbonitrile) was purchased from Synthon, Dye 1 (a coumarin derivative) was purchased from RiskReactor, Dye 2 was synthesized according to the literature⁴; these three materials are depicted in **Figure 2.1a**.

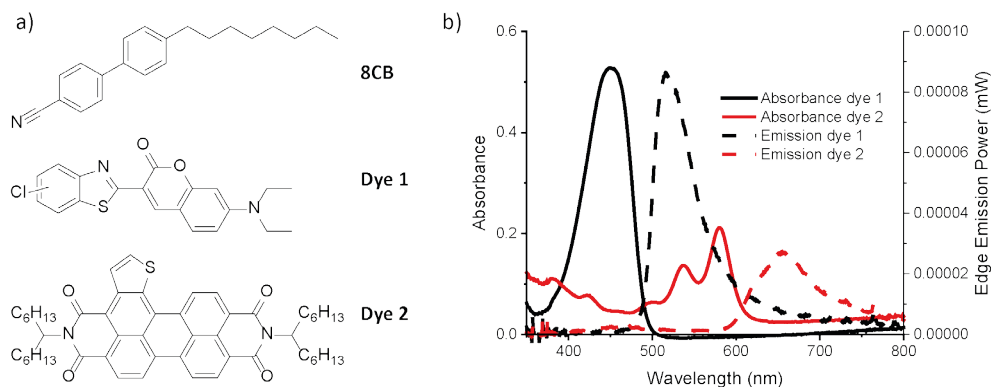


Figure 2.1: a) The chemical structures of 8CB, Dye 1 and Dye 2. b) Absorption (solid lines) and emission power (from one edge parallel to the alignment direction, dotted lines) spectra of 1 wt% of Dye 1 (black) and Dye 2 (red) in 8CB in planar aligned 6 μm gap cell.

Indium tin oxide (ITO)-coated glass plates of $3 \times 3 \text{ cm}^2$ (for transmission measurements) and $5 \times 5 \text{ cm}^2$ (for emission power measurements, LC-Tec) and glass plates of $1 \times 1 \text{ cm}^2$ with ITO interdigitated electrodes (IDE), linewidth $10 \text{ }\mu\text{m}$; line spacing $10 \text{ }\mu\text{m}$, (for transmission measurements) were cleaned and spincoated (Karl Suss RC-8 spin coater, 5000 rpm, 50 seconds) with a layer of polyimide (Optimal AL 1051, JSR corporation, for planar alignment on the ITO-coated glass plates and Nissan Polyimide Varnish, Sunever for homeotropic alignment on the IDE samples Tokyo, Japan) and cured at $180 \text{ }^\circ\text{C}$ for 90 minutes; the Optimal AL 1051-coated samples were rubbed on a velvet cloth to induce planar alignment. Cells were fabricated by gluing two coated glass plates together using $6 \text{ }\mu\text{m}$ glass spacers. The cells were filled at $\sim 80 \text{ }^\circ\text{C}$ with 1 wt% of either Dye 1 or Dye 2 in liquid crystal 8CB. The absorption and emission power spectra for the planar devices are shown in **Figure 2.1b**.

The transmission spectra of the cells were measured using a UV-vis spectrophotometer (Perkin Elmer Lambda 750); temperatures were controlled using a customized heating stage (Linkam THMS600) and electrical potentials (AC, 1000 Hz) were applied using a laboratory function generator (Agilent 33220A) coupled to a $20 \times$ voltage amplifier (FLC Electronics F20A). Edge emission powers were measured using a Labsphere SLMS 1050 integrating sphere connected to an International Light RPS900 diode array detector. Simulated solar illumination was provided by a 300 W Lot-Oriel solar simulator equipped with filters to emulate the AM 1.5 solar spectrum. Differential scanning calorimetry (DSC) was performed under a nitrogen atmosphere using a TA Instruments Q1000 DSC equipped with an RCS90 cooling accessory, New Castle, Delaware, USA. Polarized optical microscopy (POM) images were made using a Leica CTR 6000 microscope equipped with a Leica DFC420 C camera.

3.3 Results and discussion

The coumarin (Dye 1) and perylenebisimide (Dye 2) derivatives were individually dissolved at 1 wt% in 8CB. Three distinct liquid crystal phases of the dye/8CB mixtures are identified by DSC (SmA, $30\text{--}35 \text{ }^\circ\text{C}$, N, $40\text{--}45 \text{ }^\circ\text{C}$, I), similar to those found in the literature.⁵

In the planar cells, the fluorescent dyes can absorb a significant fraction of the incoming light as they are aligned with absorption axis perpendicular to the incoming light. The application of a voltage reorients the liquid crystals, which in turn reorient the dyes to a homeotropic state, to a position with the absorption axis parallel to the incoming light. Due to the dichroism of the dyes, light absorption decreases in the homeotropic orientation, resulting in a more transparent state. Increasing the temperature decreases the LC order, as seen in Table 1; the order parameters (S) of the dyes were calculated according to equation 2.1:⁶

$$S = \frac{A_{par} - A_{per}}{A_{par} + 2A_{per}} \quad (\text{eq 2.1})$$

where A_{par} and A_{per} are the peak absorbance when the film is exposed to incident light polarized parallel and perpendicular to the LC alignment direction, respectively. As the dyes become more disordered, absorption increases, as shown in **Figure 2.2**. The order parameters (see **Table 2.1**) clearly show that, as the temperature increases, the alignment of the dyes decreases as the system becomes more isotropic, finally resulting in an order parameter of 0 when the LC is fully isotropic.

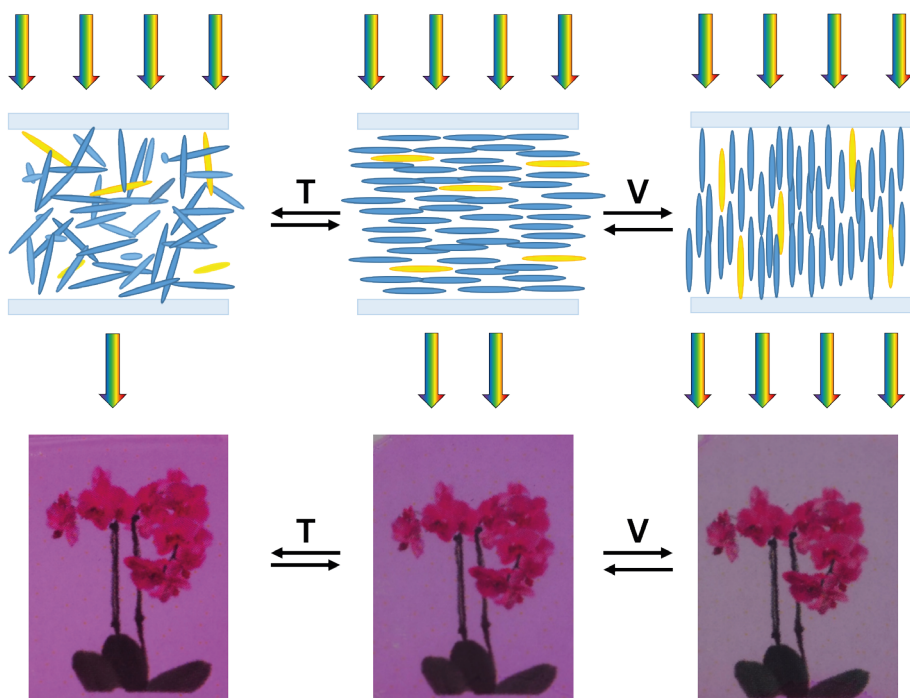


Figure 2.2: Schematic (top row) and photographs on top of an image of a flower (bottom row) of liquid crystal (blue rods) and dye (yellow rods) alignments in the initial planar state (middle column) and its changes upon the application of an electrical field (right column) or increased temperature (left column). The relative absorption characteristics are indicated by the number of rainbow-colored arrows.

Table 2.1: Order parameter of 1 wt% Dye 1 and Dye 2 in 8CB in planar cells at different temperatures.

Temperature in °C	24	27	30	33	37	41
S, Dye 1	0.25	0.24	0.27	0.24	0.11	0.00
S, Dye 2	0.27	0.24	0.20	0.12	0.00	0.00

In **Figure 2.3**, transmission at the peak absorption wavelengths of the dyes at an increased temperature and voltage for planar cells are depicted: **Figure 2.3a** shows Dye 1, and **Figure 2.3b** Dye 2. Initially, in the smectic A phase at 24 °C, a higher voltage (123 V_{pp} (peak-to-peak voltage)) is required to overcome the LC alignment and switch the dye to a homeotropic orientation, resulting in an increased light transmission. On the other hand, increasing the temperature to the nematic state increases the mobility and disorder in the system, resulting in a lower transmission and lower switching voltage to the homeotropic state (82 V_{pp} at 26 °C and even 41 V_{pp} at 30 °C). Increasing the temperature further to the isotropic state results in a minimum transmission but prevents electrical switching, as the LC phase is randomized and loses its switching properties⁷.

Emission power spectra from 5 × 5 cm² cells from the edge parallel to the LC alignment direction were measured under a solar simulator by an integrating sphere as a function of temperature and applied voltage: the results are depicted in **Figure 2.3c,d**. The emission powers for Dye 1 (Figure 2.3c) are higher compared to Dye 2 (Figure 2.3d). As the temperature increases, the emission power parallel to the absorption increases as the transmission decreases. However, increasing the temperature too much (>35 °C) reduces edge emission powers as dye orientation becomes less favorable. Applying an electric potential across the cell reorients the LC/dye, at a cost of reduced emission power as a result of less light absorption (even though the emission direction of the dye is more favorable).

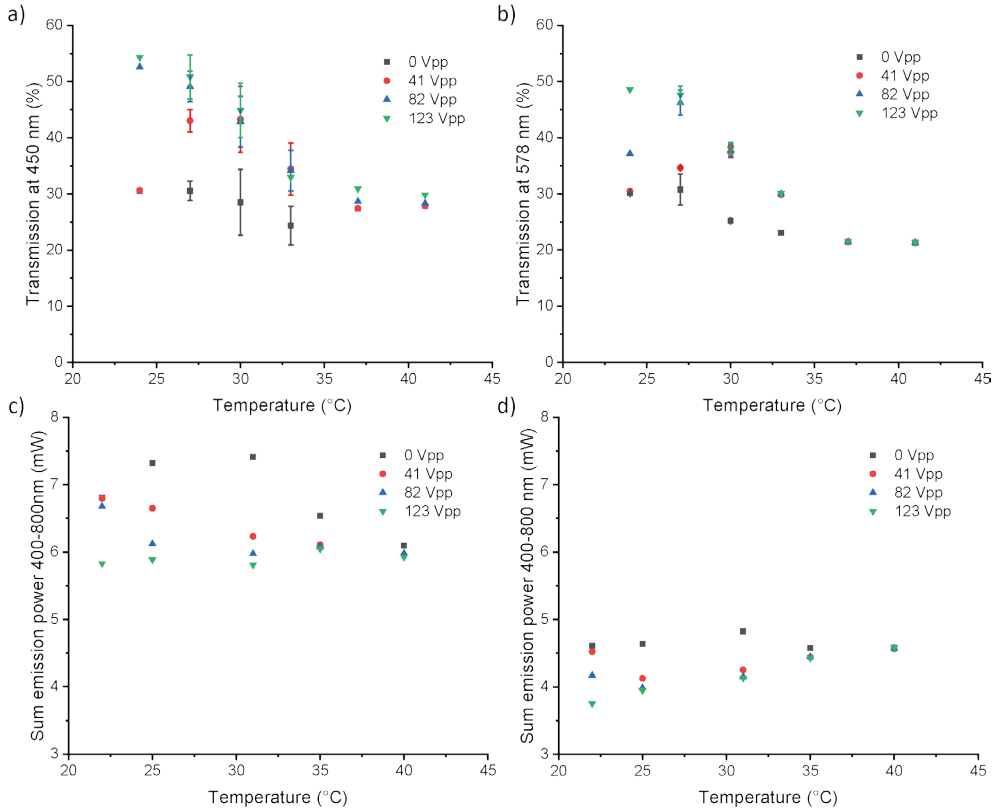


Figure 2.3: Transmission at the peak absorption of the dye at increased temperature and voltage for planar cells containing a) Dye 1; b) Dye 2. Summation of emission power spectra (from the edge with dyes aligned parallel to the LC alignment) between 400–800 nm at increased temperature and voltage for planar $5 \times 5 \text{ cm}^2$ containing c) Dye 1; d) Dye 2.

The external power efficiency (η_{ext} , energy emitted at the edges of the device as a function of the energy incident on the device) and the internal optical efficiency (η_{int} , photons emitted at the edges of the device per photons absorbed by the device)⁸ of the systems at the various temperatures and applied potentials were calculated using equation 2.2 and equation 2.3:

$$\eta_{ext} = \frac{\text{energy emitted}}{\text{incident energy}} = \frac{\int_{\text{emission}} P_{out}(\lambda_{em}) d\lambda_{em}}{\int_{\text{sol}} P_{in} d\lambda_{sol}} * 100\% \quad (\text{eq. 2.2})$$

and

$$\begin{aligned} \eta_{int} &= \frac{\text{photons emitted}}{\text{photons absorbed}} \\ &= \frac{\int_{\text{emission}} P_{out}(\lambda_{em}) \frac{\lambda_{em}}{hc} d\lambda_{em}}{\int_{\text{absorption}} P_{in}(\lambda_{abs}) \frac{\lambda_{abs}}{hc} A(\lambda) d\lambda_{abs}} * 100\% \end{aligned} \quad (\text{eq. 2.3})$$

where $P_{out}(\lambda_{em})$ is the integrated emission power from all four edges over the wavelength range (in Watts). Both one parallel and one perpendicular edge were measured and multiplied by 2 to approximate the total output. P_{in} is the incident light power from the solar simulator (in Watts), $A(\lambda)$ is the absorption of the sample (in %), λ is the wavelength range over which the summation is made, h is Planck's constant, and c the speed of light. The absorption of Dye 1 was integrated over the wavelength range 350–500 nm and the emission power over 450–700 nm, while for Dye 2 these values were 450–650 nm and 550–800 nm, respectively. The incoming solar simulator light was integrated over the wavelength range of 350–800 nm.

The external power efficiency decreases at higher applied voltages (see **Figure 2.4a,b**) as the incident light remains constant, but the emitted light decreases due to the reduced absorption of light. The internal optical efficiency increases at higher applied voltages (see **Figure 2.4c,d**) as, despite the decrease in absorption, the light that is absorbed is emitted much more effectively towards the edges of the system due to the favorable dye alignment².

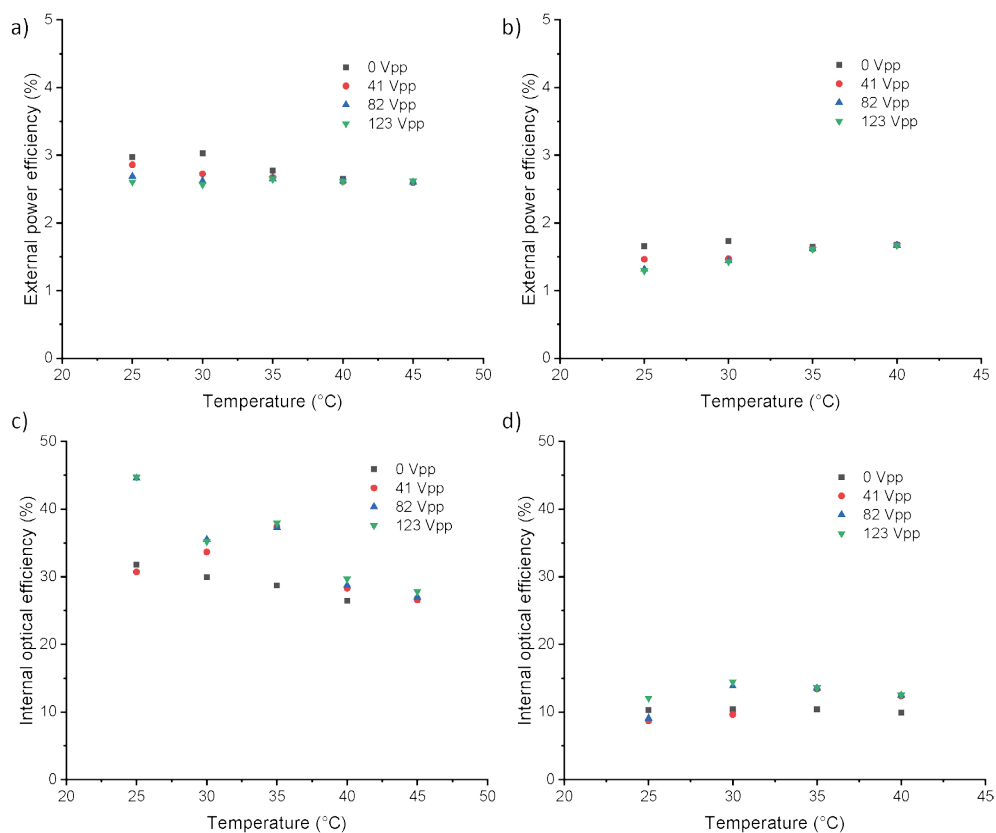


Figure 2.4: External power efficiency at different temperatures and applied electrical fields of a planar cell filled with a) Dye 1; b) Dye 2. Internal optical efficiency at different temperatures and applied electrical fields of a planar cell filled with c) Dye 1; d) Dye 2.

In many cases, it might be desirable for the ‘smart’ window to be in the most transparent state, and only upon increasing temperature or application of voltage should it become more absorbing. Such a device was fabricated by replacing the planar with a homeotropic alignment layer and switching from a fully ITO-coated glass substrate to an IDE-coated substrate. In this latter device, the thermal response is unchanged, while the LC and dye are switched from a homeotropic (transparent) alignment to a planar (absorbing) alignment by application of a voltage, as depicted in **Figure 2.5**.

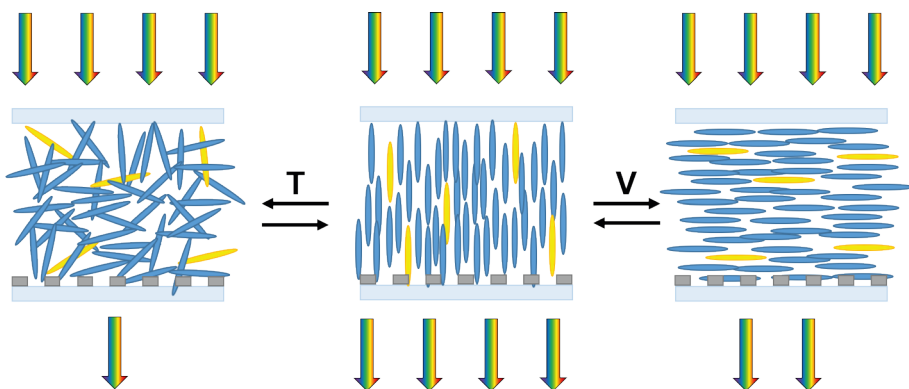


Figure 2.5: Schematic of liquid crystal (blue rods) and dye (yellow rods) alignment in an IDE-coated substrate. In an initial homeotropic state (middle) and its changes upon application of an electrical field (right) or increased temperature (left).

The transmittance at the absorption peaks of the dyes of this modified homeotropic device are shown in **Figure 2.6**. As mentioned earlier, the effect of heating is very similar to the planar device: that is, at higher temperatures the transmission decreases and the voltage required to switch the system decreases. The response to changes in potential is the opposite, however: at higher voltages, the absorption increases. The relative difference in transmission upon application of an electrical field is smaller compared to the planar ITO-coated system, most likely as the electrical field between the electrodes is less homogeneous, resulting in less uniform LC alignments. The edge emission powers for the homeotropic-aligned system with IDE could not be reliably measured as the IDE cells had a very small switching area ($1 \times 1 \text{ cm}^2$). However, the emission power spectra of the planar ITO device with potential applied should match quite closely to the homeotropic IDE system at rest.

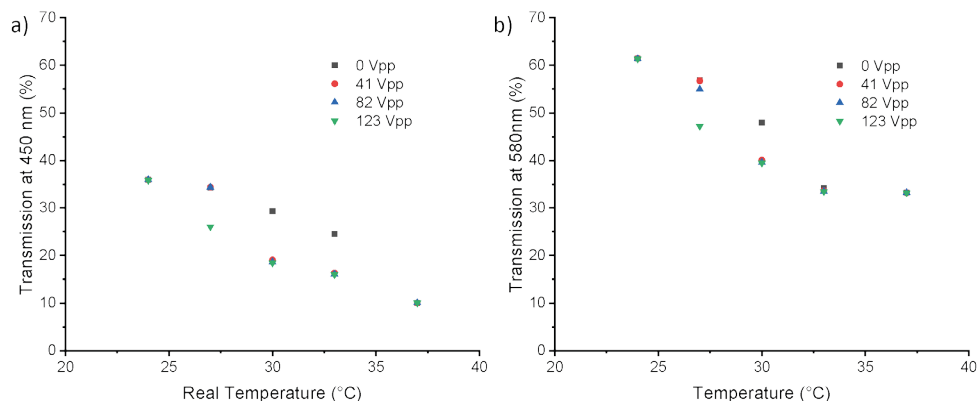


Figure 2.6: Peak transmission of an interdigitated homeotropic cell as a function of temperature and voltage filled with 8CB and 1 wt% of a) Dye 1; b) Dye 2.

Ideally, one would prefer a 'smart' window that requires the minimum use of power to operate. In regions of the world with many hours of sunlight in buildings primarily used in daytime, like office buildings, this would be a window that is in the dark, absorbing state when switched 'off'. However, there will also be situations where the opposite is desired: the windows remain transparent until some state at which light intensity is too high, and may then switch to absorbing, such as in a greenhouse, for example. In order to improve the performance of a 'smart' window with a transparent rest state, rather than using an IDE cell as described in this work, an LC could be used with a negative dielectric anisotropy in an ITO cell. This combination allows switching from a transparent homeotropic-aligned system to an absorbing planar alignment by the application of a voltage⁹. The advantage would be that a simpler ITO design can be used with better switching properties, as the IDE system inhibited full switching, and its limited in-cell gap affects the maximum absorption that can be reached, as many dyes have limited solubility in the LC host. Further performance improvements can be achieved by adjusting the structures of the dyes: enhanced alignment can be achieved, resulting in a better contrast between the 'on' and 'off' states of the electrically switched system¹⁰, and simultaneously enhancing edge emission powers as well.

2.4 Conclusion

Deploying these switchable windows could have several advantages. First, one can create windows that make better use of the incident sunlight, reducing light transmission and glare under bright, hot conditions and using this excess solar energy to generate power which could be used to allow the window to switch itself. Triggering window transmission changes to variations in external temperature allows switching to be done automatically, while the electrical switching allows for individuals to override the automatic temperature response. The temperature range for switching may be tuned by adjusting the LC host system, although the current device, which switches between about 25 °C and 35 °C, already seems appropriate.

One potential disadvantage of these LC-based devices is the reliance on the smectic phase of the LC. The smectic phase is often somewhat scattering, resulting in a slightly 'hazy' appearance to the window, as if it is somewhat soiled. What may be viewed as potential disadvantage in a commercial building actually becomes a positive feature with windows deployed in horticulture, for example, where the diffusing of light can assist plant growth by allowing more light to reach deeper into the plant canopy¹¹. Finally, the lifetime of these 'smart' window type devices is always a concern. In this particular case, the lifetime will not be very extensive due to the use of the model LC host. However, liquid-crystal based devices

have been deployed outdoors worldwide in the form of advertising displays and sporting scoreboards, so it is anticipated that with optimization of the LC mixture extended lifetimes appropriate for use as windows will be possible. Likewise, many organic dyes have already exhibited extended lifetimes¹², and it is anticipated that appropriate lifetimes may be reached for the luminescent species as well.

2.5 References

- 1 S.-W. Oh, S.-H. Kim and T.-H. Yoon, *Adv. Sustain. Syst.*, 2018, **1800066**, 1800066.
- 2 M. G. Debije, *Adv. Funct. Mater.*, 2010, **20**, 1498–1502.
- 3 J. A. H. P. Sol, G. H. Timmermans, A. J. van Breugel, A. P. H. J. Schenning and M. G. Debije, *Adv. Energy Mater.*, 2018, **8**, 1702922.
- 4 J. Wu, D. He, Y. Wang, F. Su, Z. Guo, J. Lin and H.-J. Zhang, *Org. Lett.*, 2018, **20**, 6117–6120.
- 5 P. Kahl, P. Baroni and L. Noirez, *Phys. Rev. E - Stat. Nonlinear, Soft Matter Phys.*, 2013, **88**, 050501.
- 6 J. Lub, D. J. Broer, R. T. Wegh, E. Peeters and B. M. I van der Zande, *Mol. Cryst. Liq. Cryst.*, 2005, **429**, 77–99.
- 7 T. K. Bose, B. Campbell, S. Yagihara and J. Thoen, *Phys. Rev. A*, 1987, **36**, 5767–5773.
- 8 C. Tummeltshammer, A. Taylor, A. J. Kenyon and I. Papakonstantinou, *Sol. Energy Mater. Sol. Cells*, 2016, **144**, 40–47.
- 9 P. P. Crooker and D. K. Yang, *Appl. Phys. Lett.*, 1990, **57**, 2529–2531.
- 10 A. M. Kendhale, A. P. H. J. Schenning and M. G. Debije, *J. Mater. Chem. A*, 2013, **1**, 229–232.
- 11 S. Hemming, T. A. Dueck, J. Janse and F. van Noort, *Acta Hortic.*, 2008, **801**, 1293–1300.
- 12 I. Baumberg, O. Berezin, A. Drabkin, B. Gorelik, L. Kogan, M. Voskoboynik and M. Zaidman, *Polym. Degrad. Stab.*, 2001, **73**, 403–410.

Chapter 3

Color tunable triple state 'smart' window

In this Chapter, we describe a new fluorescent red dye modified with liquid crystal side chains to be more interactive with the liquid crystal host. The dye solubilizes in the liquid crystal matrix with increasing temperature resulting in a red colored, absorbing state, recovering transparency again by aggregating within minutes upon cooling. This dye is used to fabricate a device that can be electrically switched from a red colored, absorbing to an intermediate scattering state, and at greater electrical fields, a transparent state. Using a second dichroic fluorescent dye, heating the device transitions the window's color from yellow/green to red assisted by Förster Resonance Energy Transfer. The multi-responsive optical changes could find applications in many fields including displays, smart windows, electricity generation and greenhouses.

This chapter is partially reproduced from: G. H. Timmermans, J. Wu, A. P. H. J. Schenning, J. Lin, and M. G. Debije, "Color tunable triple state 'smart' window," (submitted)

3.1 Introduction

In this Chapter, we propose a device that can alter its color and transparency in response to both heat and electrical potential. Unlike the previous Chapter, not only is the liquid crystal (LC) host responsive to temperature but the dye itself also responds to temperature changes. In earlier work, we demonstrated a thermally reversible perylene-core dye in the LC blend E7.¹ While this dye produced reversible color variation upon heating, returning to the transparent state took quite a long time (>45 minutes) which makes it less viable for use in devices where rapid reversibility are desired. We conjectured that the addition of cyano-biphenyl groups at the end of the alkyl tails of a perylene core to better match the chemical nature of the host LC would allow both enhanced interaction between the dye and the host LC, but also promote more rapid association of the dyes upon cooling. Indeed, the cyano-biphenyl groups result in faster dye reaction speeds, while maintaining excellent alignment and provide an improved electrical response. The new dye combined with a second dichroic dye and a chiral dopant is used to fabricate a color tunable triple-state 'smart' window or that is electrically switchable between a dark, 'absorbing' state and a transparent state, with an intermediate scattering state with a thermal override to a bright red color.

3.2 Experimental

CB-perylene (4',4'''-(((1,3,8,10-tetraoxo-5,6,12,13-tetraphenoxy-1,3,8,10-tetrahydroanthra[2,1,9-def:6,5,10-d'e'f]diisoquinoline-2,9-diyl)bis(4,1-phenylene))bis(dodecane-12,1-diyl))bis([1,1'-biphenyl]-4-carbonitrile)) **1** was kindly synthesized and provided by Dr. Jianbin Lin of Xiamen University China. C12-PBI (2,9-bis(4-dodecylphenyl)-5,6,12,13-tetraphenoxyanthra[2,1,9-def:6,5,10-d'e'f]diisoquinoline-1,3,8,10(2H,9H)-tetraone) **2** was synthesized as described previously.¹ Mixtures were made with 0.25 wt% of these dyes in the liquid crystal mixture E7 (Merck). For the supertwist experiments, a mixture was made of 0.25 wt% CB-perylene **1**, 1 wt% chiral dopant S1011 **3** (Merck), 0.25 wt% of the coumarin derivative **4** (RiskReactor) and in E7 (see **Figure 3.1**).

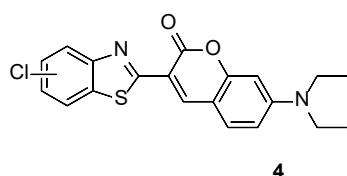
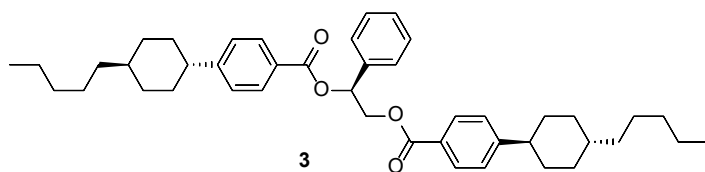
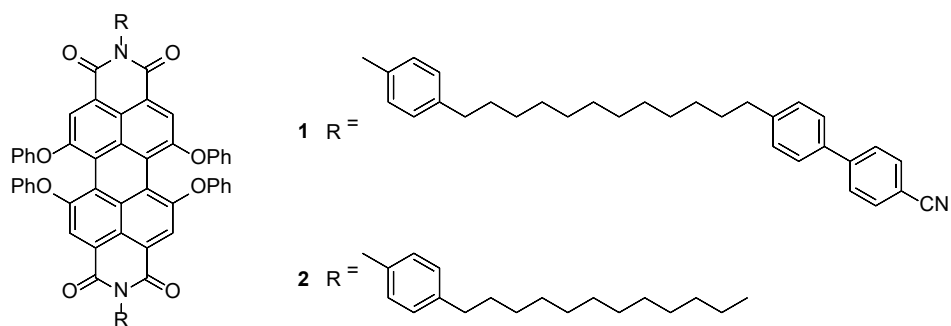


Figure 3.1: Molecular structure of **1:** dye CB-perylene, **2:** dye C12-PBI¹, **3:** chiral dopant S1011 and **4:** the coumarin derivative.

Indium tin oxide (ITO) coated glass plates of $3 \times 3 \text{ cm}^2$ were cleaned and a layer of planar polyimide (OPTMER AL 1051, JSR Corporation, Tokyo, Japan) was spin-coated (Karl Suss RC8, 40 s at 5000 rpm) onto the cleaned glass plates which were then baked for 1.5 h at $180 \text{ }^\circ\text{C}$ and rubbed over a velvet cloth to induce planar alignment. Cells were fabricated by gluing two rubbed plates together with glue containing $20 \text{ }\mu\text{m}$ glass spacer beads in an antiparallel fashion with a small offset at the edges. In addition, custom-made ITO coated cells ($5 \times 5 \text{ cm}^2$ switching area, $20 \text{ }\mu\text{m}$ spacing) from LC-Tec Displays AB were also purchased. The cells were filled with the LC mixtures in the isotropic state and allowed to cool and rest for a day before use. The $3 \times 3 \text{ cm}^2$ cells were used for the absorption measurements and the $5 \times 5 \text{ cm}^2$ cells for the edge emission power measurements.

UV-vis spectra were measured on a PerkinElmer Lambda 750 with a 150 mm integrating sphere. Edge emission powers were measured using a Labsphere SLMS 1050 integrating sphere connected to an International Light RPS900 diode array detector. Simulated solar illumination was provided by a 300 W Lot-Oriel solar simulator equipped with filters to emulate the AM1.5 solar spectrum. Sine wave voltage modulation at 1000 Hz

was applied to the cells using a laboratory function generator (Agilent 33220A) coupled to a 20× voltage amplifier (FLC Electronics F20A) in the range of 0–26 V_{RMS}. The fluorescence lifetime and photoluminescence spectra were obtained with an Edinburgh Instruments LifeSpec-ps spectrophotometer with a Peltier cooled Hamamatsu microchannel plate photomultiplier for detection and coupled to a 400 nm pulsed laser (PicoQuant LDH-C 400, 2.5 MHz; PicoQuant PDL 800-B driver): for the excitation of the analyte with power kept below 1 mW by using a diaphragm. The fluence of a single pulse was 10⁻⁸ J/cm². The fluorescence lifetime were fitted with a multiexponential fit by reconvolution of the instrument response function (IRF) using $I(t) = \int_{-\infty}^t IRF(t') \sum_{i=1}^n A_i \exp\left[-\frac{t-t'}{\tau_i}\right] dt'$, where A_i is the amplitude of the i th component with a lifetime τ_i . Using the software packaged FluoFit 4.1 of PicoQuant the decay parameters were recovered.

3.3 Results and discussion

3.3.1 CB-perylene dye

Similar to its predecessor C12-PBI,¹ most of the CB-perylene dye aggregates at 0.25 wt% in the nematic host LC E7 at room temperature, resulting a relatively colorless cell (**Figure 3.2a**). Upon increasing the temperature to >55 °C, the dye mostly dissolves, aligning parallel to the planar LC host and a red colored cell is obtained (**Figure 3.2a**). The order parameter (S) of CB-perylene in E7 was measured in the dissolved state using polarized absorption and calculated using equation 3.1:

$$S = \frac{A_{par} - A_{per}}{A_{par} + 2A_{per}} \quad (\text{eq. 3.1})$$

where A_{par} and A_{per} are the peak absorbances of the sample when incident light is polarized parallel and perpendicular to the alignment direction of the host LCs, respectively. We determine a high degree of alignment ($S = 0.6$), indicating a good interaction between the dye and the E7 host; this value is greater than that found for the coumarin derivative dye labeled **4** in **Figure 3.1**, which has been one of the highest reported in E7,^{2,3} and approximately the degree of alignment of the E7 host itself.⁴

Even though at room temperature the system is mostly transparent, application of 7 V_{RMS} rotates the E7 host to the homeotropic alignment, realigning the minor amount of non-aggregated dye, further reducing absorption since the dye is dichroic, and so absorbs little light when orientated with its molecular long axis directed towards to viewer (**Figure 3.2a**). Increasing the temperature allows the dye to de-aggregate and promote light absorption. As more dye dissolves, more dye can realign when an electrical potential is applied across the cell, reaching a maximum difference between the ‘on’ and ‘off’ states of

the window at 55 °C (see **Figure 3.2b**). Around 65 °C the E7 host becomes isotropic and no longer responds to the applied electric field.

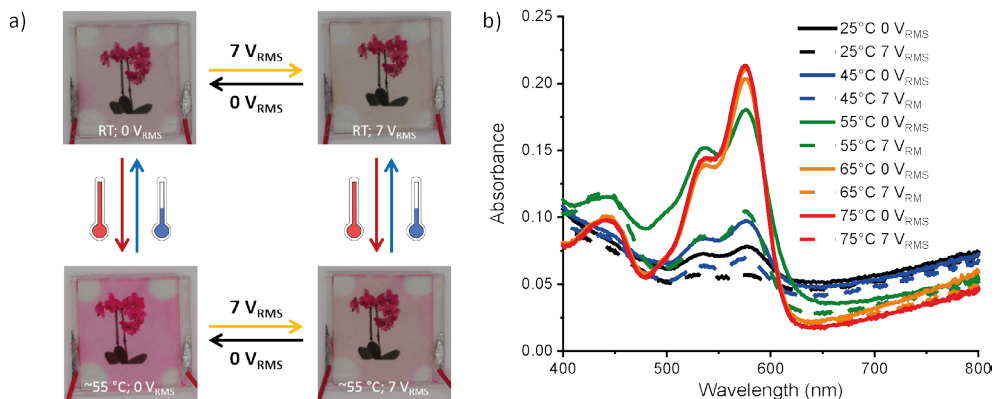


Figure 3.2: a) Photographs of the cell over an image of a flower containing 0.25 wt% CB-perylene in E7 under various conditions: (top left) RT, 0 V_{RMS}; (top right) RT, 7 V_{RMS}; (bottom left) ~55 °C, 0 V_{RMS}; (bottom right) ~55 °C, 7 V_{RMS}. b) Absorption spectra of 0.25 wt% CB-perylene in E7 at various temperatures at (solid lines) 0 V_{RMS} and (dashed lines) 7 V_{RMS}.

The recovery of the system to mostly colorless upon cooling from its colored state was measured by first heating the sample to 80 °C and measuring the absorption spectra every 5 minutes as the sample cooled at ambient conditions. The results for CB-perylene show that within 5 minutes the absorption has returned to 88% of its initial value and completely recovers to its initial state at ~25 minutes (see **Figure 3.3**). In contrast, C12-PBI, which does not boast the cyano biphenyl groups, takes much longer to recrystallize: the 88% recovery takes 45 min and still has not reached its minimum value even after 90 minutes.

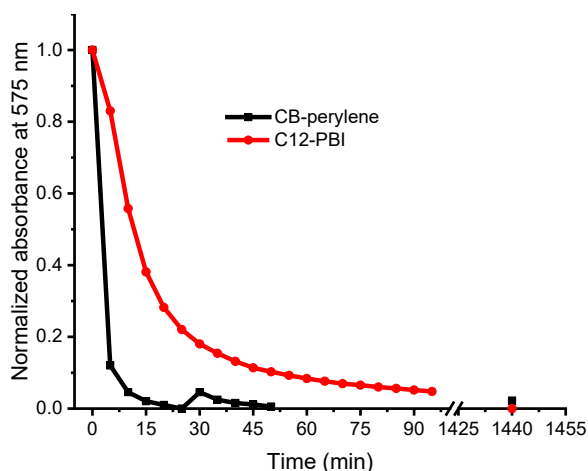


Figure 3.3: Normalized absorbance at 575 nm in time during cooling of CB-perylene and C12-PBI in E7 from 80 °C to room temperature.

3.3.2 Color tunable triple state 'smart' window

A method to create a scattering state in a switchable liquid crystal (LC) system without polymerization is by using a 'supertwist' system.⁵⁻⁸ In a supertwist system, a small amount of chiral dopant is added to a nematic LC to create a several rotations of the LC through the depth of the cell. When applying intermediate voltages, the supertwist hinders the formation of a homeotropic state, resulting in a focal conic (scattering) state; at higher voltages the homeotropic state is generated. Supertwist 'smart' windows that use dichroic dyes have increased absorption as a result of multiple alignments throughout the thickness of the samples.⁸

3

To fabricate the color tunable triple state 'smart' window we used 0.25 wt% of CB-perylene **1**, 0.25 wt% of coumarin dye **4**, and 1 wt% chiral dopant **3** dissolved in the nematic E7 host. When heating the 'smart' window, more CB-perylene dye dissolves and the window becomes increasingly red colored (**Figure 3.4a**). The dissolution of the red dye clusters was monitored using UV-vis spectroscopy (see **Figure 3.4b**). Initially, only the 450 nm absorption peak from the coumarin derivative is visible with some scattering at longer wavelengths caused by the CB-perylene agglomerates. Increasing the temperature results in the dissolving of the CB-perylene dye and the appearance of the typical perylene absorption peak, with corresponding reduction in scattering, with scattering reaching a minimum around 65 °C, the isotropic temperature of the LC mixture. Application of a voltage (**Figure 3.4c** and **Figure 3.4d** shown at RT) increases the scattering, with a maximum appearing around 9 V_{RMS} as a focal conic LC state is achieved. Further increasing the potential decreases both the absorption and scattering of the cell as a homeotropic LC state with both the two dichroic dyes aligned perpendicular to the cell surface.

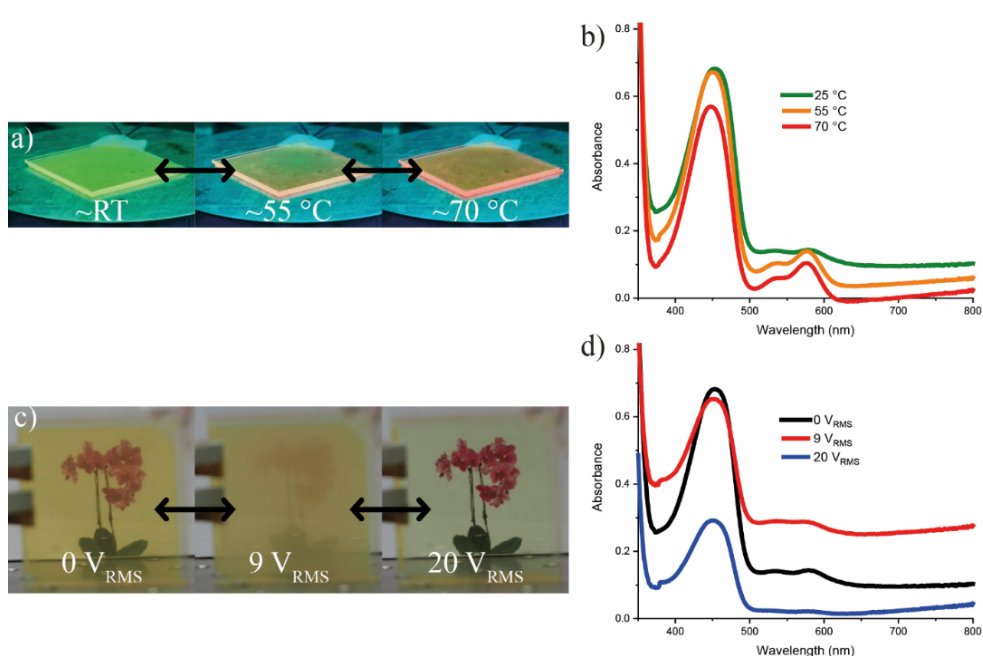


Figure 3.4: a) Photographs of the 'smart' window at (from left to right): RT, ~55 °C and ~70 °C. b) Absorption spectra of the 'smart' window at the different temperatures at 0 V_{RMS}. c) Photographs of the 'smart' window at RT and different applied voltages, from left to right: 0 V_{RMS}, 9 V_{RMS} and 20 V_{RMS}. d) Absorption spectra of the 'smart' window at various applied voltages at RT.

Not only can the 'smart' window be switched independently with temperature or applied voltage, but the two stimuli can also be applied at the same time (see **Figure 3.5a**). Until ~60 °C, the system is responsive to both temperature and electrical fields, after which the LC becomes isotropic and further application of a voltage has no effect. The effect of intermediate temperatures and voltage on the absorption of CB-perylene at 575 nm (corrected for scattering) is plotted in **Figure 3.5b**.

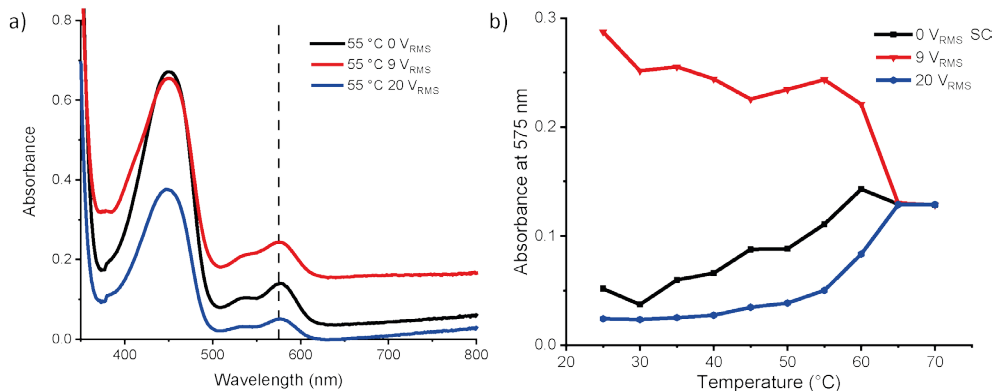


Figure 3.5: a) Absorption spectra of the 'smart' window at 55 °C and 0 V_{RMS}, 9 V_{RMS} and 20 V_{RMS} (with vertical dotted line indicating 575 nm). b) Absorption at 575 nm of the supertwist sample at various temperatures and voltages. The 0 V_{RMS} SC is baseline corrected for scattering. Lines are added between points as an aid for the eye.

Figure 3.6 schematically depicts the 'smart' window in its various states as it responds to changes in both temperature and applied electrical fields. At low temperatures most of the red dye is aggregated in a non-fluorescent form and the device is colored yellow. Application of an intermediate voltages forms a yellow scattering texture and at higher voltages a transparent, slightly yellow, state. Increasing the temperature results in a red color as the CB-perylene is dissolved to its fluorescent form and receives energy via FRET from the coumarin. At temperatures below the isotropic point of the LC (<65 °C), a red scattering texture and transparent, slightly red colored state is formed upon application of intermediate and high voltages respectively. When heated above the isotropic temperature the device can no longer respond to voltages.

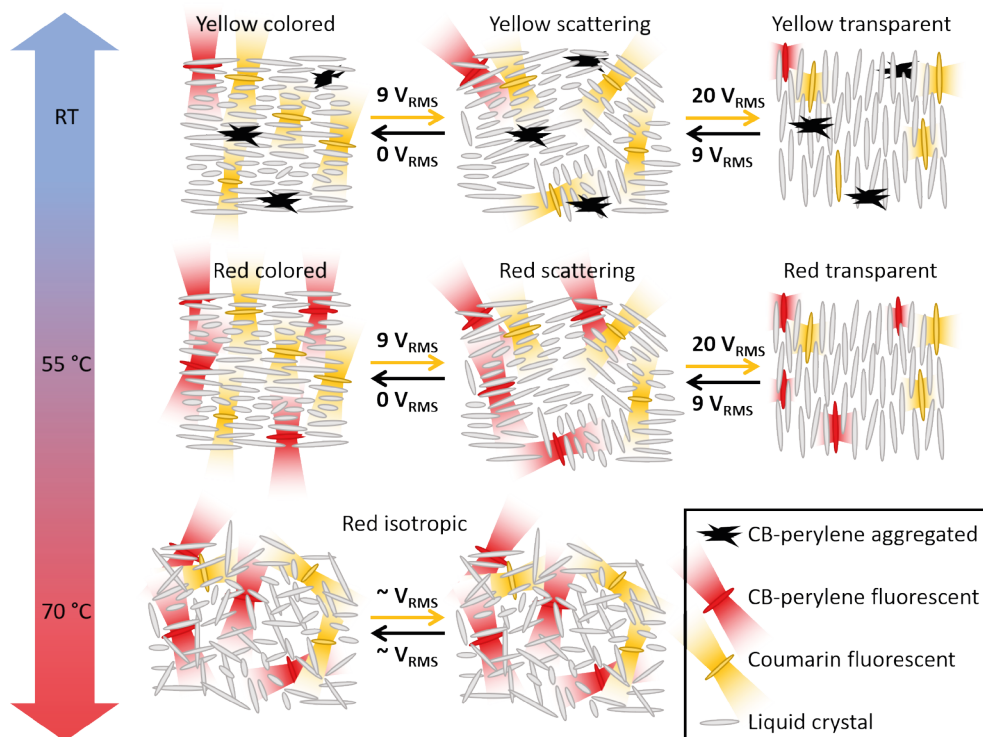


Figure 3.6: Schematic representation of the different states of the ‘smart’ window architecture. From left to right along the top row: conditions under ambient, with the visually yellow state with most CB-perylene aggregated. Upon application of intermediate potential, the LCs take a focal conic, scattering texture. Further potential increase forms the transparent, homeotropic LC alignment. Heating the sample to a higher temperature below the isotropic phase transition leads to (middle row, left to right) a red absorbing state with the CB-Perylene accepting energy transfer via FRET from the coumarin. Upon application of intermediate and higher voltages, the focal conic and homeotropic states are attained. Finally, (bottom row) heating the sample to above the isotropic phase transition leads to a random alignment and a red color that is not affected by the application of an electric field.

To investigate the performance of the ‘smart’ window for electricity generation in luminescent solar concentrator-like applications,⁹ the edge emission powers were measured as a function of temperature and applied voltage when exposed to an AM1.5 solar spectrum (**Figure 3.7a**). At the application of 20 V_{RMS} there is a decrease in emission power at every wavelength as the sample becomes homeotropic. The emission power of the coumarin derivative (450-580 nm) noticeably decrease with increasing temperature while the emission power of CB-perylene (580-750 nm) increase. This decrease of coumarin emission power is the result of increased FRET as CB-perylene is released. The fluorescent lifetime of the coumarin derivative in the supertwist system was found to be: 3.76 ns (11%) and 2.73 ns (88%) at RT and: 2.65 ns (53%) and 2.18 ns (47%) at ~ 80 °C. Average lifetimes were calculated to be 2.84 ns at RT and 2.18 ns at ~ 80 °C, while the lifetime of the coumarin only was 3.26 ns (see **Figure 3.7b**). The energy transfer efficiency (E) was calculated using equation 3.2:⁴²

$$E = 1 - \frac{\tau_{DA}}{\tau_D} \quad (\text{eq. 3.2})$$

where τ_{DA} is the lifetime of the donor in the presence of the acceptor and τ_D is the lifetime of the donor in the absence of the acceptor. From this, efficiencies for FRET of 0.13 at RT and 0.33 at $\sim 80^\circ\text{C}$ were calculated.

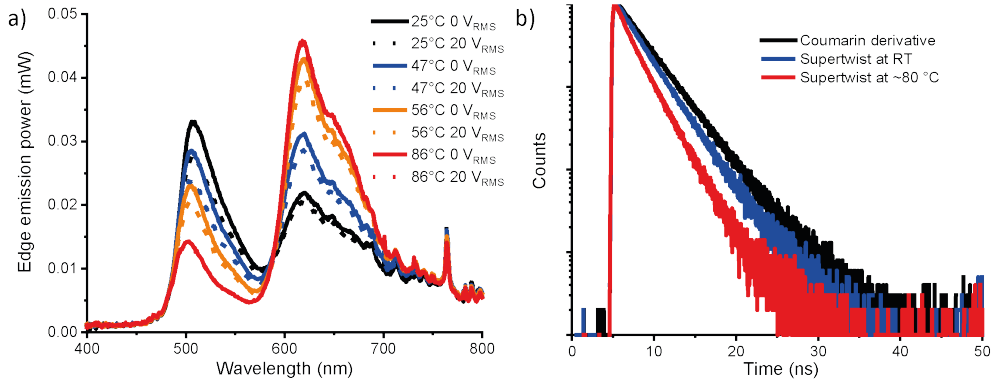


Figure 3.7: a) Edge emission power of three state system at different temperatures and voltages. b) Single photon counting measurement of the fluorescence decay of: 0.25 wt% coumarin derivative in E7 at RT (black line); supertwist sample at RT (blue line) and supertwist sample at $\sim 80^\circ\text{C}$ (red line)

3.4 Conclusion

A fluorescent dye was synthesized to have more interaction with its host LC by attaching cyano-biphenyl groups at the end of the alkyl tails on a perylene core. The dye aligns well in the nematic LC host E7, responding to an electrical field and rapidly aggregating at lower temperatures and dissolving at higher temperatures.

Using this dye in combination with a second fluorescent dichroic dye in a supertwist LC system, a color tunable triple state ‘smart’ window was fabricated. The ‘smart’ window can change its optical properties both through temperature but also through application of an electrical field. A dramatic color change from green/yellow to brilliant red with a corresponding increase of red edge emission power via enhanced fluorescence transfer was achieved by heating the device. A scattering state is generated due to the application of an intermediate voltage; it is possible to override the bright yellow/green or red colors by application of a higher field to generate a transparent system. This system has potential for application as ‘smart’ windows, and in greenhouses where the incoming solar radiation can automatically be reduced when temperatures increase too much, while a manual override to a transparent state is possible if desired.

3.5 References

- 1 J. A. H. P. Sol, V. Dehm, R. Hecht, F. Würthner, A. P. H. J. Schenning and M. G. Debije, *Angew. Chemie Int. Ed.*, 2018, **57**, 1030–1033.
- 2 P. P. C. Verbunt, A. Kaiser, K. Hermans, C. W. M. Bastiaansen, D. J. Broer and M. G. Debije, *Adv. Funct. Mater.*, 2009, **19**, 2714–2719.
- 3 M. G. Debije, C. Menelaou, L. M. Herz and A. P. H. J. Schenning, *Adv. Opt. Mater.*, 2014, **2**, 687–693.
- 4 B. Bahadur, R. K. Sarna and V. G. Bhide, *Mol. Cryst. Liq. Cryst.*, 1982, **72**, 139–145.
- 5 S. C. Guy, *Displays*, 1993, **14**, 32–38.
- 6 J.-W. Huh, B.-H. Yu, J. Heo and T.-H. Yoon, *Appl. Opt.*, 2015, **54**, 3792.
- 7 K.-H. Kim, H.-J. Jin, K.-H. Park, J.-H. Lee, J. C. Kim and T.-H. Yoon, *Opt. Express*, 2010, **18**, 16745.
- 8 J. A. H. P. Sol, G. H. Timmermans, A. J. van Breugel, A. P. H. J. Schenning and M. G. Debije, *Adv. Energy Mater.*, 2018, **8**, 1702922.
- 9 M. Debije and P. Verbunt, *Adv. Energy Mater.*, 2012, **2**, 12–35.

Chapter 4

Temperature and light responsive ‘smart’ window based on a diarylethene sunlight responsive dye

Controlling the intensity and manipulating the spectral composition of sunlight is critical for many devices including ‘smart’ windows, greenhouses and photomicroreactors, but also important in more decorative applications. Here, we use a photo responsive diarylethene dye incorporated in a liquid crystal host to create a dual-responsive ‘smart’ window regulated both by an electrical trigger and by specific wavelengths of light. By incorporating the same diarylethene dye in a polymerizable host and using inkjet printing, coatings can be made with complete freedom in the applied pattern design, although the electrical response is lost. The color change of the diarylethene dye can be controlled in simulated sunlight by concurrent light exposure from a LED source, allowing a manual override for outdoor use. Photoluminescence of the closed isomer of the diarylethene from the lightguide edges could be used for lighting or electricity generation in a luminescent solar concentrator architecture.

This chapter is partially reproduced from: G. H. Timmermans, B. W. H. Saes, and M. G. Debije, "Dual-responsive “smart” window and visually attractive coating based on a diarylethene photochromic dye," *Appl. Opt.* 58, 9823 (2019).

4.1 Introduction

Thus far, all systems described in this thesis have been responsive to (both) thermal and electrical stimuli. Because temperature control is often the goal of ‘smart’ windows, temperature responsive systems that can function autonomously are desirable. However, photo responsive systems can directly change their properties when the lighting conditions change without waiting for the temperature to rise. This is especially desired in greenhouse applications where an overload of light can be detrimental to plants. A manual override via an electrical trigger remains advantageous in all cases.

One way to help in the introduction of ‘smart’ windows into the built environment and reduce manufacturing costs is by using ‘smart’ coatings. Coatings are easier to scale up and produce, especially when the need for electrodes is removed. Inkjet printing such coatings allows for creative patterns to be produced that can be made more visually attractive.

In this Chapter, we demonstrate the concept of a dual electrical- and photo-switchable ‘smart’ window which can be used to generate electricity. Additionally, an exclusively photo-switchable system was fabricated by inkjet printing which could ease the application of energy generating ‘smart’ windows in the urban setting via its visually pleasing aesthetics. To our knowledge, no other light switchable, color-changing LSC coatings have been reported in the literature.

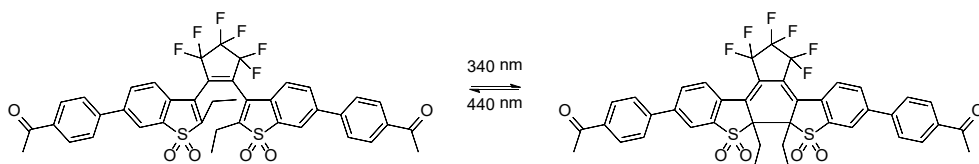


Figure 4.1: Molecular structures of the photochromic diarylethene dye in its open, non-fluorescent form (left) and its closed, fluorescent form (right).

The key component is a diarylethene photochromic dye (see **Figure 4.1**), which, due to its small conformational change upon isomerization, enables switching between the colored and transparent states when embedded in a polymeric host.^{1,2} Photochromic diarylethenes have previously found application in fields including optical data storage,^{3,4} thermosensors,⁵ display materials,⁶ and in biotechnology.⁷ However, diarylethenes with fluorescent quantum yields above 0.7 (required for LSC applications) are uncommon.^{5,8–11}

4.2 Experimental

1,2-Bis(2-ethyl-6-(4-acetylphenyl)-1-benzothiophen-1,1-dioxide-3-yl)perfluorocyclopentene (hereafter labelled the 'diarylethene dye') was synthesized according to procedures found in literature⁹. Lumogen F Red 305¹² was purchased from BASF SE and the nematic LC mix E7 was purchased from Merck KGaA. A proprietary solution was used for the inkjet printing. Custom-made indium tin oxide (ITO) coated cells (about 50 × 50 mm² switching area, coated with planar aligned polyimide, 20 μm spacing) were purchased from LC-Tec Displays AB. Samples were printed on 50 × 50 × 5 mm³ PMMA substrates (Plano Plastics). Inkjet printing was performed on a Dimatix DMP-2831 printer equipped with a DMC11610 printhead (10 pl). Polymerization of the ink was performed with a Thorlabs M365LP1 LED under N₂ at a dose rate of 35 mW/cm².

0.25 wt% of the diarylethene dye was dissolved in E7, a commonly-used liquid crystal (LC)^{13,14} mixture which is nematic at room temperature and used to fill the ITO coated, glass cells. In this setup, dual electrical-optical switching behavior could be tested

UV-vis spectra were measured on a PerkinElmer Lambda 750 with a 150 mm integrating sphere. Edge emission powers were measured using a Labsphere SLMS 1050 integrating sphere connected to an International Light RPS900 diode array detector. Simulated solar illumination was provided by a 300 W Lot-Oriel solar simulator equipped with filters to emulate the AM1.5 solar spectrum. Additional illumination was provided with Thorlabs LEDs of 340 nm at ~2 mW/cm² (M340L4) and 440 nm at ~8 mW/cm² (M455L3) with collimation adapters placed approximately 19 cm above the sample at 700 mA. A function generator (Agilent 33220A) was used to apply a 10 V_{pp}, 100 Hz sine wave.

4.3 Results and discussion

The choice for this diarylethene dye (see Figure 4.1) is mainly based on its high fluorescence quantum yield (ϕ_f) in the ring-closed isomer (in 1,4-dioxane, $\phi_f = 0.87$).⁸ Diarylethene dyes with S,S-dioxidized benzothiophene heterocycles have a significantly increased ϕ_f compared to their thiophene heterocycle appended counterparts.¹⁵ Extension of the conjugation raises the ϕ_f from 0.22 to ≈ 0.8 : this is why the molecule features acetophenone rings in conjugation with the benzothiophene heterocycles. In addition, from a series of molecules where the length of linear alkyl substituents on the reactive carbons of similar diarylethenes is varied from methyl up to n-butyl in order to increase ϕ_f , substituents longer than methyl on the benzothiophene 2-position are most effective.¹⁵ However, the introduction of ethyl alkyl chains may diminish the fatigue resistance of diarylethenes compared to their methyl substituted counterparts: however, for proof-of-principle we valued the increased ϕ_f over the increased fatigue resistance.

The order parameter (S) of the dye in the cell was determined by comparing the absorption of light polarized parallel (A_{par}) and perpendicular (A_{per}) to the alignment of the dye using equation 4.1:

$$S = \frac{A_{par} - A_{per}}{A_{par} + 2A_{per}} \quad (\text{eq. 4.1})$$

These measurements resulted in a relatively high order parameter of $S = 0.53$, comparable to the order parameter of the better-aligning dyes used in previous studies.^{16,17}

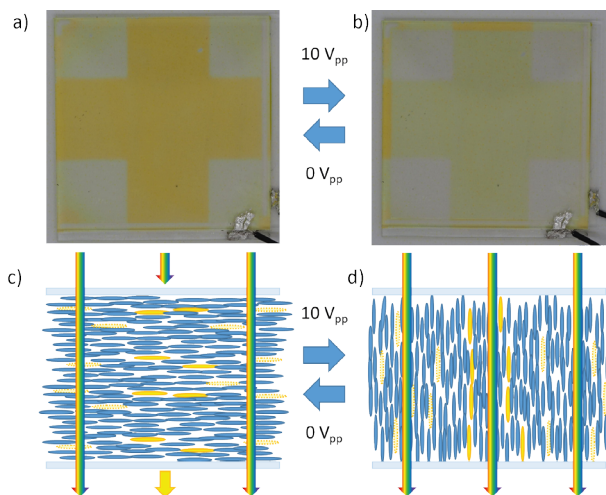


Figure 4.2: a) Photograph of a 20 μm cell of 0.25 wt% diarylethene dye in the host liquid crystal E7 exposed for 2 hours to 440 nm light through a cross shaped mask. b) The same sample with 10 V_{pp} at 100 Hz applied. c) Schematic representation of the alignment of the LCs and the dye in both open and closed forms in rest state (0 V_{pp}). d) Schematic representation of the alignment of the LCs and the dye in both open and closed states in the homeotropic orientation (10 V_{pp}).

The center of the planar cell was then covered with an opaque photomask in the shape of a cross, and the device exposed for 2 hours to light from a 440 nm LED. Upon removal of the photomask, a dark yellow cross corresponding to the unexposed areas was visible on a mostly transparent background from the exposed regions, as can be seen in **Figure 4.2a**. **Figure 4.2c** shows schematically that light is able to pass the sample in the exposed areas where the dye has undergone a ring opening to the transparent state while the light is absorbed at the unexposed areas. By application of a small AC field (*i.e.* 10 V_{pp} at 100 Hz) the LC (and hence the diarylethene dye) could be reoriented into a homeotropic state within a second (see **Figure 4.2b**). Due to the dichroism of the dye, the absorption is much reduced in the regions with homeotropic orientation compared to the planar (rest) state, resulting in the dark yellow areas becoming more transparent while the background became even clearer. **Figure 4.2d** shows the realignment of the LCs and the dye, resulting in a non-absorbing state across the sample allowing more light to pass through the device. Removal

of the potential allows the LCs to return to their initial orientation within seconds. These multiple visual effects are not normally possible in ‘smart’ windows using static fluorescent dichroic dyes.

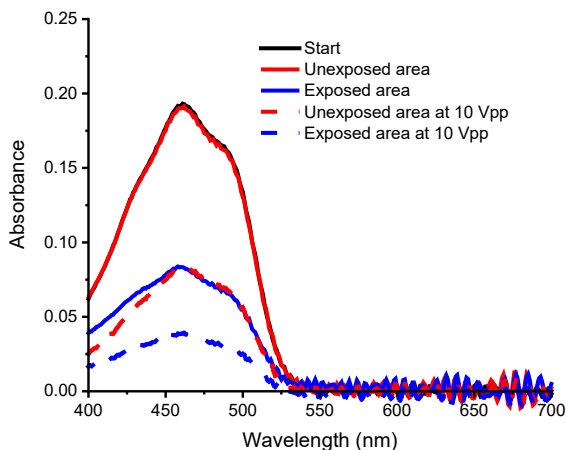


Figure 4.3: Absorption spectra of the exposed (blue) and unexposed (red) regions of the masked cell containing 0.25 wt% diarylethene dye in E7 at rest (solid lines) and under an applied field of 10 V_{pp} at 100 Hz (dotted lines).

The absorption spectra of the exposed and unexposed regions of the sample are shown in **Figure 4.3**. The unexposed area covered by the mask retained its initial absorbance, indicating that no isomerization has occurred, in contrast to the region exposed to the LED for 2 hours, where a decrease of the absorbance peak from 0.19 to 0.08 was observed. The LC (and hence the diarylethene dye) reoriented reversibly upon application of a potential across the cell to align homeotropically, resulting in a drop in the measured absorption of the exposed areas to only 0.04, while the absorption of the masked area reduced to 0.08. In future, to reduce the switching times without affecting the fluorescent quantum yield it may be possible to modify the dye to have an increased thermal relaxation.

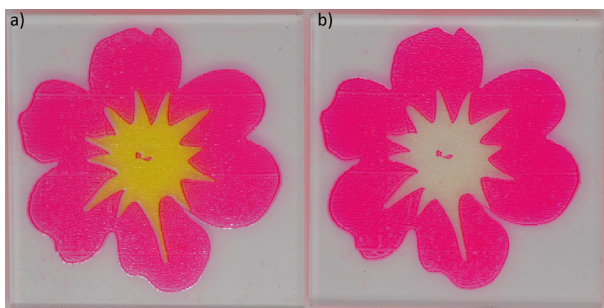


Figure 4.4: Examples of an inkjet-printed pattern containing diarylethene dye (yellow) and Lumogen F Red 305 (red): a) A flower; b) A flower after switching to the transparent state (2 hours of 440 nm light).

By incorporating the diarylethene dye in a solution, inkjet printing allows for the construction of intricate, light-sensitive art, making the system more visually pleasing to the observer. For example, **Figure 4.4a** displays a sample printed in the shape of a flower, with the center yellow region containing the diarylethene dye and the outer red region containing BASF Lumogen F Red 305, a common dye used in LSC studies.^{12,18–21} The sample, containing 0.45 wt% of diarylethene dye in a binder was printed onto 50 × 50 × 5 mm³ polymethylmethacrylate (PMMA) plates. The printed layer was subsequently photopolymerized under nitrogen with a 365 nm LED to form a solid film. During the polymerization, photocyclization of the diarylethene took place accompanied with the enhancement of the absorption band at around 455 nm. **Figure 4.4b** shows the same flower after switching to the transparent state (2 hours of 440 nm light), resulting in a fading of the color of the flower center, with only the red petal color remaining. This allows for decorative designs that could be used for advertisement purposes where part of the message can be reversibly displayed.

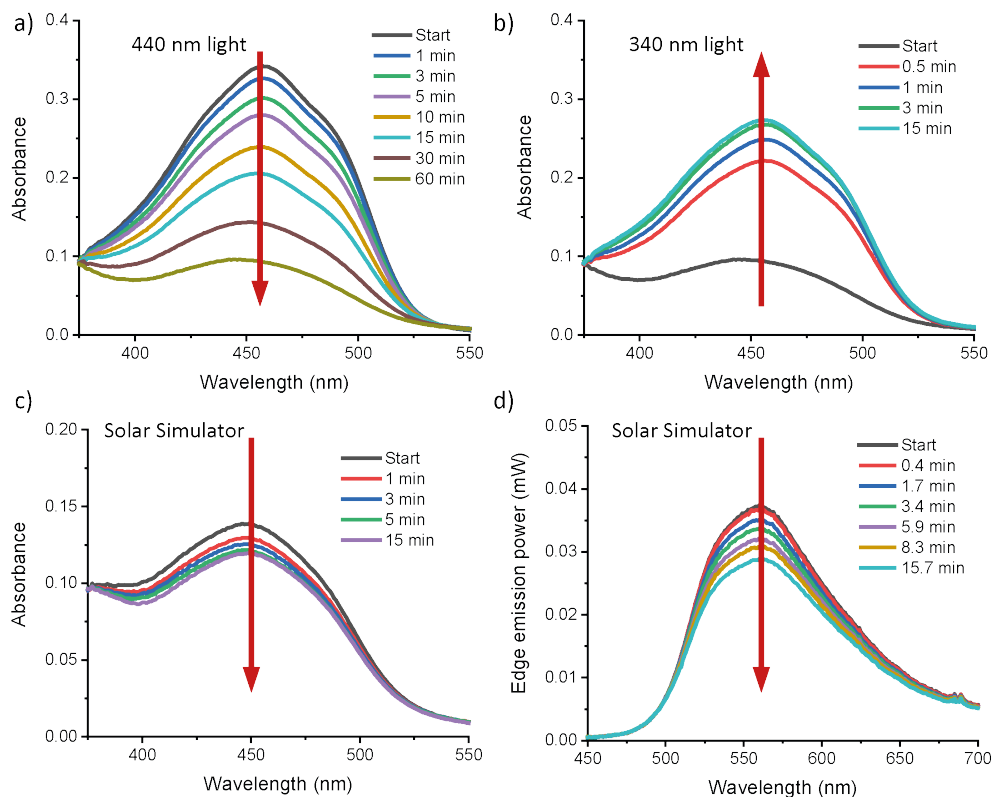


Figure 4.5: Absorption spectra of the coating containing the diarylethene dye on a PMMA lightguide. a) During exposure with 440 nm light. b) During subsequent exposure with 340 nm light. c) During subsequent exposure with solar simulator AM1.5 illumination. d) Edge emission power spectra of the diarylethene dye on a PMMA lightguide during exposure with solar simulator AM1.5 illumination

To study the switching speed and light being emitted from the edges of the lightguide, the diarylethene dye was printed to fully cover the 50 x 50 mm² surface of a PMMA plate. After photopolymerization (and photocyclization of the diarylethene) of the binder, the sample was exposed to light from a 440 nm LED at 22 mW/cm², causing an photoinduced cycloreversion and gradual reduction of the absorption peak center at 455 nm (see **Figure 4.5a**), changing the film color from yellow to essentially colorless over an hour of exposure. To regenerate the absorption peak and device color, the sample was exposed to 340 nm light from an LED at 1.5 mW/cm², reaching the photostationary state (PSS) within 3 minutes. Already more than 80% of the maximum absorption at 455 nm of the pristine coating was recovered within the first 30 seconds (**Figure 4.5b**). The PSS was also monitored under a solar simulator. This resulted in a 14% decrease of the absorption from the initial fluorescent state (see **Figure 4.5c**). The dye reached this PSS in less than 15 min of exposure to the solar simulator, which generates a continuous spectrum, simultaneously exciting both the open and closed isomers of the diarylethene.

The fluorescent light emitted by the dye is largely retained in the high refractive index PMMA lightguide by total internal reflection, and exits the material primarily through the edges of the plate. The fluorescent light emitted from one edge of the lightguide during exposure to the solar simulator was captured with an integrating sphere and spectrally resolved (see **Figure 4.5d**). The intensity of the emitted light decreases in time, concurrent with the decrease of absorption at 455 nm. The internal optical efficiency²² (photons emitted at the edges of the device per photons absorbed by the device) of the initial closed isomer, high absorbance state was calculated using equation 4.2:

$$\eta_{int} = \frac{\text{photons emitted}}{\text{photons absorbed}} = \frac{\int_{\text{emission}} P_{\text{out}}(\lambda_{\text{em}}) \frac{\lambda_{\text{em}}}{hc} d\lambda_{\text{em}}}{\int_{\text{absorption}} P_{\text{in}}(\lambda_{\text{abs}}) \frac{\lambda_{\text{abs}}}{hc} A(\lambda) d\lambda_{\text{abs}}} * 100\% \quad (\text{eq. 4.2})$$

where $P_{\text{out}}(\lambda_{\text{em}})$ is the emission power of all four edges over the wavelength range (in Watt). Because only 1 edge at a time could be physically measured, total output was approximated by multiplying the single measurement by four. $P_{\text{in}}(\lambda_{\text{abs}})$ is the incoming light spectra from the solar simulator (in Watt), $A(\lambda)$ is the absorption of the sample (in %), λ is the wavelength range over which the summation is made, h is Planck's constant, and c the speed of light. For the active wavelength range (absorption 350-800 nm, emission power 450-700 nm) the calculated internal optical efficiency was $\eta_{\text{int}} = 40\%$ (10% for a single edge).

Illumination of the sample with exclusively 440 nm light initially resulted in a high emission power which dropped by more than 50% within 30 min due to the ring opening reaction to the transparent, non-fluorescent state. Illumination with 340 nm light resulted in only negligible emission power as the closed isomer shows practically no absorption at this wavelength.

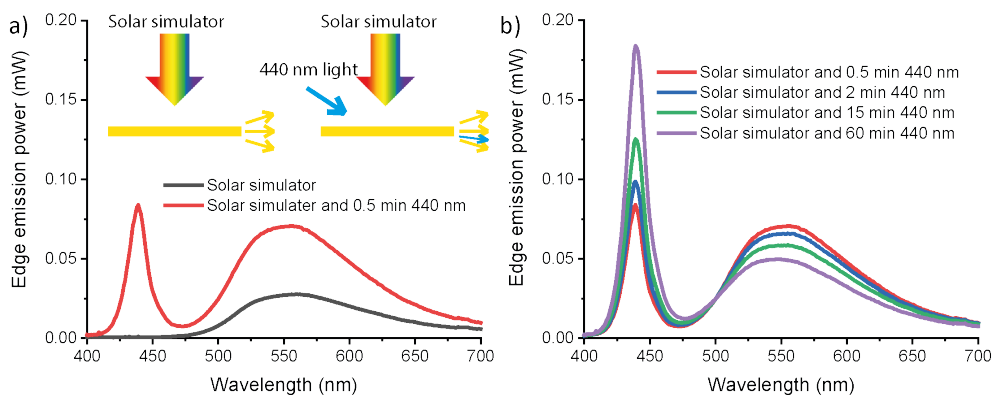


Figure 4.6: Edge emission powers of the diarylethene dye film a) upon initial illumination by a solar simulator (black line) and with additional 440 nm LED (red line) illumination (inset: schematic of the setup) followed by b) time evolution of the edge emission power during continuous exposure to solar simulator light with additional 440 nm light illumination. The short wavelength peak in the spectra is the result of LED light scattered to and escaping the edge of the lightguide; the peak increases over time as the sample becomes more transparent to these wavelengths over time.

For future applications, it would be desirable to control the color change in the LSC device in an outdoor environment, where constant solar light is illuminating the device. This control is simulated by illumination with a solar simulator until the PSS is reached, followed by supplementing the solar simulator with an additional 440 nm LED light source to alter the PSS (this sequence is illustrated as an inset in **Figure 4.6a**) and drive the device towards its open, transparent isomer. The addition of the 440 nm LED increases the light intensity on the sample resulting in an increase of emission power between 500-700 nm (see **Figure 4.6a**). After the initial increase, the transition towards the open and transparent isomer decreases the emission power (see **Figure 4.6b**), indicating that the PSS and the accompanying color and fluorescence states can be tuned to desired levels.

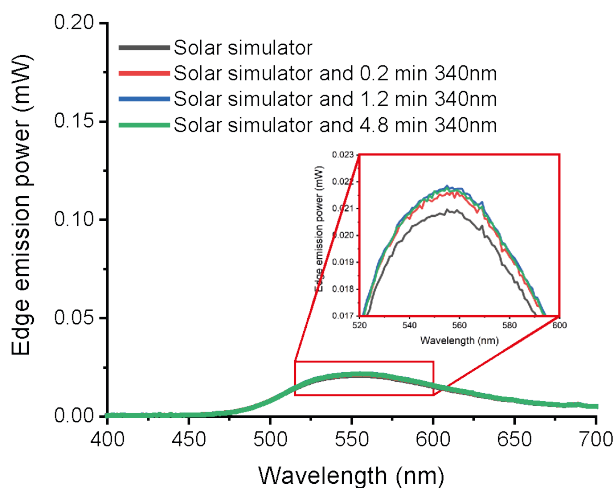


Figure 4.7: Time evolution of the edge emission power under illumination of AM1.5 solar spectrum. Inset: enlargement of the emission power peak.

To restore the original state, illumination with the 440 nm LED was ceased, allowing the sample to return to the PSS under simulated solar illumination. This was followed by illumination with a 340 nm LED, driving the dye towards its closed fluorescent state, resulting in increased emission power. The principle of this tuning is shown in **Figure 4.7**; however, the changes in the emission power are minor, resulting from the large difference in intensity between the 340 nm LED and the solar simulator (1.5 mW/cm^2 versus 22.5 mW/cm^2 , respectively) and competitive absorption of the binder, allowing for only a minor shift in the PSS of the device.

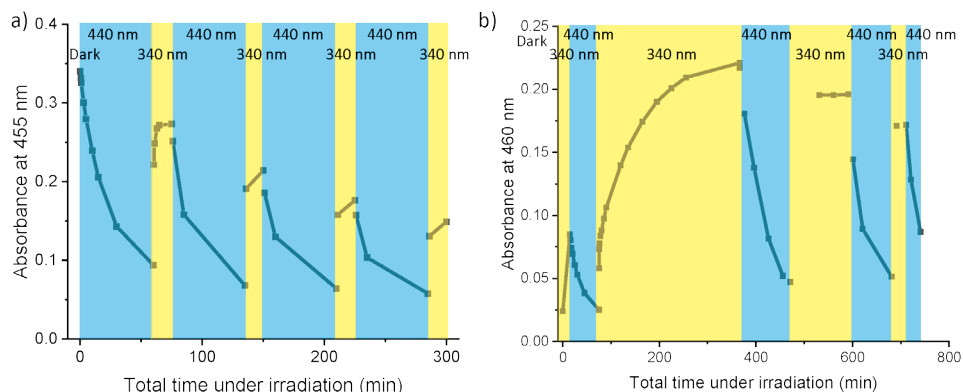


Figure 4.8: Absorbance of diarylethene dye in time during four cycles of 440 nm light and 340 nm light being applied. a) Absorbance at 455 nm in polymer matrix; b) absorbance at 460 nm in LC host.

The switching repeatability of the dye in the solid coating used in these experiments was investigated by performing four photoswitching cycles and monitoring the peak absorbance at 455 nm (see **Figure 4.8a**). The absorbance in the transparent state drops after the first cycle and reaches the same minimum value in subsequent cycles. The decreased absorbance during the 2nd cycle could be due to the PSS not having been reached. Exposure to 340 nm light results in PSS formation after 5 min, while subsequent illuminations for 15 min fail to return the previous peak value. Thus, the absorbance of the colored state drops steadily after every cycle indicating a limited repeatability.

The repeatability of the system in E7 was also tested (see **Figure 4.8b**). Since behavior similar to the polymer matrix was expected, the initial exposure to 340 nm was only 15 min and no PSS was reached. During the second exposure to 340 nm, a PSS appeared to be attained after more than 4.5 hours which is more than 50 times longer than expected from the polymer matrix. In the third cycle a PSS was achieved within 60 mins but it is likely that the PSS was already reached before that time. In the fourth cycle the PSS was already attained within 10 min which is comparable with the experiments with the polymer matrix. A possible explanation for this difference in behavior is that the dye in the polymer matrix underwent an activation during the photo polymerization step. If the first full cycle to the PSS is different compared to the subsequent cycles, the first cycle could not be monitored during polymerization while it was monitored in the E7 matrix. Therefore, it is possible that in subsequent cycles the dye shows similar behavior in both matrices.

It is unknown what the cause is for the continuous decrease in absorption peak with each cycle. Generally, diarylethene dyes are valued for their high photostability and durability in cycling.¹ For diarylethenes of which both (benzo)thiophene rings have been S,S-oxidized, thermally induced degradation has not been found. However, for diarylethenes bearing just one thiophene-S,S-dioxide it is known that a thermally induced intramolecular reaction leads to the formation of degradation products.^{23–25} As most degradation studies investigate stability of the dyes in isolation, it is unknown what effect other components in the polymer used and LC host mixture might have.

For future development and commercialization, the library of switchable fluorescent molecules should be extended to exhibit a wider variety of colors. Fortunately, the color of these molecules can be easily altered, suggesting deployment in the built environment from the aesthetic standpoint could be possible as ‘smart’ windows as advertisement banners where parts of the message could be reversibly manipulated. Finally, the color switching could find application in the LSC-photomicroreactor concept,^{21,26} allowing various reactions to be catalyzed from solar light by simply switching the color state of the embedded diarylethene.

4.4 Conclusions

In this Chapter, we have shown a diarylethene-based electrically- and photo-switchable ‘smart’ window with a potential for electricity generation. Additionally, using inkjet printing, diarylethene based coatings could be created allowing for more visually appealing designs. Printing these coatings results in the loss of the electrical switching response but will also lower the manufacturing costs as electrodes are no longer needed. The coating is capable of switching its coloration when exposed to light from LEDs as well as solar simulated light; the fluorescence escaping the edge of the underlying lightguide is affected by the switching state of the dye. The color change is reversible, although the stability at this time must be improved before real applications can be considered. A ‘manual override’ for the color change under the solar simulator was created by adding additional light from an LED. If desired, it is possible to maintain the color of the dye to a significant degree, even under full simulated sunlight. These systems could help reduce energy consumption in greenhouses and buildings by being employed as ‘smart’ windows or signage, for example.

4.5 References

- 1 M. Irie, T. Fukaminato, K. Matsuda and S. Kobatake, *Chem. Rev.*, 2014, **114**, 12174–12277.
- 2 M. Morimoto, S. Kobatake and M. Irie, *Chem. - A Eur. J.*, 2003, **9**, 621–627.
- 3 M. Irie, *Chem. Rev.*, 2000, **100**, 1685–1716.
- 4 M. Yu, H. Wang, Y. Li, P. Zhang, S. Chen, R. Zeng, Y. Gao and J. Chen, *J. Appl. Polym. Sci.*, 2019, **136**, 1–7.
- 5 D. Kitagawa and S. Kobatake, *Chem. Rec.*, 2016, **16**, 2005–2015.
- 6 S. Kobatake, H. Imagawa, H. Nakatani and S. Nakashima, *New J. Chem.*, 2009, **33**, 1362–1367.
- 7 X. Su, Y. Ji, W. Pan, S. Chen, Y.-M. Zhang, T. Lin, L. Liu, M. Li, Y. Liu and S. X.-A. Zhang, *J. Mater. Chem. C*, 2018, **6**, 6940–6948.
- 8 Y. Takagi, T. Kunishi, T. Katayama, Y. Ishibashi, H. Miyasaka, M. Morimoto and M. Irie, *Photochem. Photobiol. Sci.*, 2012, **11**, 1661.
- 9 K. Uno, H. Niikura, M. Morimoto, Y. Ishibashi, H. Miyasaka and M. Irie, *J. Am. Chem. Soc.*, 2011, **133**, 13558–13564.
- 10 M. Morimoto, Y. Takagi, K. Hioki, T. Nagasaka, H. Sotome, S. Ito, H. Miyasaka and M. Irie, *Dye. Pigment.*, 2018, **153**, 144–149.
- 11 R. Kashihara, M. Morimoto, S. Ito, H. Miyasaka and M. Irie, *J. Am. Chem. Soc.*, 2017, **139**, 16498–16501.
- 12 G. Seybold and G. Wagenblast, *Dye. Pigment.*, 1989, **11**, 303–317.
- 13 M. E. McConney, T. J. White, V. P. Tondiglia, L. V. Natarajan, D. Yang and T. J. Bunning, *Soft Matter*, 2012, **8**, 318–323.
- 14 H. Khandelwal, R. C. G. M. Loonen, J. L. M. Hensen, M. G. Debije and A. P. H. J. Schenning, *Sci. Rep.*, 2015, **5**, 11773.
- 15 M. Irie and M. Morimoto, *Bull. Chem. Soc. Jpn.*, 2018, **91**, 237–250.
- 16 P. P. C. Verbunt, A. Kaiser, K. Hermans, C. W. M. Bastiaansen, D. J. Broer and M. G. Debije, *Adv. Funct. Mater.*, 2009, **19**, 2714–2719.
- 17 M. G. Debije, *Adv. Funct. Mater.*, 2010, **20**, 1498–1502.
- 18 L. H. Slooff, E. E. Bende, A. R. Burgers, T. Budel, M. Pravettoni, R. P. Kenny, E. D. Dunlop and A. Büchtemann, *Phys. status solidi - Rapid Res. Lett.*, 2008, **2**, 257–259.
- 19 J. C. Goldschmidt, M. Peters, A. Bösch, H. Helmers, F. Dimroth, S. W. Glunz and G. Willeke, *Sol. Energy Mater. Sol. Cells*, 2009, **93**, 176–182.
- 20 L. Desmet, A. J. M. Ras, D. K. G. de Boer and M. G. Debije, *Opt. Lett.*, 2012, **37**, 3087–9.

- 21 D. Cambié, F. Zhao, V. Hessel, M. G. Debije and T. Noël, *Angew. Chemie Int. Ed.*, 2017, **56**, 1050–1054.
- 22 C. Tummeltshammer, A. Taylor, A. J. Kenyon and I. Papakonstantinou, *Sol. Energy Mater. Sol. Cells*, 2016, **144**, 40–47.
- 23 H. Shoji and S. Kobatake, *Chem. Commun.*, 2013, **49**, 2362.
- 24 D. Kitagawa, K. Tanaka and S. Kobatake, *J. Mater. Chem. C*, 2017, **5**, 6210–6215.
- 25 H. Shoji, D. Kitagawa and S. Kobatake, *New J. Chem.*, 2014, **38**, 933–941.
- 26 D. Cambié, J. Dobbelaar, P. Riente, J. Vanderspikken, C. Shen, P. H. Seeberger, K. Gilmore, M. G. Debije and T. Noël, *Angew. Chemie - Int. Ed.*, 2019, **58**, 14374–14378.

Chapter 5

Flexible Nanoporous Liquid Crystal Networks as Matrixes for FRET

Förster resonance energy transfer (FRET) is important not only to the fields of biology and biophysics, but also in opto-electronics and light guiding systems. Different matrixes are being investigated that facilitate FRET, including zeolites and metal-organic frameworks. In this Chapter, a new matrix for FRET generation is proposed: nanoporous liquid crystal networks. These liquid crystal networks can be easily processed and are able to align dichroic fluorescent dyes. A base treatment can create nanopores in the network, which are then able to absorb a second fluorescent dye in an aqueous phase while still retaining good alignment. Using lifetime measurements, we provide proof that even in this non-optimized system, around 70% of the energy was transferred via the FRET mechanism from one dye to the other. Liquid crystal networks have many advantageous over current matrixes as they are easy fabricate, flexible and could be modified to selectively and reversely absorb dyes, allowing many new applications.

This chapter is partially reproduced from: G. H. Timmermans, M. van der Heijden, B. M. Oosterlaken, S. C. J. J. Meskers, A. P. H. J. H. J. Schenning, and M. G. Debije, "Flexible Nanoporous Liquid Crystal Networks as Matrixes for Förster Resonance Energy Transfer (FRET)," *ACS Appl. Nano Mater.* 3, 3904–3909 (2020)

5.1 Introduction

For a more fundamental look at light guiding, we investigate an anisotropic nanoporous polymer matrix for facilitating the transfer of energy between different fluorescent dyes via Förster resonance energy transfer (FRET).¹ FRET is an important physical phenomenon whose applications have expanded tremendously in the last 30 years, especially in the biological and biophysical fields.²⁻⁴ Additional applications include optoelectronics,^{2,5} micro fluidic sensors,⁶ reducing Stokes shift losses in luminescent solar concentrators^{7,8} and slowing the effects of photodegradation in dyes.⁹

There are a few criteria that must be satisfied for FRET to occur efficiently between two molecules: 1) the fluorescence emission spectrum of the donor and absorption spectrum of the acceptor need to overlap,⁵ 2) the donor and the acceptor need to be in close proximity to one another, typically 1 to 10 nm^{5,10,11} 3) the transition dipoles of the donor and acceptor need to be approximately parallel^{2,5} and 4) the fluorescence lifetime of the donor must be sufficiently long to allow FRET to occur.²

It would be desirable to generate FRET by bringing donor and acceptor molecules into close contact without relying on high concentrations to minimize the distance between the molecules,^{11,12} but not only from a cost perspective: in biological sensing applications, for example, one prefers to deploy the minimum dose of foreign species in the living system.^{3,6} High concentrations of dyes in light control systems may also result in strong reabsorption of emitted light leading to reduced efficiency.⁷ Furthermore, solubility of the dyes in the host medium is often limited, so higher concentrations are often not even possible.¹³ Current techniques to minimize the distance between the luminophores without relying on high doping concentrations are by physically linking the interacting molecules¹⁴ or incorporating them in highly aligned structures¹⁵ such as metal organic frameworks (MOF),^{16,17} zeolites,^{18,19} or other materials.^{20,21}

In this Chapter, we propose a new way of bringing two dyes at low concentrations into close proximity in a controlled manner for efficient FRET generation by using a self-assembling, all-organic flexible network with aligned fluorescent molecules in liquid crystal (LC) host films containing reversible channel structures. By opening the channels using a base treatment, nanopores are created in the LC film which allow absorption of a second fluorescent dye, bringing the two dyes in close contact, one in the LC network, one in the channel. Liquid crystals networks (LCNs) have shown to be able to selectively absorb²² and align organic dyes,^{23,24} and even facilitate FRET,^{8,25,26} but never has the selective absorption been combined with the alignment of a second fluorescent dye for the purpose of FRET generation.

5.2 Experimental

Monomer 1 4-(4-(4-(6-acryloyloxyhexyloxy)benzoyloxy)benzoyloxy)-(6-acryloyloxyhexyloxy)benzene was supplied and synthesized by Synthron Chemicals as described in the literature²⁷ and monomer 2 (4-(6-acryloyloxyhexyloxy)benzoic acid) was supplied by Synthron Chemicals. The photo-initiator (1-hydroxycyclohexylphenylketone) was obtained from Ciba Specialty Chemicals and the thermal inhibitor (p-methoxyphenol) from Sigma Aldrich. These chemical structures are shown in **Figure 5.1**. Dye 1 (DFSB-K160, a coumarin derivative from RiskReactor), Dye 2 (Rhodamine B, $\geq 95\%$ (HPLC), obtained from Sigma Aldrich) and Dye 3 (Fluorescein, 95%, obtained from Sigma Aldrich) were used as received. Dye 2 is water soluble and exists in a protonated acidic or an unprotonated zwitterionic salt form at pH 2 and 8, respectively.^{28–30}

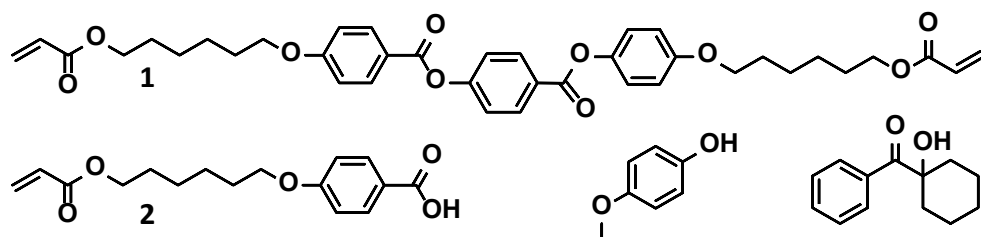


Figure 5.1: The chemical structures of: monomer 1 (top), monomer 2 (bottom left), the thermal inhibitor (bottom center), the photo initiator (bottom right).

An LC mixture was made based on the literature^{31,32} with monomers 1 and 2 in a 50/50 w/w ratio. Additionally, 0.2 wt% of Dye 1, 0.5 wt% of the photoinitiator and 0.2 wt% of the thermal inhibitor were added.

Glass plates of 3 x 3 cm² were cleaned and a layer of planar polyimide (OPTMER AL 1051, JSR Corporation, Tokyo, Japan) was spincoated (Karl Suss RC8, 40 seconds at 5000 rpm) onto the cleaned glass plates. After spincoating, the glass plates were baked for 1.5 hours at 180 °C and rubbed over a velvet cloth to induce planar alignment. Cells were fabricated by gluing two rubbed plates together using glue containing 20 μm glass spacer beads in an antiparallel fashion with a small offset at the edges.

Cells were filled with the LC mixture in the isotropic phase at 120 °C by capillary action. After filling, the cells were cooled to 107 °C and then slowly cooled to 95 °C (smectic phase A)³³ at 1 °C per minute (see Figure S1). The LC mixture was photopolymerized at 95 °C using a high intensity UV-lamp (Omnicure EXFO, series 2000) at 2–4 mW/cm² for 10 minutes. After photopolymerization, the cell was opened and a free-standing film was obtained.

The films were immersed in a 0.1 M potassium hydroxide (KOH) solution for 1 hour to open the hydrogen bonds and create a porous structure.³⁴ Thereafter, two different dye concentrations c_1 and c_2 (0.0014 and 0.0010 wt% of Dye 2 in water, respectively), were allowed to infiltrate into the nanopores for 24 hours.

A schematic overview of the process is shown in **Figure 5.2**. Differential scanning calorimetry (DSC) was performed under a nitrogen atmosphere using a TA Instruments Q1000 DSC equipped with an RCS90 cooling accessory. Polarized optical microscopy (POM) studies were conducted on a Leica DM2700 microscope equipped with a Leica MC170 HD camera, or on a Leica DM 6000 M microscope using a Leica DFC420 C camera. The absorption spectra were measured with a Perkin Elmer Lambda 750 UV/Vis/NIR spectrophotometer equipped with a 150 mm integrating sphere. Infrared (IR) spectra of the films were measured with a Varian 670-IR FT-IR spectrometer equipped with a golden gate (an ATR accessory).

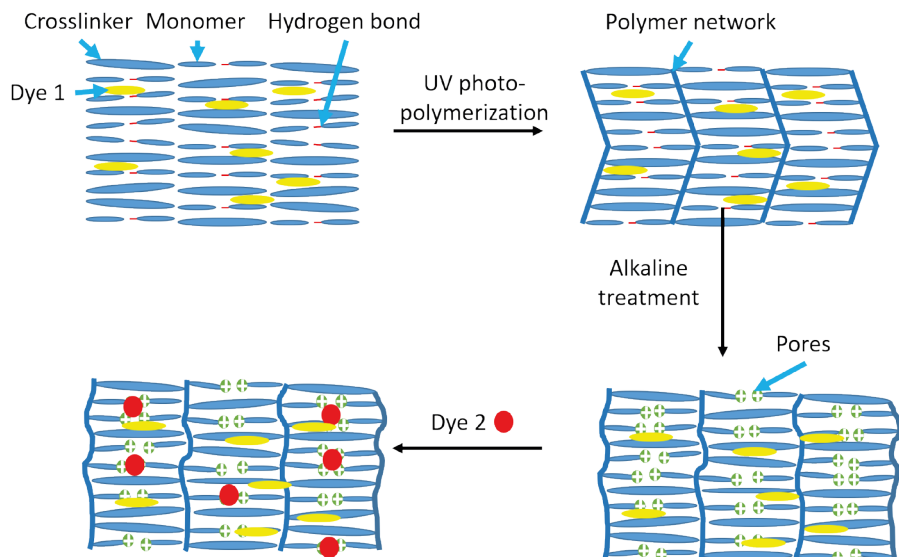


Figure 5.2: Schematic overview of the porous film fabrication process. (Top left) The initial smectic aligned LC film containing aligned Dye 1. (Top right) Polymerization by exposure to UV light. By exposing the films to a KOH alkaline treatment, the hydrogen bonds are broken (Bottom right). Dye 2 is introduced in solution and competes out the K^+ in the channels of the LC film, bringing the two dyes in close proximity to each other (Bottom left).

The fluorescence lifetime and photoluminescence (PI) spectra were obtained with an Edinburgh Instruments LifeSpec-ps spectrophotometer with a Peltier cooled Hamamatsu microchannel plate photomultiplier for detection and coupled to a 400 nm pulsed laser (PicoQuant LDH-C 400, 2.5 MHz; PicoQuant PDL 800-B driver) for the excitation of the

analyte with power kept below 1 mW using a diaphragm. The fluence of a single pulse is 10^{-8} J/cm². The fluorescence lifetime were fitted with a multiexponential fit by reconvolution of the instrument response function (IRF) using $I(t) = \int_{-\infty}^t IRF(t') \sum_{i=1}^n A_i \exp\left[-\frac{t-t'}{\tau_i}\right] dt'$, where A_i is the amplitude of the i th component with a lifetime τ_i . Using the software packaged FluoFit 4.1 of PicoQuant the decay parameters were recovered. Confocal microscopy was performed on a Leica DMI8 microscope equipped with a Leica HC PL APO CS2 (20x/0.75 DRY) objective, three lasers (405 nm, 488 nm and 638 nm) and a Leica hybrid detector (HyD) and a normal photomultiplier (PMT) detector.

A Transmission Electron Microscope (TEM) was used to obtain the layer-spacing of the LCN, calculated with Fast Fourier Transform (FFT). The LCN was embedded in EMS Epofix embedding resin and was cross cut using a Reichert-Jung Ultracut-E ultramicrotome set to 70 nm thickness and 3 mm/s cutting speed. Slices were picked up with an EMS perfect loop and placed on a continuous carbon TEM grid, 200 mesh copper support. TEM imaging was performed under 4 μ m defocus on a Tecnai 20, type Sphera, operating at 200 kV and equipped with an LaB6 filament. The images were acquired with an electron dose of 4 e- \AA^{-2} per image on a 2k x 2k Gatan CCD camera.

5.2.1 Determining the fluorescence quantum yield

The fluorescence quantum yield (ϕ_f) of Dye 1 was determined using Dye 3 (fluorescein) as reference. The fluorescence emission and absorption spectra of Dye 1 in xylene and Dye 3 in 0.1 M NaOH were measured (see **Figure 5.3**).

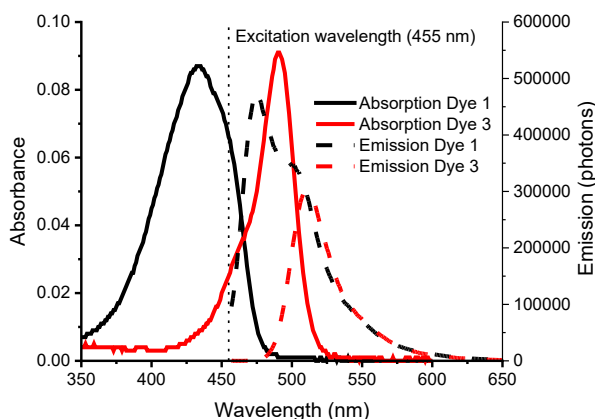


Figure 5.3: Absorption (solid lines) and emission (dotted lines) of Dye 1 in xylene (red) and Dye 3 in 0.1 M NaOH (black).

The ϕ_f could then be calculated from equation 5.1:³⁵

$$\phi_{f,i} = \frac{F_i * f_r * n_i^2}{F_r * f_i * n_r^2} * \phi_r \quad (\text{eq. 5.1})$$

where, F is the integrated fluorescent emission (excited at 455 nm), f is the absorption factor (at 455 nm), n is the refractive index and the subscript r and i refer to the reference and the sample, respectively. Using the values in **Table 5.1** and equation 5.1 results in an ϕ_f for Dye 1 in xylene of ~ 0.97 .

Table 5.1: Measured and literature data of Dye 3 in 0.1 M NaOH and Dye 1 in xylene for ϕ_f determination.

Sample	Integrated fluorescent emission (F)	Absorption factor (f)	Refractive index (n)	ϕ_f
Dye 3 in 0.1 M NaOH	12.8 *106	0.056	1.3336	0.9237
Dye 1 in xylene	26.7*106	0.141	1.5038	0.97

5.3 Results and discussion

The fluorescent dyes chosen as the donor and acceptor should have a good overlap of the emission spectrum of the donor (Dye 1) and the absorption spectrum of the acceptor (Dye 2) for efficient FRET. The donor chosen was a coumarin based dye (Dye 1) with a $\phi_f > 90\%$ and good solubility and alignment in the LC host.³⁰ The acceptor needed to be water soluble with good spectral overlap with Dye 1: as a model system, we selected Rhodamine B (Dye 2, ϕ_f in water $\sim 20\%$).³⁹ Coumarin/Rhodamine dye pairs have been used previously in FRET pair studies.⁴⁰ The absorption and emission of the two dyes is shown in **Figure 5.4** from which it was calculated that Dye 2 is able to absorb $\sim 46\%$ of the emission spectra of Dye 1.

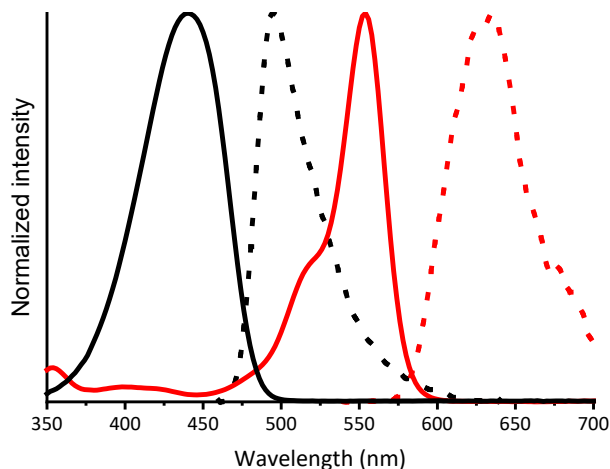


Figure 5.4: Normalized absorption (solid black line) and emission (dotted black line) spectra of Dye 1 and normalized absorbance (solid red line) and emission (dotted red line) spectra of Dye 2 in the LCN.

The fabricated films were flexible and could easily be bent by hand without damaging the structures, as shown in **Figure 5.5a**. To confirm the formation and opening of the LCN nanopore structure, the hydrogen bonds formed between the carboxylic acid moieties of the monoacrylates were monitored with Fourier Transform Infrared (FTIR). In **Figure 5.5b**, one follows the three sample preparation steps: immediately after polymerization, after KOH treatment, and after infiltration of Dye 2. The formation of the hydrogen bonds is monitored by the 1678 cm^{-1} peak, associated with the C=O stretch vibration in cyclic carboxylic acid dimers.³² After the alkaline treatment with 0.1 M KOH for 1 hour, the FTIR spectrum showed the breaking of the hydrogen bonds and the formation of carboxylic anions (COO^- formation at 1539 cm^{-1} and 1384 cm^{-1}). The formation of carboxylic anions is accompanied with the activation of the LCN and therefore the formation of the anionic nanopores. After the infiltration of Dye 2, the absorbance peaks at 1678 cm^{-1} increased again, indicating that some hydrogen bonds reformed, while the peaks at 1538 cm^{-1} and 1383 cm^{-1} decreased, indicating that the number of carboxylic anion groups decreased.

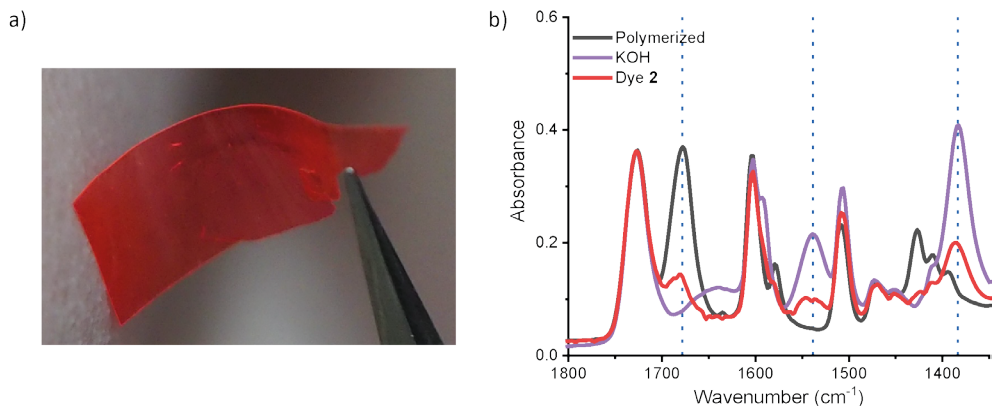


Figure 5.5: a) Photograph of a piece of a typical LCN film showing its flexibility. b) FTIR spectra of sample immediately after polymerization (black line), after KOH treatment (violet line) and after infiltration of Dye 2 (red line). Vertical blue lines denote the positions of H-bonds (1678 cm^{-1}), and carboxylate anions (1539 cm^{-1} and 1384 cm^{-1}).

POM (see **Figure 5.6**) confirms the ordering of LC in the film retains smectic C order throughout the nanopore opening procedure in correspondence with literature.³³

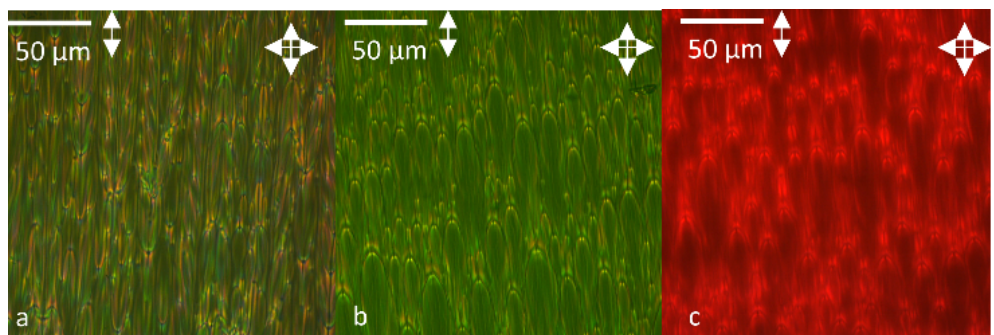


Figure 5.6: POM photographs of the LCN at 500x magnification. a) After polymerization; b) after base treatment, and c) after infiltration with Dye 2. The single arrow shows the alignment direction of the substrate and the crossed arrows represent the axes of the crossed polarizers.

Alignment of dyes in the LCN can be described using the order parameter, S , where S is defined using equation 5.2 as:⁴¹

$$S = \frac{A_{par} - A_{per}}{A_{par} + 2A_{per}} \quad (\text{eq. 5.2})$$

where A_{par} and A_{per} are the peak absorbance when the film is exposed to light polarized parallel and perpendicular to the LC alignment direction, respectively. The order parameter for Dye 1 was determined to be $S = 0.3$ and showed only minor fluctuations (± 0.03) during the entire process, indicating alignment within the LCN. After infiltration it was found that the disc-like Dye 2 did not align with the LCN nanopores ($S = 0.05$), but as this dye does not show alignment in LCN matrixes, either,²³ this result was expected. Ideally, one would desire a dye that would align in a controlled way in the nanopores, and future work will involve identifying such dyes.

TEM was used to study the layer spacing of the samples. The red arrow in **Figure 5.7a** shows the alignment of the layers of the LCN after infiltration with Dye 2. For a hydrogen-bonded network with the same monomer composition, literature reports a layer-spacing of 3.8 nm for the polymerized LCN and a layer-spacing of around 3.4 nm after alkaline treatment.³² Fast Fourier Transform (FFT) of the TEM image (**Figure 5.7b**) resulted in an intermediate value 3.65 ± 0.02 nm, which is expected, as after infiltration of Dye 2 the LCN has reformed some hydrogen-bonds, resulting in a layer-spacing intermediate to the hydrogen-bonded and fully opened networks.

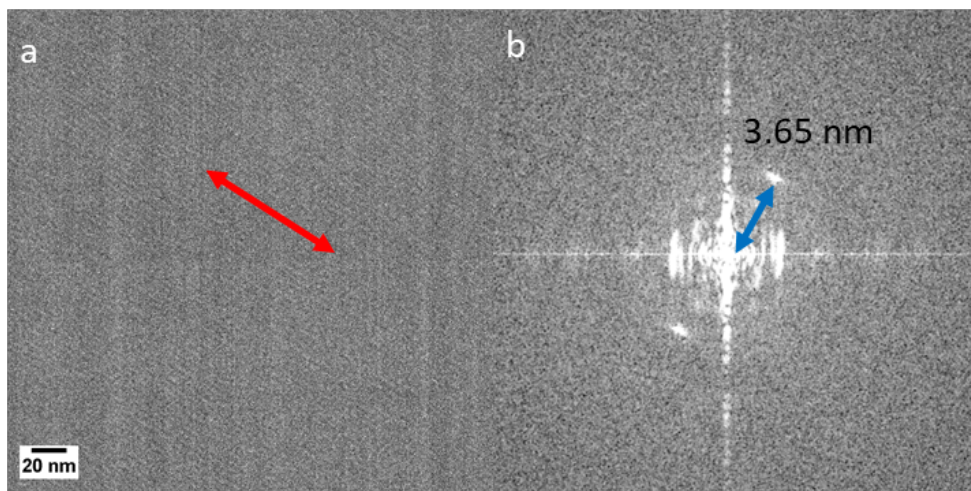


Figure 5.7. a) TEM picture of the cross-cut of the LCN with the red arrow showing the alignment direction of the nanopores and b) FFT of the TEM image showing the layer-spacing of 3.65 nm.

The weight fraction of Dye 2 (w_2) adsorbed in the network was investigated by measuring the absorption of the Dye 2 solutions before and after soaking the samples and calculated by equation 5.3:

$$w_2 = \frac{V(c_i - c_a) * M_w}{M_f} \quad (\text{eq. 5.3})$$

where c_i and c_a are the concentrations of Dye 2 in the initial solution [mol L^{-1}] and after soaking, respectively, V is the volume of the Dye solution [L], M_w is the molecular weight of Dye 2 [gram mol^{-1}] and M_f is the weight of the film [gram]. The Dye 2 concentration in the solution before and after absorption was calculated from their absorption peaks and the Lambert-Beer law. From these calculations it was estimated that film c1 contained 0.30 wt% Dye 2 and film c2 contained 0.26 wt% of Dye 2, which are in the same range as the 0.20 wt% of Dye 1 present in the film.

Fluorescent confocal microscopy was used to estimate the distribution of Dye 2 through the depth of an infiltrated freestanding film. With two lasers, Dye 1 and Dye 2 could be separately excited and the resulting fluorescence measured over a $0.6 \times 0.6 \text{ mm}^2$ area. By comparing the dye penetration of Dye 1 and Dye 2, the diffusion of the Dye 2 into the network can be evaluated, as Dye 1 is assumed to be evenly spread through the network. The spectrum of a freestanding film with 0.73 wt% Dye 2 is shown in **Figure 5.8**: the distribution of the measured fluorescence is relatively constant throughout the film depth and follows the fluorescence of Dye 1 quite closely, suggesting an equal distribution of Dye 2 throughout the freestanding film depth.

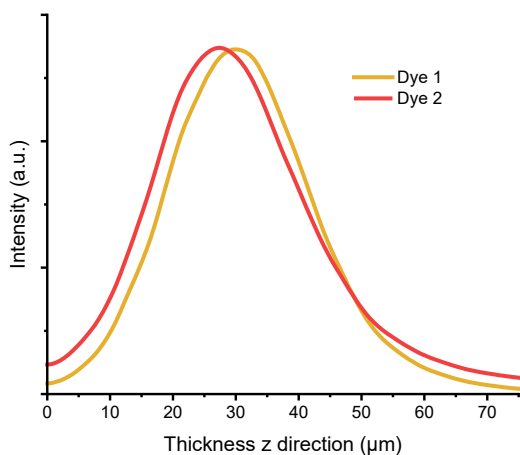


Figure 5.8: The normalized intensity of the fluorescence of Dye 1 (orange) and Dye 2 (red) over the approximately 20 μm thickness of a freestanding film using fluorescent confocal microscopy.

The photoluminescence emission spectra of the films c1 and c2 excited at 400 nm both show the characteristic emission peaks of Dye 1 at 495 nm and of Dye 2 at 588 nm; see **Figure 5.9**. This indicates that there is energy transfer from Dye 1 to Dye 2, as Dye 2 itself has almost no absorption at 400 nm (see Figure 5.4).

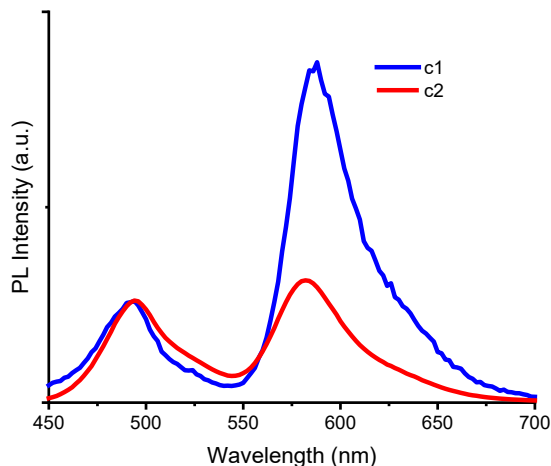


Figure 5.9: The fluorescence emission spectra of films c1 and c2, each excited at 400 nm, normalized to unit intensity for the first peak.

To distinguish if the energy transfer from Dye 1 to Dye 2 is primarily due to FRET or simple reabsorption and reemission events, fluorescence lifetimes were measured. In **Figure 5.10**, the lifetime spectra of a film with only Dye 1 and two films containing both Dye 1 and Dye 2 (c1 and c2), show that the films containing Dye 2 have a faster decay in the lifetime. The decay of the fluorescence can be described by a biexponential function and a non-linear least squares analysis taking into account the finite instrument response yields the following excited state lifetimes for Dye 1 for c1 : 0.61 ns (70%) and 1.85 ns (30%). For c2: 1.01 ns (49%) and 2.16 ns (51%). From this, an average lifetime was calculated to be 0.98 ns for c1 and 1.60 ns for c2, while the lifetime for a system containing only Dye 1 was 3.04 ns. The energy transfer efficiency (E) was calculated using equation 5.4:⁴²

$$E = 1 - \frac{\tau_{DA}}{\tau_D} \quad (\text{eq. 5.4})$$

where τ_{DA} is the lifetime of the donor in the presence of the acceptor and τ_D is the lifetime of the donor in the absence of the acceptor. From this, efficiencies for energy transfer via non-trivial mechanisms of 0.7 for film c1 and 0.5 for film c2 were calculated, which are comparable to other non-liquid crystal based systems.^{43,44}

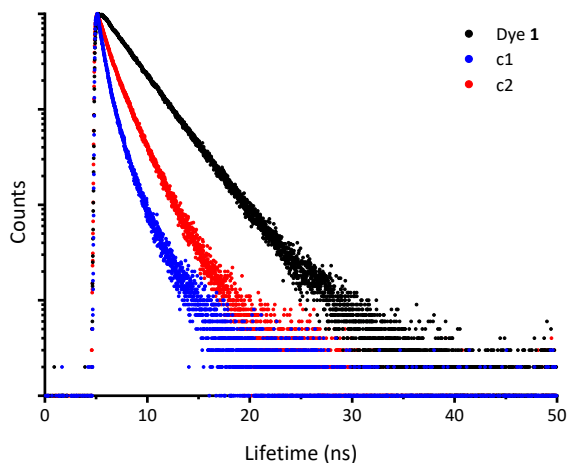


Figure 5.10: Normalized single photon counting measurement of the fluorescence decay for a film containing only Dye 1 (black line), and for film c1 (blue line) and film c2 (red line). Excitation with a light pulse of 400 nm wavelengths and ~ 100 ps temporal width.

Adding Dye 2 directly to the initial LC mixture (0.1; 0.2; 0.4 wt%) without opening of the pores and polymerizing in the isotropic state also results in energy transfer from Dye 1 to Dye 2, as can be seen in **Figure 5.11a**. However, the average fluorescence lifetimes were determined to be between 2.3-2.4 ns for all concentrations (**Figure 5.11b**). These lifetimes correspond to much lower energy transfer efficiencies, *i.e.* 0.2-0.3. This low energy transfer efficiency shows that the ordering of Dye 1 in the smectic C phase and absorption of Dye 2 in the pores significantly improves the energy transfer via the FRET mechanism over random mixing.

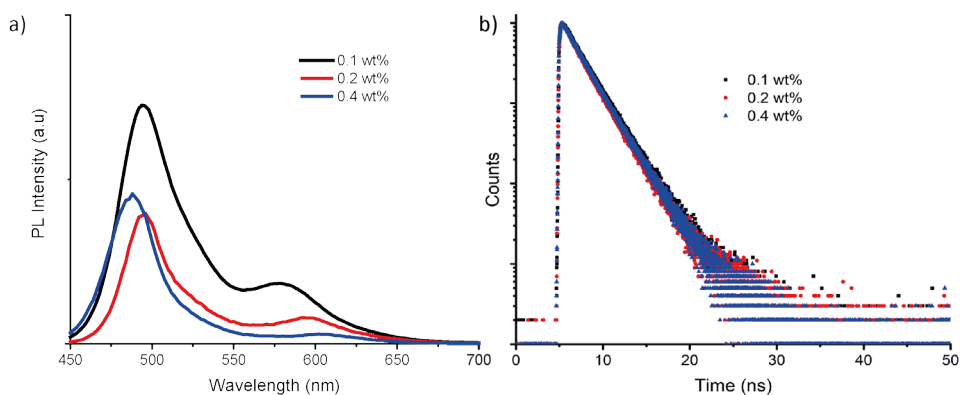


Figure 5.11: a) The fluorescence emission spectra, and b) the normalized single photon counting measurement of the fluorescence decay for isotropic films containing 0.1; 0.2; 0.4 wt% Dye 2. Excitation with a light pulse of 400 nm wavelengths and ~ 100 ps temporal width

While we have demonstrated FRET between the LC-embedded Dye 1 and the channel infiltrated Dye 2, the performance of this dye coordination system could be significantly improved. Firstly, Dye 2 is a rather poor performing dye; replacing it with one with higher ϕ_f could have considerable impact on emissions. It should also be possible to compete out the infiltrated dye with other dyes which have higher affinity for the nanopores, or by changing pH to displace the occupying dye,^{22,45} again increasing the system versatility. Modification of the nanopore size, layer spacing,^{22,46} ordering⁴⁷ and binding nature of the nanopore interior could allow alignment of dyes within the channels, improving the degree of control over the light emission directions.⁴⁸ Better control of directionality of light emission open up potential applications in solar energy,⁷ daylighting,⁴⁹ and horticulture.⁵⁰

5.4 Conclusions

A flexible organic host matrix for enhanced light control was investigated. An aligned liquid crystal polymer network containing a fluorescent dye was created. After opening the nanopores in the network, a second fluorescent dye was infiltrated. During these procedures the alignment and ordering of the network remained constant. This network was able to transfer almost 70% of the energy of the donor dye in the liquid crystal to the acceptor dye in the channels via FRET. Liquid crystal networks potentially provide many new opportunities for sensing and light guiding purposes.

5.5 References

- 1 Z. Dai, L. Dähne, E. Donath and H. Möhwald, *J. Phys. Chem. B*, 2002, **106**, 11501–11508.
- 2 S. A. Hussain, *ResearchGate*.
- 3 R. M. Clegg, in *FRET and film techniques*, Elsevier B.V., 2009, vol. 33, pp. 1–57.
- 4 L. M. S. Loura, R. F. M. de Almeida, L. C. Silva and M. Prieto, *Biochim. Biophys. Acta - Biomembr.*, 2009, **1788**, 209–224.
- 5 Z. Limpouchová and K. Procházka, Springer, Third edit., 2016, pp. 91–149.
- 6 S. S. Varghese, Y. Zhu, T. J. Davis and S. C. Trowell, *Lab Chip*, 2010, **10**, 1355–1364.
- 7 M. G. Debije and P. P. C. Verbunt, *Adv. Energy Mater.*, 2012, **2**, 12–35.
- 8 J. Ter Schiphorst, A. M. Kendhale, M. G. Debije, C. Menelaou, L. M. Herz and A. P. H. J. Schenning, *Chem. Mater.*, 2014, **26**, 3876–3878.
- 9 A. M. Mooney, K. E. Warner, P. J. Fontecchio, Y.-Z. Zhang and B. P. Wittmershaus, *J. Lumin.*, 2013, **143**, 469–472.
- 10 H. C. Ishikawa-Ankerhold, R. Ankerhold and G. P. C. Drummen, *Molecules*, 2012, **17**, 4047–4132.
- 11 C. Tummeltshammer, A. Taylor, A. J. Kenyon and I. Papakonstantinou, *J. Appl. Phys.*, 2014, **116**, 173103.
- 12 B. Balaban, S. Doshay, M. Osborn, Y. Rodriguez and S. A. Carter, *J. Lumin.*, 2014, **146**, 256–262.
- 13 R. O. Al-Kaysi, T. Sang Ahn, A. M. Müller and C. J. Bardeen, *Phys. Chem. Chem. Phys.*, 2006, **8**, 3453–3459.
- 14 C. Tummeltshammer, M. Portnoi, S. A. Mitchell, A. T. Lee, A. J. Kenyon, A. B. Tabor and I. Papakonstantinou, *Nano Energy*, 2017, **32**, 263–270.
- 15 K. V. Rao, K. K. R. Datta, M. Eswaramoorthy and S. J. George, *Chem. - A Eur. J.*, 2012, **18**, 2184–2194.

- 16 E. A. Dolgoplova, A. M. Rice, C. R. Martin and N. B. Shustova, *Chem. Soc. Rev.*, 2018, **47**, 4710–4728.
- 17 O. Shekhhah, J. Liu, R. A. Fischer and C. Wöll, *Chem. Soc. Rev.*, 2011, **40**, 1081.
- 18 D. Brühwiler, G. Calzaferri, T. Torres, J. H. Ramm, N. Gartmann, L.-Q. Dieu, I. López-Duarte and M. V. Martínez-Díaz, *J. Mater. Chem.*, 2009, **19**, 8040.
- 19 A. Devaux and G. Calzaferri, *Int. J. Photoenergy*, 2009, **2009**, 1–9.
- 20 S. Peralta, J.-L. Habib-Jiwan and A. M. Jonas, *ChemPhysChem*, 2009, **10**, 137–143.
- 21 D. Dinda, A. Gupta, B. K. Shaw, S. Sadhu and S. K. Saha, *ACS Appl. Mater. Interfaces*, 2014, **6**, 10722–10728.
- 22 H. P. C. van Kuringen, G. M. Eikelboom, I. K. Shishmanova, D. J. Broer and A. P. H. J. Schenning, *Adv. Funct. Mater.*, 2014, **24**, 5045–5051.
- 23 P. P. C. Verbunt, A. Kaiser, K. Hermans, C. W. M. Bastiaansen, D. J. Broer and M. G. Debije, *Adv. Funct. Mater.*, 2009, **19**, 2714–2719.
- 24 A. M. Kendhale, A. P. H. J. Schenning and M. G. Debije, *J. Mater. Chem. A*, 2013, **1**, 229–232.
- 25 B. Zhang, C. Gao, H. Soleimaninejad, J. M. White, T. A. Smith, D. J. Jones, K. P. Ghiggino and W. W. H. Wong, *Chem. Mater.*, 2019, **31**, 3001–3008.
- 26 J. A. H. P. Sol, V. Dehm, R. Hecht, F. Würthner, A. P. H. J. Schenning and M. G. Debije, *Angew. Chemie Int. Ed.*, 2018, **57**, 1030–1033.
- 27 R. A. M. Hikmet, J. Lub and A. J. W. Tol, *Macromolecules*, 1995, **28**, 3313–3327.
- 28 C. J. Stephenson and K. D. Shimizu, *Org. Biomol. Chem.*, 2010, **8**, 1027–32.
- 29 F. Lopez Arbeloa, T. Lopez Arbeloa, M. J. Tapia Estevez and I. Lopez Arbeloa, *J. Phys. Chem.*, 1991, **95**, 2203–2208.
- 30 H. Weininger, J. Schmidt and A. Penzkofer, *Chem. Phys.*, 1989, **130**, 379–387.
- 31 D. Dasgupta, I. K. Shishmanova, A. Ruiz-Carretero, K. Lu, M. Verhoeven, H. P. C. van Kuringen, G. Portale, P. Leclère, C. W. M. Bastiaansen, D. J. Broer and A. P. H. J. Schenning, *J. Am. Chem. Soc.*, 2013, **135**, 10922–10925.
- 32 C. L. Gonzalez, C. W. M. Bastiaansen, J. Lub, J. Loos, K. Lu, H. J. Wondergem and D. J. Broer, *Adv. Mater.*, 2008, **20**, 1246–1252.
- 33 B. M. Oosterlaken, Y. Xu, M. M. J. Rijt, M. Pilz da Cunha, G. H. Timmermans, M. G. Debije, H. Friedrich, A. P. H. J. Schenning and N. A. J. M. Sommerdijk, *Adv. Funct. Mater.*, 2020, **30**, 1907456.
- 34 I. K. Shishmanova, C. W. M. Bastiaansen, A. P. H. J. Schenning and D. J. Broer, *Chem. Commun.*, 2012, **48**, 4555–4557.
- 35 A. M. Brouwer, *Pure Appl. Chem.*, 2011, **83**, 2213–2228.
- 36 Z.-C. Yang, M. Wang, A. M. Yong, S. Y. Wong, X.-H. Zhang, H. Tan, A. Y. Chang, X. Li and J. Wang, *Chem. Commun.*, 2011, **47**, 11615.
- 37 J. Shen and R. D. Snook, *Chem. Phys. Lett.*, 1989, **155**, 583–586.
- 38 K. M. Sumer and A. R. Thompson, *J. Chem. Eng. Data*, 1968, **13**, 30–34.
- 39 U. Brackmann, *Lambdachrome Laser Dyes*, Lambda Physik, Göttingen, Germany, 2nd Revise., 1997.
- 40 X. Luo, X.-D. He, Y.-C. Zhao, C. Chen, B. Chen, Z.-B. Wu and P.-Y. Wang, *J. Heterocycl. Chem.*, 2017, **54**, 2650–2655.
- 41 J. Lub, D. J. Broer, R. T. Wegh, E. Peeters and B. M. I van der Zande, *Mol. Cryst. Liq. Cryst.*, 2005, **429**, 77–99.
- 42 Y. Sun, H. Wallrabe, S. Seo and A. Periasamy, *ChemPhysChem*, 2011, **12**, 462–474.
- 43 S. Ramachandra, Z. D. Popovic', K. C. Schuermann, F. Cucinotta, G. Calzaferri and L. De Cola, *Small*, 2011, **7**, 1488–1494.
- 44 F. Cucinotta, A. Guenet, C. Bizzarri, W. Mróz, C. Botta, B. Milián-Medina, J. Gierschner and L. De Cola, *Chempluschem*, 2014, **79**, 45–57.
- 45 M. Moirangthem, R. Arts, M. Merx and A. P. H. J. Schenning, *Adv. Funct. Mater.*, 2016, **26**, 1154–1160.
- 46 A. Longo, D. J. Mulder, H. P. C. van Kuringen, D. Hermida-Merino, D. Banerjee, D. Dasgupta, I. K. Shishmanova, A. B. Spoelstra, D. J. Broer, A. P. H. J. Schenning and G. Portale, *Chem. - A Eur. J.*, 2017, **23**, 12534–12541.
- 47 T. Liang, H. P. C. van Kuringen, D. J. Mulder, S. Tan, Y. Wu, Z. Borneman, K. Nijmeijer and A. P. H. J. Schenning, *ACS Appl. Mater. Interfaces*, 2017, **9**, 35218–35225.
- 48 P. P. C. Verbunt, T. M. de Jong, D. K. G. de Boer, D. J. Broer and M. G. Debije, *Eur. Phys. J. Appl. Phys.*, 2014, **67**, 10201.
- 49 A. A. Earp, G. B. Smith, J. Franklin and P. Swift, *Sol. Energy Mater. Sol. Cells*, 2004, **84**, 411–426.
- 50 C. Corrado, S. W. Leow, M. Osborn, I. Carbone, K. Hellier, M. Short, G. Alers and S. A. Carter, *J. Renew. Sustain. Energy*, 2016, **8**, 043502.

Chapter 6

Technological assessment

This chapter is partially reproduced from: G. H. Timmermans, S. Hemming, E. Baeza, E. A. J. van Thoor, A. P. H. J. Schenning, and M. G. Debije, "Advanced Optical Materials for Sunlight Control in Greenhouses," *Adv. Opt. Mater.* 8, 2000738 (2020)

6.1 Introduction

In Chapters 2-4, various ‘smart’ windows have been described that can tune their optical properties upon exposure to external stimuli by making use of dichroic dyes and liquid crystals (LCs). The electrical and thermal responses originated from the LC host in Chapter 2, but in Chapter 3 the dye was designed to respond to changes in temperature. To enable a more rapid change, a photochromic dye was developed in Chapter 4 which could also be printed as a coating. In Chapter 5, LCs were used to fabricate a nanoporous matrix that facilitates Förster resonance energy transfer (FRET) between two fluorescent dyes for efficient light guiding.

In this Chapter, a technological assessment is given on the advanced optical materials presented in the thesis. The two main limitations of these devices (their untested stabilities and uncertain scalabilities) are discussed, and a short evaluation on the potential impacts of these systems on greenhouses is given. In addition, preliminary work on ‘smart’ blinds is presented as a potentially more robust alternative to standard ‘smart’ windows, and on lightguides for improving lighting conditions in lower areas of greenhouses.

The work in this thesis is developed in an academic environment and therefore a large gap remains before this research can be implemented industrially. When implementing this research, the initial focus should be a high margin market, where the technology can have a large impact. For this reason, high value crops such as ornamentals (*e.g.* potted plants, flowers) are of interest; alternatively, initial deployment could be in the built environment. As most of the systems in this thesis decrease the total amount of photosynthetically active radiation (PAR), shade loving plants and regions with high sunlight intensities are of special interest for application.

6.2 Stability

Perhaps the main roadblock to widespread acceptance of responsive optical materials, besides the potential additional costs, is the fatigue of the materials. The devices discussed in this thesis use polymers, dyes and LCs that have been known to degrade from UV exposure, for example. For growers to seriously consider using these devices, extended lifetimes are required. Therefore, the stability of the new devices should be determined.

Although not extensively covered in this thesis, there are many strategies to extend the lifetime of the various devices described here. A simple way to greatly reduce the harmful effects of UV-light on the stability is addition of UV-absorbers to prevent the harmful irradiation from reaching the UV-sensitive components. LCD screens (containing LCs and

using similar technologies) have long lifetimes and are even used outdoors by making use of UV-protective coatings, indicating that these stability issues can be overcome.¹

The coating from Chapter 4 might experience polymer degradation and the standard solution of adding UV-absorbers would probably hinder the photo-switching. A solution to these issues would be to develop dyes that respond to longer wavelengths of light, but care must be taken not to affect the PAR light. Dyes are especially sensitive to irradiation and (depending on the host material) stabilities are generally not good², however dyes with longer lifetimes have been made.³ An interesting study by Mooney *et al.*⁴ suggest that the lifetime of the donor dye is improved in a FRET pair. This gives an additional advantage to the system in Chapter 5 as dyes with short lifetimes could be made more stable in a flexible nanoporous liquid crystal network matrix for FRET.

The electrical switching can cause damage over repeated uses; however, the devices from Chapter 2-4 were stable for multiple switching cycles. For applications, more switching cycles need to be tested but similar devices have already shown to be able to switch 100,000 times.⁵

6.3 Scalability

To truly test the potential of these systems and determine their effects on crops, they should be incorporated in model greenhouses. Only when tested in an actual greenhouse can the effects on growth rate, crop quality, temperature and electricity generation truly be measured. As the systems described in this thesis have had a maximum size of 5 x 5 cm², this is impractical to test in a greenhouse without first scaling up the system to at least ~1 x 1 m² size panels.⁶

The main devices in Chapters 2-4 consist of a LC material filling a glass cell. Commercially available 'smart' windows such as eyerise⁷ and priva-lite⁸ are based on similar principles, indicating that large scale manufacturing is possible. Systems that require a polymerization step (the coating from Chapter 4 and the film from Chapter 5) are generally more difficult to produce but systems of 40 x 50 cm² have been fabricated.⁵

Probably the easiest way to create large area devices is by making use of coatings and they could even be applied as part of a retrofitting operation to the glass of existing structures. As most systems in this thesis require a LC phase, it is difficult to transform them to a coating. A solution to this could be using stratification techniques to form a hard top layer with a LC material underneath from a single coating.⁹ Stratification techniques could potentially be used for the thermal responsive systems described in this thesis but for electrical response, flexible transparent electrodes¹⁰ on the substrate are required as well.

The photochromic dye in Chapter 4 doesn't require a LC phase to function and was already made into a coating, and is therefore a good system to start scaling up.

6.4 Predicted effects

In section 1.2.1 the effects of scattered light on crops are discussed and some examples are shown of systems that can regulate haze. In Chapter 3 we presented a 'smart' window which has a scattering state based on a supertwist structure. In the work by Sol *et al.*¹¹ a very similar system is described where a scattering state of 66% haze is reached. Similar haze values are expected for our system in Chapter 3 or even higher due to the additional scattering of the aggregates dyes. Having a greenhouses cover with 50% haze could increase the production of cucumbers by 8-10%.¹² From these results we expect that the 66% haze will have a significant impact on crop production.

To get an indication of the amount of cooling gained by using a 'smart' window, a simple model of a greenhouse was made using LBNL Optics and DesignBuilder.^{13,14} For simplicity, permanent absorption was assumed and the absorption spectra in Chapter 2 of dye 2 (System 1) was used and a combination of dye 1 and double the amount of dye 2 (System 2). No ventilation was assumed, and greenhouses were modeled in three locations: De Bilt, the Netherlands (NL); Almeria, Spain (ES) and Riyadh, Saudi Arabia (SA). In **Table 6.1** the yearly average temperatures and cooling gains for the proposed devices (compared to standard greenhouse quality glass) are shown, as well as the temperature and cooling gains for the 26th of June at 15:00, a typical summer time (TST). On a yearly average the cooling gain is fairly limited (less than 1 °C) for System 1 and about 3 times larger for System 2. However, on a TST System 1 can lower the interior temperature by 0.7 °C in the Netherlands and double that amount in Spain and Saudi-Arabia. The stronger absorbing System 2 can even triple that cooling gain resulting in temperature decrease of more than 4 °C. As mentioned in section 1.3, temperatures both too high as well as too can be detrimental to crop production. The modeling results demonstrate that even our imperfect systems could have a significant impact in preventing temperatures from becoming too high, while, due to the option of switching to a transparent state, the system has no negative impact when it is cold.

Table 6.1: Modeled temperature and cooling gain in a greenhouse when using absorbing coatings in three locations for a yearly average and at a typical summer time.

	<i>Temperature (°C)</i>				<i>Cooling gain (°C)</i>	
	Outdoor	Glass	System 1	System 2	System 1	System 2
<i>NL avg</i>	10.8	14.3	14.1	13.7	0.2	0.6
<i>ES avg</i>	19.0	28.6	28.2	27.2	0.5	1.4
<i>SA avg</i>	26.4	37.3	36.7	35.5	0.6	1.7
<i>NL TST</i>	22.3	39.6	38.9	37.5	0.7	2.1
<i>ES TST</i>	23.9	58.0	56.6	53.5	1.5	4.6
<i>SA TST</i>	39.6	67.7	66.4	63.5	1.4	4.3

As mentioned in section 1.4, changing the color of light that reaches the crops can result in photomorphogenetic responses. Most systems in this thesis use red fluorescent materials alone or in combination with yellow/green fluorescent dye. The effect of red light on plant growth is disputed: for example, some researches using only red light¹⁵ or red fluorescent covers¹⁶ claimed mainly negative effects, while in contrast a fluorescent red cover on crops have also been reported that indicate positive effects.¹⁷ It is unclear if the positive effects on growth are due to the resulting reduction in temperature or if the red light itself is beneficial.¹⁷ While photosynthetic activity may be higher for red light¹⁶ (see also **Figure 1.2c**¹⁸) the actual effects on plant growth is debated. Thus, the impact of our color changing capabilities still must be determined.

In section 1.5 it was proposed that luminescent solar concentrators (LSCs) can be used by greenhouses to generate electricity. An estimation of the potential electrical generation of such a device was made for our system in Chapter 2. As depicted in **Figure 2.4a**, external power efficiencies of around 2.5% are obtained. With a sunlight intensity of 1000 W/m² and a solar cell efficiency of 20%¹⁹ that would result in a 5 W/m² production of electricity. The electricity production could be further increased by adding more and/or another dye to increase the amount of absorbed light. More light collected will result in even less light reaching the crops, so a careful balance between light energy collected and transmitted needs to be considered. Additionally, PV cells have different responses to different wavelengths of light and this should be matched with the LSCs.²⁰ When upscaling LSCs for the electrical production it should be noted that the optimal dye concentration changes with different sizes of LSCs.²¹ Test on greenhouses with LSCs have shown that 20 W/m² of electricity could be generated.²²

6.5 'Smart' blinds

An alternative to 'smart' windows could be 'smart' blinds that can open and close automatically based on ambient temperatures. Potential advantages of this system over 'smart' windows are that they could be easier to produce and could be more robust as damage to a single blind will not affect other blinds.

'Smart' microblinds have been reported by Lamontagne *et al.*²³ based on an array of curled electrodes created by laser patterning of a strained transparent conductive oxide layer. The curled electrodes bend when electricity is applied, which closes the blinds. Light can still pass through in the closed state, but the window will be darkly colored, rather than only reflecting IR light. Other examples of automatic closing shutters are the flectofins²⁴ and the flectofold²⁵. A significant disadvantage of these systems is that all wavelengths of light are blocked. In this section, we describe 'smart' blinds that reflect IR while remaining transparency to visible light; by rotating the reflector panels, the 'smart' blinds become transparent to the IR light as well. These 'smart' blinds are made from two parts: a cholesteric reflective panel and a LC actuator acting as a hinge (see **Figure 6.1**). The panel only allows visible light to pass and reflects IR radiation at rest, while the rotation of the hinge realigns the reflective panel to allow IR passage, permitting dynamic modulation of IR light reflection while retaining constant visible light access.

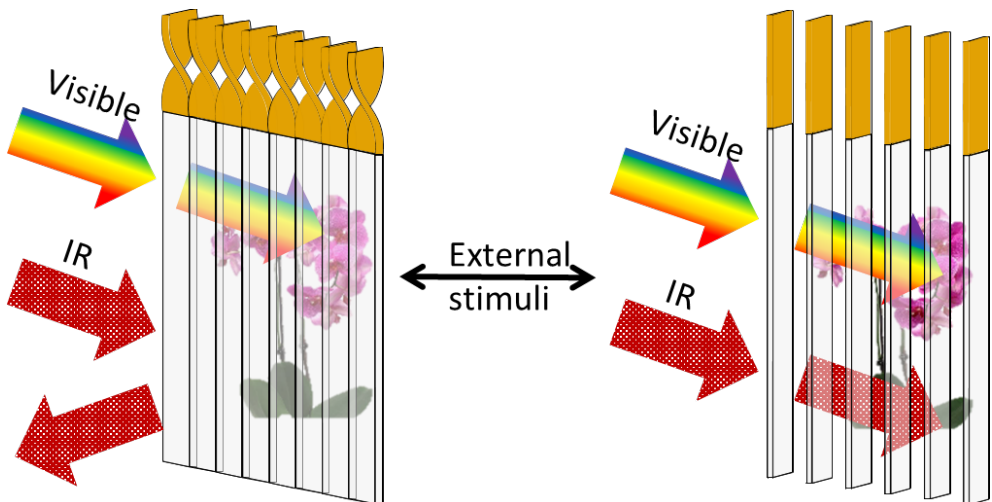


Figure 6.1: Schematic representation of the principle of the 'smart' blinds made from reflective panel that is transparent in the visible region and reflects IR light attached to a LC actuator.

Although heat is the desired stimulus for switching the window IR transparency, these initial experiments are done with light responsivity for easier control. The reflector is made

by bar-coating a chiral nematic LC mixture on a polyethylene terephthalate (PET) substrate.²⁶ The hinge section of the blind is made by bar coating an azobenzene-containing LC mixture on a PET substrate.²⁷ The azobenzene is responsive to light and isomerizes from *trans* to *cis* upon exposure to 365 nm light and back to *trans* upon exposure to 455 nm light. If embedded in an aligned LC network, this isomerization causes contraction in the direction of the director and expansion in the perpendicular direction, resulting in a bending motion.

Actuator strips were cut from the coated PET substrate and bent when exposed to either 365 nm or 455 nm LED light, see **Figure 6.2a**. To test the ‘smart’ blinds, a piece of reflector panel of similar size was attached to the actuator strip (**Figure 6.2b**). The ‘smart’ blind shows a 90° twisting motion when illuminated with 365 nm light and twists back when exposed to 455 nm light. The twisting is probably caused by the weight of the reflector attached to the actuator and the size of the film strip preventing the actuator from bending, as happens without the piece of reflector attached.

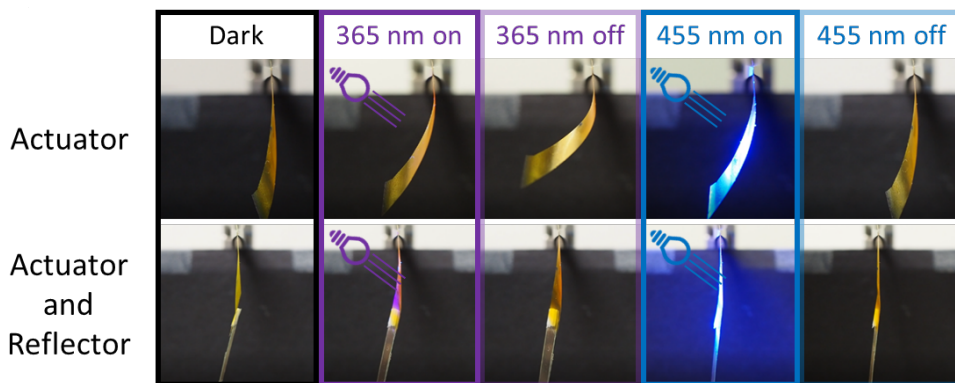


Figure 6.2: Actuation of: (top) free actuator and (bottom) a ‘smart’ blind consisting of a reflector piece attached to the same actuator.

To address the issue of temperature response: LCs are temperature sensitive, where increasing the temperature causes a decrease in order which will lead to contraction along the director and expansion in the perpendicular directions. In a polymerized LC network this expansion and contraction leads to bending similar to that shown for the light response with the azobenzene-containing LCs. To make this system temperature responsive, the isotropic temperature of the LC mixture will need to be tuned to rotate the reflector at the desired temperature (~30 °C).

6.6 Switchable Light guide

In greenhouses, diffusers are used to ensure light is not only absorbed by the top leaves of the crop but also reaches the lower canopy.^{12,28} Here, we propose a new method to selectively increase light irradiation deeper in the leaf canopy of plants by using LSCs. Additional illumination at the sides or bottom is expected to lead to an increase in crop growth.²⁹

Figure 6.3 shows two very basic schematic representations of possible greenhouse configurations. The light which would normally not illuminate the plants directly is absorbed by the LSC. Hereafter the light is guided to the desired position and then selectively extracted from the lightguide at the most advantageous locations to stimulate plant growth.

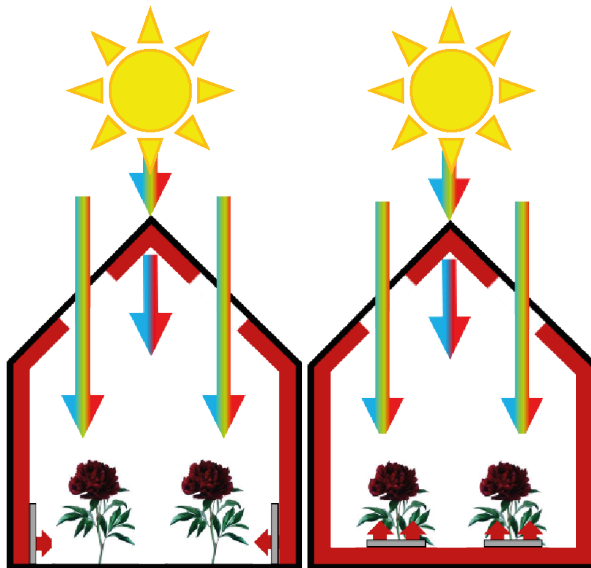


Figure 6.3: Two schematic representations of possible greenhouse configurations to increase crop production using LSCs (red parts). The color of the arrows represents the wavelengths of the corresponding light and the grey rectangles represent the (switchable) outcoupling structures.

In a typical LSC, light is absorbed by fluorescent dyes over the entire panel surface and the re-emitted light is concentrated primarily at the four edges (**Figure 6.4a**). We propose to create a slanted edge at one end of the LSC where the trapped light will be released towards the bottom instead of the edge (**Figure 6.4b**). In initial experiments it was found that 3.2% of the photons absorbed at one end of the LSC could be released at the other end (~20 cm further) using the slanted structure as depicted in Figure 6.4b.

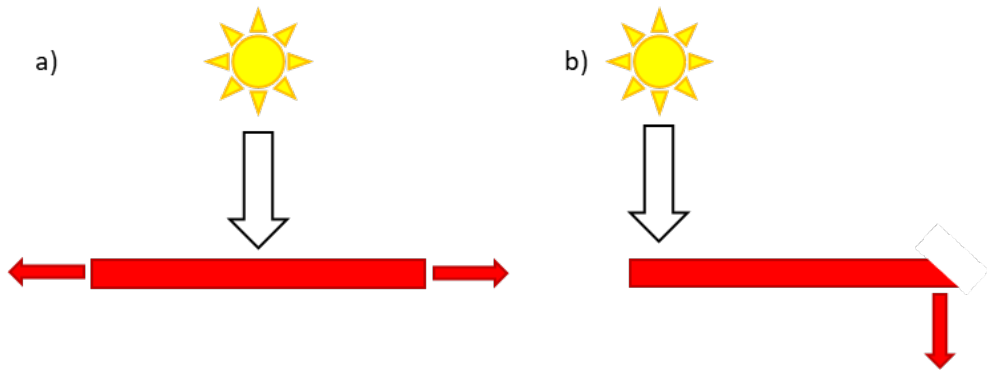


Figure 6.4: a) Standard LSC design, where light is concentrated to the four edges of the panel. b) Light distributing LSC, where light is outcoupled at the far end by creation of a slanted edge.

The light distributing LSC could be made switchable by addition of a layer that can become alternatively reflective/absorbing and transparent such as cholesterics^{9,30,31} or dichroic dye doped LC^{32–34} systems at the outcoupling area for selective extraction of light. The efficiency of the light transport could be further improved by addition of scattering structures where the light needs to be released and by doping only the area of the LCS that absorbs light with dye while the rest is transparent to prevent reabsorption losses.³⁵

6.7 Conclusion

Currently there are no systems available that can rapidly and reversibly, sometimes autonomously, alter their optical properties for use in greenhouses. To remedy this a variety of advanced optical materials were fabricated as described in this thesis. Most of these systems are designed as ‘smart’ windows to control the incoming sunlight based on the combination of fluorescent dichroic dyes and LCs. These systems can quickly change from absorbing to transparent and some also to scattering in response to electrical and thermal or light triggers. The next step in the development of these devices would be to incorporate them in an actual greenhouses to investigate their effects on crops. Further development is needed before they can be applied in the greenhouse industry, paying special attention to the two main hurdles (stability and scalability) that are discussed in this Chapter. If these issues can be overcome, we foresee a bright (green) future for these devices!

6.8 References

- 1 <https://abrisatechnologies.com/2010/02/using-uv-blocking-glass-to-protect-liquid-crystal-displays/> (accessed January 2021).
- 2 I. Baumberg, O. Berezin, A. Drabkin, B. Gorelik, L. Kogan, M. Voskobojnik and M. Zaidman, *Polym. Degrad. Stab.*, 2001, **73**, 403–410.
- 3 W. G. J. H. M. van Sark, K. W. J. Barnham, L. H. Slooff, A. J. Chatten, A. Büchtemann, A. Meyer, S. J. McCormack, R. Koole, D. J. Farrell, R. Bose, E. E. Bende, A. R. Burgers, T. Budel, J. Quilitz, M. Kennedy, T. Meyer, C. D. M. Donegá, A. Meijerink and D. Vanmaekelbergh, *Opt. Express*, 2008, **16**, 21773.
- 4 A. M. Mooney, K. E. Warner, P. J. Fontecchio, Y.-Z. Zhang and B. P. Wittmershaus, *J. Lumin.*, 2013, **143**, 469–472.
- 5 X. Hu, X. Zhang, W. Yang, X. Jiang, X. Jiang, L. T. Haan, D. Yuan, W. Zhao, N. Zheng, M. Jin, L. Shui, A. P. H. J. Schenning and G. Zhou, *J. Appl. Polym. Sci.*, 2020, **48917**, 48917.
- 6 Personal communication with S. Hemming and E. Baeza, Wageningen University (2020).
- 7 <https://www.eyrise.com> (accessed March 2020).
- 8 <https://www.privalite.com/> (accessed March 2020).
- 9 H. Khandelwal, E. P. A. van Heeswijk, A. P. H. J. Schenning and M. G. Debije, *J. Mater. Chem. C*, 2019, **7**, 7395–7398.
- 10 H. Peng, W. Dang, J. Cao, Y. Chen, D. Wu, W. Zheng, H. Li, Z.-X. Shen and Z. Liu, *Nat. Chem.*, 2012, **4**, 281–286.
- 11 J. A. H. P. Sol, G. H. Timmermans, A. J. van Breugel, A. P. H. J. Schenning and M. G. Debije, *Adv. Energy Mater.*, 2018, **8**, 1702922.
- 12 S. Hemming, T. A. Dueck, J. Janse and F. van Noort, *Acta Hortic.*, 2008, **801**, 1293–1300.
- 13 J. L. M. Hensen and R. Lamberts, Eds., *Building Performance Simulation for Design and Operation*, Routledge, Second edition. | Abingdon, Oxon ; New York, NY : Routledge, 2019., 2019.
- 14 C. Lee, P. Hoes, D. Cóstola and J. L. M. Hensen, *Energy*, 2019, **175**, 534–545.
- 15 W. van Ieperen, *Acta Hortic.*, 2012, **956**, 131–139.
- 16 M. E. Loik, S. A. Carter, G. Alers, C. E. Wade, D. Shugar, C. Corrado, D. Jokerst and C. Kitayama, *Earth's Futur.*, 2017, **5**, 1044–1053.
- 17 G. Alers, *Luminescent Enhancement for Combined Solar and Agriculture*, Argonne, IL (United States), 2020.
- 18 K. J. McCree, *Agric. Meteorol.*, 1972, **10**, 443–453.
- 19 V. Avrutin, N. Izyumskaya and H. Morkoç, *Superlattices Microstruct.*, 2011, **49**, 337–364.
- 20 M. Debije and P. Verbunt, *Adv. Energy Mater.*, 2012, **2**, 12–35.
- 21 A. A. Earp, G. B. Smith, P. D. Swift and J. Franklin, *Sol. Energy*, 2004, **76**, 655–667.
- 22 C. Corrado, S. W. Leow, M. Osborn, I. Carbone, K. Hellier, M. Short, G. Alers and S. A. Carter, *J. Renew. Sustain. Energy*, 2016, **8**, 043502.
- 23 B. Lamontagne, P. Barrios, C. Py and S. Nikumb, *Proc. Glas. Perform. Days 2009*, 2009, 637–639.
- 24 J. Lienhard, S. Schleicher, S. Poppinga, T. Masselter, M. Milwich, T. Speck and J. Knippers, *Bioinspiration and Biomimetics*, DOI:10.1109/CoDIT.2017.8102714.
- 25 A. Körner, L. Born, A. Mader, R. Sachse, S. Saffarian, A. S. Westermeier, S. Poppinga, M. Bischoff, G. T. Gresser, M. Milwich, T. Speck and J. Knippers, *Smart Mater. Struct.*, 2018, **27**, 017001.
- 26 E. P. A. van Heeswijk, J. J. H. Kloos, J. de Heer, T. Hoeks, N. Grossiord and A. P. H. J. Schenning, *ACS Appl. Mater. Interfaces*, 2018, **10**, 30008–30013.
- 27 R. C. P. Verpaalen, M. Pilz da Cunha, T. A. P. Engels, M. G. Debije and A. P. H. J. Schenning, *Angew. Chemie Int. Ed.*, 2020, **59**, 4532–4536.
- 28 S. Hemming, V. Mohammadkhani and T. Dueck, *Acta Hortic.*, 2008, **797**, 469–475.
- 29 N. S. Makarov, K. Ramasamy, A. Jackson, A. Velarde, C. Castaneda, N. Archuleta, D. Hebert, M. R. Bergren and H. McDaniel, *ACS Nano*, 2019, **13**, 9112–9121.
- 30 H. Khandelwal, R. C. G. M. Loonen, J. L. M. Hensen, M. G. Debije and A. P. H. J. Schenning, *Sci. Rep.*, 2015, **5**, 11773.
- 31 A. J. J. Kragt, N. C. M. Zuurbier, D. J. Broer and A. P. H. J. Schenning, *ACS Appl. Mater. Interfaces*, 2019, **11**, 28172–28179.
- 32 S.-W. Oh, S.-H. Kim and T.-H. Yoon, *Adv. Sustain. Syst.*, 2018, **1800066**, 1800066.
- 33 V. K. Baliyan, K.-U. Jeong and S.-W. Kang, *Dye. Pigment.*, 2019, **166**, 403–409.
- 34 G. H. Sheetah, Q. Liu, B. Senyuk, B. Fleury and I. I. Smalyukh, *Opt. Express*, 2018, **26**, 22264.
- 35 A. A. Earp, G. B. Smith, J. Franklin and P. Swift, *Sol. Energy Mater. Sol. Cells*, 2004, **84**, 411–426.

Samenvatting

Er zijn meer gewassen en van een hogere kwaliteit nodig om de groeiende en steeds welvarender wereldbevolking te voeden. Broeikassen zijn uitstekende systemen om de productiviteit van een afgebakend stuk grond te verhogen. Er zijn veel factoren onderzocht om te proberen de opbrengst van kassen te verhogen, maar in veel moderne kassen is de hoeveelheid en de spreiding van het licht dat de gewassen bereikt nog steeds de beperkende factor. Er zijn momenteel nog weinig mogelijkheden om het invallende zonlicht te beheersen en er zijn bijna geen systemen beschikbaar waarvan de optische eigenschappen snel kunnen veranderen. In dit proefschrift laten we verschillende systemen zien die hun optische eigenschappen wel snel kunnen veranderen in reactie op omgevingsfactoren. Deze 'slimme' ramen kunnen hun absorptie en/of lichtverstrooiing veranderen als reactie op bijvoorbeeld temperatuur, licht of een elektrisch veld.

Eerst werd in hoofdstuk 2 beschreven hoe een op absorptie gebaseerd 'slim' raam wordt gemaakt door een dichroïsche fluorescente kleurstof op te lossen in een vloeibaar kristallijn materiaal. De ordening van de vloeibare kristallen kan worden gewijzigd door een elektrisch veld aan te leggen of door verandering van de temperatuur. De dichroïsche kleurstof volgt de ordening van de vloeibare kristallen en daardoor verandert de absorptie van het systeem. Hierdoor wordt – naarmate het warmer wordt – meer licht geabsorbeerd, waardoor de temperatuur in de broeikas gestabiliseerd wordt. Het 'slimme' raam kan handmatig in een transparantere toestand worden gebracht door een elektrisch veld aan te leggen. Omdat de dichroïsche kleurstof fluorescent is, wordt een deel van het geabsorbeerde licht opnieuw uitgezonden en wordt het geconcentreerd aan de randen van het raam zoals in een fluorescente lichtgeleider. Het geconcentreerde licht kan met behulp van zonnecellen worden omgezet in elektriciteit of worden doorgestuurd naar planten om hun groei te bevorderen.

In hoofdstuk 3 wordt beschreven hoe een 'slim' raam wordt gemaakt waarin niet alleen de ordening van de fluorescente kleurstof wordt veranderd, maar de kleurstof zelf temperatuurgevoelig is. Bij hogere temperaturen is de kleurstof fluorescent, maar bij afkoeling aggregereert ze tot een kleurloze, niet-fluorescente vorm. Mede dankzij Förster resonantie energieoverdracht zorgt toevoeging van een tweede fluorescente kleurstof voor een gele kleur bij lage temperaturen en een helderrode kleur bij hogere temperaturen. Door het aanbrengen van een elektrisch veld heroriënteren zowel de vloeibaar kristallijne gastheer als de fluorescente kleurstof zich, waardoor het 'slimme' raam transparant wordt. Door de vloeibare kristallen gedraaid te ordenen wordt bij tussenliggende elektrische

spanningen lichtverstrooiing gecreëerd. Lichtverstrooiing is in het algemeen gunstig voor de groei van gewassen in broeikassen en kan ook dienst doen als privacy toestand in gebouwen. Omdat het systeem gebruikmaakt van een fluorescente kleurstof, kan het ook dienen als een fluorescente licht geleider.

Om gewassen snel tegen hoge lichtintensiteiten te kunnen beschermen, werd in hoofdstuk 4 een lichtgevoelig 'slim' raam gemaakt. In tegenstelling tot de systemen in hoofdstuk 2 en 3 kan dit systeem direct reageren op veranderingen in het licht, voordat de temperatuur in de broeikas oploopt. Dit systeem is gebaseerd op een fluorescente lichtgevoelige kleurstof die sterker gekleurd wordt bij blootstelling aan licht van 340 nm en minder gekleurd bij blootstelling aan licht van 440 nm. Het systeem kan nog steeds handmatig transparant worden gemaakt door het aanleggen van een elektrisch veld. Ook hier zou het systeem eveneens kunnen worden gebruikt als fluorescente lichtgeleider om elektriciteit op te wekken. Het 'slimme' raam werd ook omgevormd tot een 'slimme' lichtgevoelige coating om het makkelijker toepasbaar te maken in broeikassen of gebouwen.

In tegenstelling tot de hoofdstukken 2-4 wordt in hoofdstuk 5 geen 'slim' raam beschreven maar wordt beschreven hoe een systeem kan worden gemaakt waarin efficiënte Förster resonantie energieoverdracht kan plaatsvinden. Met vloeibare kristallen wordt een fluorescente kleurstof gemanipuleerd om een geordende matrix te creëren. Na onderdompeling in een base wordt de vloeibaar kristallijne matrix nano poreus en wordt een tweede kleurstof geabsorbeerd, waardoor de twee kleurstoffen nauw met elkaar in contact komen. De ordening en de korte afstand tussen de twee fluorescente kleurstoffen vergemakkelijkt de Förster resonantie energieoverdracht. Dergelijke systemen zijn niet alleen interessant als detectoren, maar deze efficiënte energieoverdracht kan ook gunstig zijn voor zonnecellen, fluorescente lichtgeleiders en broeikassen.

Conclusie, dit proefschrift geeft meerdere voorbeelden van potentiële 'slimme' ramen op basis van fluorescente kleurstoffen en vloeibare kristallen. Deze ramen kunnen hun absorptie zowel op commando als in reactie op veranderende omgevingsfactoren veranderen, om de binnentemperatuur van gebouwen en broeikassen te stabiliseren. Het geabsorbeerde licht kan worden gebruikt om elektriciteit op te wekken als een fluorescente licht geleider of kan worden omgeleid naar de gewassen in broeikassen. Behalve in broeikassen zijn deze systemen ook interessant voor gebouwen, elektriciteitsopwekking en detectoren.

Acknowledgments

After four years as a PhD student there are many people to thank, not only for helping me create this thesis but also for making the time I spend at SFD so wonderful.

Als eerste wil ik mijn promotor, prof. dr. Albert Schenning, bedanken voor al zijn steun en hulp. Albert, al sinds ik als masterstudent bij SFD zat, verbaasde ik me erover hoe anders ik een vergadering met jou verliet dan ik binnenkwam. Het maakte niet of ik problemen had of zeker was van mijn ideeën, na overleg met jou bleek het vaak handig om het nét wat anders te doen en verliet ik jouw kantoor weer vol goede moed. Bedankt voor al het advies, het heeft mijn werk veel beter gemaakt!

Many thanks to Dr. Michael Debije, my copromotor and daily supervisor. Michael, you introduced me to this project and with your guidance I managed to create this thesis. Meetings with you had a tendency to run a bit long, not only due to you being eager to teach me something, or the dozen suggestions that you had for my work, but also because we would have many nice chats about politics, books and the university. Thank you, for teaching me how to be a good researcher and many other things, including not to use the word 'thingy' anymore (although I still have difficulty with responds and response).

I would also like to thank my committee members, prof. dr. Wilfried van Sark, dr. Rachel Evans, prof. dr. Angèle Reinders, dr. Stefan Meskers and dr. Silke Hemming for being on my committee and giving me valuable feedback to improve my thesis. Angèle, I always valued our meetings and enjoyed the LSC PV workshop you organized at the TU/e. Stefan, thank you for always being available to help me or my students with the various fluorescence measurements and taking an interest in my work. Silke, you organized and chaired all the PPS Smart Materials meetings we had. The meetings were not only very informative but also very fun and that was largely due to your excellent organization and teambuilding skills.

My project was funded as a part of the PPS Smart Materials program and this led me to meet various interesting people from different companies (FME, LTO Glaskracht Nederland, Wageningen University, BASF, Fujifilm, Sabic, Saint-Gobain, Mardenkro, Glascom, DA Glass and RKW-Hyplast). During the four years of our project, the people that were members of this group changed but everyone was very helpful and enthusiastic. Your talks and suggestions during our meetings were very valuable and I greatly enjoyed visiting your companies and getting a closer look at the industry (and of course the dinners and drinks

afterwards!). A special thanks to Silke, Esteban, Bram and Cecilia of Wageningen University, your enthusiasm about plants and all things greenhouse really made a difference. Thank you, for helping me with measurements and teaching me about plants, light and greenhouses.

Dr. Jianbin Lin, thank you for synthesizing various dye molecules for us. Your help and enthusiasm allowed us to design new molecules with interesting properties, the results of which can be seen in two Chapters of this thesis.

Dr. Roel Loonen and Agata Rijs, thank you for quickly building a model to estimate the energy savings of my materials, it made my technological assessment much better.

I would also like to thank Audrey. Thank you for helping me with my scientific writing, which helped to improve my papers and thesis. It was always fun to chat with you when we ran into each other or when you were working in Michael's office.

Bart, hartelijk bedankt voor de fijne samenwerking die resulteerde in Hoofdstuk 4 van deze thesis. Jij bleef altijd erg enthousiast en samen hebben we het tot een goed einde weten te brengen.

Bernette, ook jij bedankt voor de vele samenwerkingen. Jouw ervaring met smectische systemen en TEM hebben mijn Hoofdstuk 5 naar grotere hoogten getild. Ik was ook erg blij dat ik jou heb kunnen helpen met je onderzoek en zelfs coauteur mocht worden van een van je papers. Veel succes met het voltooien van je PhD en ik kijk er naar uit om samen met jou de paranimfen voor Davey te zijn!

Ik wil graag Johan bedanken voor zowel onze discussies over kleurstoffen (en vele andere dingen) als voor het controleren van mijn werk op fouten, vooral de structuurformules. Alle fouten die zijn blijven staan, zijn natuurlijk mijn schuld.

Tijdens mijn PhD heb ik een hoop studenten mogen begeleiden. De resultaten daarvan zijn te zien in deze thesis en ook waar het niet direct te zien is, heeft het mij enorm geholpen. Jeroen, Joey, Nieké, Robin, Maxime, Joey (opnieuw) en Jop, ik vond het erg fijn met jullie samen te werken en wens jullie het beste in jullie verder carrière.

De excellente wetenschappelijk staf maakt SFD tot een succesvolle vakgroep, maar iedereen binnen SFD weet dat niks zou functioneren zonder Marjolijn en Tom. Marjolijn, officieel ben je de secretaresse van de groep maar je bent en doet veel meer dan dat. Buiten het geregeld, papierwerk en organiseren van evenementen en conferenties zorg je ook voor iedereen. Als er nieuwe mensen in de groep komen, help je ze met van alles zodat ze zich meteen thuis voelen en met mij was dat niet anders. In mijn laatste jaar mocht ik eindelijk

samen met jou een activiteit organiseren en alhoewel het online moest, was het zeker een zeer geslaagde avond! Hartelijk bedankt voor alle hulp en gezelligheid (de mooie UCSc prijs) en zodra het weer mag, moeten we een keertje samen een pubquiz doen!

Tom, je bent een echt mannetje van alles, techneut, reparateur, veiligheidsman, voorraadbeheerder en contactpersoon voor alles en iedereen op het lab. Ondanks je (soms te) drukke werk was het altijd gezellig met jou op kantoor en geen enkele vrijdagmiddag hoefden we ons te vervelen. Bedankt voor al je hulp gedurende mijn project, van dingen repareren tot slimme suggesties voor metingen of een goed idee voor mijn cover!

Too all my colleagues from SFD (and the people from Rints group): you made it a treat to come to work every day! You were always willing to help, discuss problems or have some fun. Our lunches were legendary (especially if there were kipcorns!) and although they lunches and coffee breaks took a lot of time, it was worth every second. We went to many awesome parties, BBQs and even a few weddings! My favorite was obviously the F.O.R.T. drinks at 4 o'clock and I'm very sad we won't be able to enjoy it one last time. When this is all over we should definitely have a big party to make up for everything! Please keep the tradition (three times is a tradition!) of having UCScs ('Ugly Christmas Sweater' competitions). Hopefully a new SFD-UCSc-Oc (Stimuli-responsive Functional materials and Devices 'Ugly Christmas Sweater' competition Organizational committee) will get to organize a real-life event and not an OC/T/hC/UCScms (Online Coffee/Tea/hot Chocolate/UCSc-meetings) like last year. Thank you: Alberto, Annelore, Anping, Arne, Davey, Diederik, Dirk-Jan, Ellen, Eveline, Fabian, Frankje, Huiyi, Jeroen, other Jeroen, Li, Marc, Marina, Niki, Patri, Pei, Roel, Sebastian, Rob, Sean, Shajesh, Simon, Sterre, Stijn, Yari, Yuanyuan, Xiaohong, Xinglong, Wanshu, Wei and Wilson.

I would also like to thank the older generation of PhDs: Anne-Hélène, Dirk-Jan, Hitesh, Jody, Koen, Marcos, Matthew, Monali and Sarah. Although we haven't been colleagues for long, you immediately made me feel welcome to the group and invited me to join you for many fun activities. A special mention to Hitesh for being my supervisor during my master project and first introducing me to the wonders of SFD!

Ik wil ook graag mijn paranimfen bedanken: Davey en Ellen. Davey, we zijn rond dezelfde tijd begonnen als PhD en al snel bleken we het goed met elkaar te kunnen vinden. We begonnen te trainen naar Utrecht voor RPK-C met naderhand wat drankjes en al gauw spraken we na de F.O.R.T. af voor eten en spelletjes. Iedereen was altijd welkom om mee te doen, maar jij, Ellen, Eveline en ik waren altijd de harde kern. Nadat ik een paar keer onbewust als chaperon ben mee geweest met jullie eerste dates, kreeg je een relatie met Eveline. Gelukkig heeft dit helemaal niks veranderd aan de gezelligheid, behalve dat we nu afspreken bij het huis van jou én Eveline. Bedankt voor alle gezelligheid en veel succes met je eigen verdediging binnenkort! Ik kijk er naar uit om jouw paranimf te zijn!

Lieve Ellen, ik ken je al sinds onze introweek in 2010 waar bleek dat jij mijn lang verloren zusje was. Nadat jij wat gewend was aan al die Limbo's en ik aan dat rare taaltje van jou (Ik ben net afgewerkt, dus ik kom zo aangereden, houdoe!) werden we snel goede vrienden. Gedurende onze hele studententijd hadden we veel plezier, zowel in als buiten de collegebanken. Toen ik na mijn stage terugkwam bij SFD, werden we collega's en kantoorgenoten. Dit kwam erg goed uit, want zo hadden we altijd iemand die meteen ja zei voor koffiepauze (eigenlijk thee/chocomel pauze) of om naar de F.O.R.T. te gaan. Het enige nadeel was dat jij al een jaar eerder klaar was dan ik en ik daarna naar een leeg bureau moest kijken... Bedankt voor de leuke tijd en goeie herinneringen, mogen er nog vele volgen!

Lieve oud-studiegenoten, oud-klasgenoten, lang verloren broertje, (zelfbenoemde) subsidie verstrekkers of gewoon lieve vriendjes en vriendinnetjes: Annelies, Bea, Bianca, Ellen, Gijs, Jan Willem, Laurent, Marijne, Nicky, Remco, Rick, Sander en Tom. In het kort: jullie zijn fantastisch! In het lang: bedankt voor alle gezelligheid en al het plezier dat we gehad hebben. Het was altijd erg leuk om met jullie samen verjaardagen, dagjes Efteling, HOUSEWARMING, bruiloften, weekendjes weg, F.O.R.T., filmmarathons, vakanties, gewoon wat hangen en héél soms wat drankjes te doen. Ik denk met veel plezier aan alles terug en ik hoop nog veel meer met jullie te beleven!

Lieve familie, Mam, Pap, Guy en Joyce. Bedankt voor de (op)voeding, liefde en steun. Jullie konden niet altijd helemaal volgen wat ik aan het doen was maar ik kon altijd naar jullie toe met mijn problemen.

Iedereen hartelijk bedankt!

Thank you all!

-Gilles

Curriculum Vitae

Gilles Timmermans was born on the sixth of January, 1992 in Heerlen, the Netherlands. After finishing high school in 2010 at Grotius college in Heerlen, he moved to Eindhoven to study Chemical Engineering at Eindhoven University of Technology (TU/e). In 2016 he completed his master project within the Stimuli-responsive Functional materials and Devices (SFD) group on: 'Smart windows based on cholesteric liquid crystals'. After an internship at DSM in Geleen he received his master degree in 2017. Later in the same year he started his PhD at the same group under the supervision of prof.dr. Albert Schenning and dr. Michael Debije. In his PhD project on smart materials for greenhouses he worked in collaboration with various industrial partners and Wageningen University & Research. The most important results of his research are presented in this thesis.



List of Publications

Publications related to this thesis

- G. H. Timmermans, S. Hemming, E. Baeza, E. A. J. van Thoor, A. P. H. J. Schenning and M. G. Debije, Advanced Optical Materials for Sunlight Control in Greenhouses. *Advanced Optical Materials*, 8, 2000738 (2020).
- G. H. Timmermans, R. F. Douma, J. Lin and M. G. Debije, Dual Thermal-/Electrical-Responsive Luminescent ‘Smart’ Window. *Applied Sciences*, 10, 1421 (2020).
- G. H. Timmermans, J. Wu, A. P. H. J. Schenning, J. Lin, and M. G. Debije, "Color tunable triple state ‘smart’ window," (submitted)
- G. H. Timmermans, B. W. H. Saes and M. G. Debije, Dual-responsive “smart” window and visually attractive coating based on a diarylethene photochromic dye. *Applied Optics* 58, 9823 (2019).
- G. H. Timmermans, M. van der Heijden, B. M. Oosterlaken, S. C. J. J. Meskers, A. P. H. J. H. J. Schenning and M. G. Debije, Flexible Nanoporous Liquid Crystal Networks as Matrixes for Förster Resonance Energy Transfer (FRET). *ACS Applied Nano Materials*, 3, 3904–3909 (2020).

Other publications

- H. Khandelwal, G. H. Timmermans, M. G. Debije and A. P. H. J. Schenning, Dual electrically and thermally responsive broadband reflectors based on polymer network stabilized chiral nematic liquid crystals: the role of crosslink density. *Chemical Communications*, 52, 10109–10112 (2016).
- J. A. H. P. Sol, G. H. Timmermans, A. J. van Breugel, A. P. H. J. Schenning and M. G. Debije, Multistate Luminescent Solar Concentrator “Smart” Windows. *Advanced Energy Materials*, 8, 1702922 (2018).
- B. M. Oosterlaken, Y. Xu, M. M. J. Rijt, M. Pilz da Cunha, G. H. Timmermans, M. G. Debije, H. Friedrich, A. P. H. J. Schenning and N. A. J. M. Sommerdijk, Nanohybrid Materials with Tunable Birefringence via Cation Exchange in Polymer Films. *Advanced Functional Materials*, 30, 1907456 (2020).